NASA Contractor Report 3347

Satellite Power Systems (SPS) Laser Studies

Volume II: Meteorological Effects on Laser Beam Propagation and Direct Solar Pumped Lasers for the SPS

R. E. Beverly III

CONTRACT NAS8-32475
NOVEMBER 1980

NASA

NASA Contractor Report 3347

Satellite Power Systems (SPS) Laser Studies

Volume II: Meteorological Effects on Laser Beam Propagation and Direct Solar Pumped Lasers for the SPS

R. E. Beverly III
Rockwell International
Columbus, Ohio

Prepared for
Marshall Space Flight Center
under Contract NAS8-32475

NASA
National Aeronautics
and Space Administration

Scientific and Technical
Information Branch

1980

FOREWORD

This document, prepared in two volumes, presents the results of two laser studies performed as part of a Satellite Power System (SPS) study (NAS8-32475, for NASA/MSFC) during the period October 19 through June 1980. Both studies were performed by Dr. R. E. Beverly, III.

The first study, *Laser Environmental Impact* (Subcontract M9M8BNB-896662D), is presented in Volume I of this document. The second study (Subcontract MOL8GNS-897409D), in two parts, *Meteorological Effects on Laser Beam Propagation* and *Direct Solar Pumped Lasers for the Satellite Power System*, is presented in Volume II.

Special thanks are extended to the following people for assistance during the study activity resulting in Volume I of this technical report: Mr. Daryl J. Monson at NASA Ames Research Center for providing preprints of his work on CO lasers prior to publication; Professor K. Narahari Rao at the Physics Department of The Ohio State University for supplying high-precision spectroscopic data relative to CO laser transitions; and to Mr. David C. Applebaum, Dr. Russell H. Barnes, Jr., and Dr. Henry L. LaMuth at Battelle Columbus Laboratories for numerous technical discussions. The technical assistance given by Mr. Charles R. Agne and Mr. Steve A. Rohr of Control Data Corporation went far beyond the call of duty and is greatly appreciated. The discussions with Mr. A. I. Gordon of Rockwell International Corporation were extremely beneficial in guiding the present study.

If any questions regarding the technical content of these reports arise, please contact Dr. R. E. Beverly, III, at (614) 457-1242. Questions regarding the basic Satellite Power System program should be directed to either Mr. G. M. Hanley, Rockwell International, at (213) 594-3911, or Mr. A. I. Gordon, Rockwell International, at (213) 594-3687.

CONTENTS

ILLUSTRATIONS

TABLES

1.0 METEOROLOGICAL EFFECTS ON LASER BEAM PROPAGATION

1.1 INTRODUCTION

Lasers are presently being evaluated as an alternate power beaming technique to microwaves for space-to-earth power transmission. Although preliminary studies [Beverly (1980)] indicate that laser power transmission has the advantages of negligible environmental damage and small land requirements associated with the receptor sites, meteorological conditions influence the transmission efficiency to a much greater extent than with microwaves. With proper selection of laser wavelength, clear-air propagation can be very efficient; however, haze, fog, clouds, and rain can severely attenuate the beam.

This study investigates potential mitigation techniques which may minimize this effect by a judicious choice of laser operating parameters. Using these techniques, the availability of power at selected sites is determined using statistical meteorological data for each site. Where technically feasible, siting criteria and laser parameters are defined such that the power availability is comparable to the microwave SPS concept or to conventional electric power plants.

1.2 PROPAGATION CHARACTERISTICS UNDER VARIOUS METEOROLOGICAL CONDITIONS

1.2.1 PHYSICAL MECHANISMS

The attenuation of laser radiation passing through the earth's atmosphere is termed linear attenuation if the processes responsible are independent of the beam intensity. In general, molecular scattering, molecular absorption, aerosol scattering, and aerosol absorption contribute to linear attenuation. To calculate the transmittance of any single laser line in propagating from outside the earth's atmosphere to a terrestrial receptor site, the attenuation coefficient due to each of the above processes must be known at a sufficient number of points along the beam path. This implies the necessity for local atmospheric data as well as basic physical parameters related to absorption and scattering.

If the attenuation depends on the beam intensity, however, the propagation is termed nonlinear. The most commonly encountered nonlinear mechanism in connection with high-energy laser propagation is thermal blooming [see, for example, Gebhardt (1976)]. Thermal blooming is characterized by self-induced spreading, distortion, and bending of the laser beam as a result of molecular and aerosol absorption with the beam path. Absorption leads to heating of the air causing density and, hence, refractive index gradients which act as a distributed lens. Another nonlinear mechanism is aerosol droplet vaporization. With sufficiently large laser power densities, hole boring through various types of meteorological formations may be affected with a concomitant increase in transmission efficiency.

1.2.2 MITIGATION TECHNIQUES

A number of high transparency spectral "windows" are present for which laser radiation will propagate from space to earth with only minimal attenuation due to molecular absorption. During periods of heavy cloud cover or precipitation, however, a severe loss in transmission efficiency will occur because of aerosol absorption and scattering. The transmission efficiency may be improved during adverse meteorological conditions by (1) selection of a wavelength region which minimizes the effects of aerosol absorption and scattering, (2) increasing the elevation of receptor sites, (3) using a vertical propagation path (zenith angle θ - 0°) rather than line-of-sight propagation from a satellite in geosynchronous equatorial orbit ($\theta \simeq 50°$), and (4) by hole boring, i.e., vaporization of the aerosol droplets within the beam path.

Wavelength Selection

Preliminary information [Ruppersberg et al. (1975); Orlov et al. (1976); Tomasi and Tampieri (1976)] indicates that operation in the spectral region around 11 μm may reduce and partially mitigate the loss in transmission efficiency caused by light fog and light cloud cover. This phenomenon occurs for two reasons: (1) the real part of the complex refractive index of water has a minimum at about 12 μm and (2) the aerosol size distribution of certain fogs and clouds decreases more steeply than $(\text{particle radius})^{-2}$ above 7-10 μm radius, thus reducing the scattering and absorption coefficients. Numerical investigations conducted by Ruppersberg et al. (1975) assumed that all droplets were homogeneous and composed of pure water; furthermore, their data were reported as relative coefficients and ice-crystal clouds were not investigated. All of these restrictions are removed in this study.

The clear-air transmission efficiency (considering molecular absorption only) is, unfortunately, undesirably low everywhere in the 11-μm window except for high-elevation receptor sites. Alternately, we have identified an extremely high-transmission region around 2 μm in which molecular absorption is negligible concurrent with a minimum in the aerosol absorption coefficient of water based droplets. The attenuation due to various types of meteorological aerosols and molecular absorption is extensively investigated in both spectral regions.

Receptor Elevation

The selection of receptor sites at high elevation can reduce the deleterious effects of haze and can mitigate the problems caused at lower elevations (river valleys, coastal regions, etc.) by many types of advection and radiation fogs. In addition, if water vapor is an important molecular absorber for a specific laser line, high elevation receptor sites can "get above" a large fraction of the humid air in the lower troposphere and result in improved transmission efficiency. However, we must recognize that constraining receptor siting to high elevations may jeopardize the viability of the laser-SPS concept as an alternate energy source.

Zenith Angle

The space-to-earth transmission efficiency for all linear attentuation mechanisms and a propagation zenith angle θ scales as $\exp(-\sec\theta)$. If molecular absorption is strong, for example, operation at a propagation zenith angle of 0° rather than 50° results in a significant improvement in the transmission efficiency. If the laser wavelength is properly optimized, however, vertical propagation does not afford a significant improvement in the power availability (all meteorological conditions considered) and cannot be justified in terms of the increased cost and complexity of the required space hardware. This effect is discussed further in connection with the power availability model.

Hole Boring

Hole boring through monodisperse and polydisperse aerosols has been addressed for both continuous-wave (cw) and pulsed lasers. Numerous theoretical studies and experimental measurements using artificial and natural aerosols have been conducted over a wide range of parameters. Steady-state evaporation, which is the simplest model and which is applicable to small-diameter particles irradiated at lower intensities, assumes that the energy liberated in the droplet is proportional to its volume and the temperature rise in the droplet is uniform [Bukatji and Pogodaev (1972); Glicker (1971); Lamb and Kinney (1969); Mullaney et al. (1968); Kuzikovskii and Khmelevitsov (1968); Shifrin and Zolotova (1966); Sutton (1970)]. Hence, the absorption coefficient is proportional to water content and is independent of the details of the particle-size distribution. Inclusion of diffusion, heat conduction, and Stefan flow in the evaporation model was investigated by Kuzikovskii (1970), Kuzikovskii et al. (1971), and Zuev et al. (1973). Introduction of fresh aerosol into the beam path by wind convection was included in the steady-state model by Belyayev et al. (1975), Harney (1977), Sukhorukhov and Shumilov (1973), Sukhorukhov et al. (1971), and Volkovitskii (1977), where Sukhorukhov's papers also include the effects of diffusional blurring. All of the aforementioned effects (diffusion, heat conduction, Stefan flow, and wind) were included in the work of Gordin and Strelkov (1975a). The effects of non-uniform internal temperature profiles were considered by Caledonia and Wray (1974), Rudash et al. (1974), and Semenov and Svirkunov (1974). Solution of the evaporation equations self-consistently with absorption and scattering coefficients which explicitly depend on the droplet radius was performed by Bedair and Aly (1975), Bukatyi et al. (1975), Romanov and Pustovalov (1972), and Sutton (1978). At higher intensities, such as obtained with pulsed lasers, droplet explosion can occur [Friedman et al. (1979); Kuzikovitskii (1971); Sutton (1978)]. This process is considerably more efficient than simple evaporation and can reduce the energy requirement necessary to clear a given volume.

Using hole-boring models applicable to the range of laser-beam parameters of interest for power transmission, we have estimated the power densities necessary to affect aerosol clearing under various meteorological conditions. Laser hole boring through certain types of hazes, fogs, and clouds may be possible consistent with safety and environmental concerns. In particular, all but the thickest cirriform clouds and all stratiform clouds with the exception of nimbostratus can be penetrated without the need for weapon-quality beams. For lasers operating in the 11- μm window, cw power densities of 100-200 W/cm^2 are

required. Because of the small aerosol absorption coefficient in the 2-μm window, hole boring at these wavelengths using a cw beam alone will be ineffective. A train of short-duration pulses superimposed on the "main" cw beam will, however, affect penetration under these circumstances. More detailed calculations are given in the section describing the power availability model.

Several other physical mechanisms must be considered in conjunction with hole boring. Intensity fluctuations can be induced by temperature and water-vapor gradients within the beam path [Almayev et al. (1978); Volkovitskii (1975)] and gross refractive bending of the beam can be enhanced under certain conditions by droplet vaporization [Akhmanov et al. (1968); Bukatyi et al. (1973); Kolosov and Kuzikovskii (1979); Nerushev and Semenov (1976); Svirkunov (1978); Vorob'yev (1975)]. For laser-power transmission, intensity fluctuations which do not result in significant beam spreading should be of no concern. We have examined the regime in which refractive bending occurs and found that severe distortion should be negligible for the power densities and beam diameters under consideration here. Another phenomenon which has been recently considered is droplet recondensation in a laser-vaporized path. Overheating of the particles produces local supersaturation, resulting in the production of a large number of fine particles which may attenuate the beam and limit its penetration [Gordin and Strelkov (1975b); Kuzikovskii and Khmelevtsov (1975); Volkovitskii et al. (1976)]. This effect is pronounced at higher radiation intensities, for larger particles, and at lower temperatures. Again, for conditions anticipated here, this effect should not occur.

1.2.3 PROPAGATION CALCULATIONS—AEROSOLS

Models

Aerosol scattering, absorption, and extinction coefficients and differential scattering cross sections were calculated for haze, advection and radiation fogs, various types of clouds, and rain and snow distributions at various precipitation rates. These calculations require detailed properties of the various aerosols, such as composition, size distribution, particle concentration, and complex index of refraction as a function of wavelength. Literature sources for these data are listed in Table 1.2-1. Index of refraction data is given in Table 1.2-2. For the calculations involving haze, absorption and scattering coefficients for the various aerosol models were taken directly from the work of Shettle and Fenn (1975). For most types of fogs and precipitation, it is a good approximation to assume that the particles consist of pure water with the appropriate index of refraction data from Table 1.2-2. For clouds, which consist of nuclei surrounded by condensed water, this assumption may not be valid. Severeal different compositions are modeled in the present study.

In the Mie scattering regime, scattering, absorption, and extinction coefficients and differential scattering cross sections are calculated using the code HSPHR developed by Ruck (1980). The code is restricted to spherical particles, but does have provisions for heterogeneous compositions in which a spherical nucleus of radius a_o and complex index of refraction n_o is surrounded by a second material having a concentric radius a and complex index of refraction n. The code was modified by the present author to allow modeling of dispersive particle distributions. Graphical plotting capabilities were also

Table 1.2-1. Particle Distribution Models and Observational Measurements

Haze	Elterman (1968) Shettle and Fenn (1975)
Fog	Bisyarin and Sokolov (1974) Bisyarin et al. (1978) Chýlek (1978) Eldridge (1966) Eldridge (1971) Garland (1971) Garland et al. (1973) Goodmann (1977) Kumai (1973) Kunkel (1971) Roach et al. (1976) Pilié et al. (1975) Pinnick et al. (1978) Pinnick et al. (1979) Tampieri and Tomasi (1976) Tomasi and Tampieri (1976)
Clouds	Bartlett and Jonas (1972) Carrier et al. (1967) Cohen (1975) Deirmendjian (1964) Deirmendjian (1969) Gates and Shaw (1960) Lewis (1951) McCartney (1976) Platt and Bartusek (1974) Platt (1976) Schickel (1972) Warner (1969) Warner (1973) Yamamoto et al. (1971)
Rain	Chu and Hogg (1968) Galakhov et al. (1976) Joss et al. (1968) Laws and Parsons (1943) List and Gillespie (1976) McTaggart-Cowan and List (1975) Rensch and Long (1970) Sokolov (1970) Takahashi (1978) Wang et al. (1979) Wilson and Penzias (1966)
Snow	Galakhov et al. (1976) Nakajima et al. (1973) Passarelli (1978) Sekhon and Srivastava (1970) Sokolov (1970) Wilson and Penzias (1966)

Table 1.2-2. Complex refractive indices (n=n'-ik) for characteristic components of aerosol particles [Nilsson (1979].

Wavelength (μm)	Water soluble fraction		Water insoluble fraction		Sea salt		Soot		Water	
0.2000	1.530	0 070	1.530	0.070	1.450	0.000			1.396	0.000
0.2500	1.530	0.030	1.530	0.030	1.450	0.000			1.362	0.000
0.3000	1.530	0.008	1.530	0.008	1.450	0.000			1.349	0.000
0.3371	1.530	0.005	1.530	0.008	1.450	0.000			1.345	0.000
0.4880	1.530	0.005	1.530	0.008	1.450	0.000	1.560	0.490	1.335	0.000
0.5145	1.530	0.005	1.530	0.008	1.450	0.000	1.560	0.490	1.334	0.000
0.5500	1.530	0.005	1.530	0.008	1.450	0.000	1.570	0.500	1.333	0.000
0.6328	1.530	0.006	1.530	0.008	1.450	0.000	1.570	0.480	1.332	0.000
0.6943	1.530	0.007	1.530	0.008	1.450	0.000	1.570	0.480	1.331	0.000
0.7000	1.530	0.007	1.530	0.008	1.450	0.000	1.570	0.480	1.331	0.000
0.8000	1.524	0.010	1.524	0.008	1.450	0.000	1.570	0.480	1.329	0.000
0.8600	1.520	0.012	1.520	0.008	1.450	0.000	1.580	0.490	1.329	0.000
0.9100	1.520	0.013	1.520	0.008	1.450	0.000	1.590	0.510	1.328	0.000
1.0600	1.520	0.017	1.520	0.008	1.450	0.000	1.610	0.540	1.326	0.000
1.1300	1.519	0.018	1.502	0.008	1.450	0.000	1.620	0.540	1.325	0.000
1.5360	1.510	0.023	1.400	0.008	1.450	0.000	1.660	0.570	1.318	0.000
1.7000	1.478	0.018	1.351	0.008	1.450	0.000	1.680	0.580	1.315	0.000
2.0000	1.420	0.008	1.260	0.008	1.450	0.000	1.720	0.600	1.306	0.001
2.1600	1.420	0.009	1.234	0.008	1.450	0.000	1.740	0.610	1.298	0.000
2.4000	1.420	0.011	1.196	0.009	1.450	0.000	1.770	0.620	1.279	0.001
2.5000	1.420	0.012	1.180	0.009	1.425	0.007	1.780	0.620	1.261	0.002
2.6000	1.410	0.034	1.180	0.011	1.414	0.009	1.790	0.610	1.242	0.003
2.7000	1.400	0.055	1.160	0.013	1.410	0.012	1.790	0.610	1.188	0.019
2.8000	1.407	0.044	1.173	0.013	1.418	0.014	1.800	0.610	1.142	0.115
2.9500	1.417	0.027	1.163	0.012	1.527	0.006	1.810	0.610	1.292	0.298
3.0000	1.420	0.022	1.160	0.012	1.607	0.005	1.820	0.600	1.371	0.272
3.1500	1.428	0.011	1.205	0.011	1.520	0.003	1.820	0.590	1.483	0.135
3.2000	1.430	0.008	1.220	0.010	1.509	0.002	1.820	0.590	1.478	0.092
3.3923	1.430	0.007	1.260	0.013	1.489	0.002	1.830	0.570	1.422	0.021
3.5000	1.450	0.005	1.280	0.011	1.485	0.002	1.830	0.570	1.400	0.009
3.7500	1.452	0.004	1.270	0.011	1.476	0.001	1.840	0.590	1.369	0.004
3.8000	1.453	0.004	1.268	0.011	1.474	0.001	1.840	0.590	1.364	0.003
4.0000	1.455	0.005	1.260	0.012	1.476	0.002	1.850	0.600	1.351	0.005
4.5000	1.460	0.013	1.260	0.014	1.486	0.004	1.850	0.580	1.332	0.013
4.7300	1.455	0.014	1.251	0.016	1.478	0.003	1.850	0.580	1.330	0.016
5.0000	1.450	0.016	1.240	0.018	1.465	0.003	1.850	0.570	1.325	0.012
5.3000	1.444	0.017	1.228	0.020	1.449	0.003	1.870	0.540	1.312	0.010
5.5000	1.440	0.018	1.220	0.021	1.439	0.003	1.900	0.530	1.298	0.012
5.9000	1.416	0.022	1.164	0.034	1.423	0.011	1.950	0.500	1.248	0.062
6.0000	1.410	0.023	1.150	0.037	1.429	0.015	1.960	0.490	1.265	0.107
6.2000	1.430	0.027	1.142	0.039	1.574	0.022	1.980	0.510	1.363	0.088
6.5000	1.460	0.033	1.130	0.042	1.479	0.005	2.000	0.540	1.339	0.039
7.0000	1.417	0.059	1.323	0.051	1.449	0.006	2.040	0.510	1.317	0.032
7.2000	1.400	0.070	1.400	0.055	1.439	0.008	2.060	0.520	1.312	0.032
7.9000	1.200	0.065	1.150	0.040	1.404	0.018	2.090	0.560	1.294	0.034
8.2000	1.010	0.100	1.130	0.074	1.413	0.022	2.120	0.630	1.286	0.035
8.5000	1.300	0.215	1.300	0.090	1.461	0.027	2.160	0.730	1.278	0.037
8.7000	2.400	0.290	1.400	0.100	1.566	0.029	2.190	0.820	1.272	0.038
9.0000	2.560	0.370	1.700	0.140	1.667	0.028	2.220	0.980	1.262	0.040
9.2000	2.200	0.420	1.720	0.150	1.627	0.026	2.230	1.070	1.255	0.042
9.5000	1.950	0.160	1.730	0.162	1.584	0.022	2.250	1.150	1.243	0.044
10.0000	1.820	0.030	1.750	0.162	1.534	0.016	2.300	1.290	1.218	0.051
10.5910	1.760	0.070	1.620	0.120	1.510	0.014			1.179	0.072
10.7000	1.749	0.065	1.620	0.116	1.506	0.014			1.172	0.078
11.0000	1.720	0.050	1.620	0.105	1.494	0.014			1.153	0.097
12.0000	1.670	0.053	1.545	0.103	1.466	0.015			1.111	0.199
12.4900	1.646	0.054	1.508	0.101	1.428	0.017			1.123	0.258
13.0000	1.620	0.055	1.470	0.100	1.412	0.019			1.146	0.305
14.8000	1.400	0.100	1.570	0.100	1.434	0.030			1.258	0.396
15.0000	1.420	0.200	1.570	0.100	1.440	0.032			1.270	0.402
17.2000	2.080	0.240	1.630	0.100	1.668	0.084			1.386	0.429
18.5000	1.850	0.170	1.648	0.120	1.737	0.113			1.443	0.421
19.5000	2.030	0.203	1.669	0.187	1.750	0.138			1.476	0.404
20.0000	2.120	0.220	1.680	0.220	1.747	0.149			1.480	0.393
25.0000	1.880	0.280	1.970	0.248	1.738	0.214			1.531	0.356
27.9000	1.840	0.290	1.890	0.320	1.744	0.251			1.549	0.339
30.0000	1.820	0.300	1.800	0.420	1.745	0.279			1.551	0.328
32.0000	1.860	0.340	1.840	0.452	1.741	0.383			1.546	0.324
35.0000	1.920	0.400	1.900	0.500	1.735	0.553			1.525	0.336
40.0000	1.860	0.500	2.100	0.600	1.707	0.000			1.519	0.385

added. Theoretical treatments of the Mie problem are well documented in the literature and will not be repeated here. The method adopted here is the classical numerical treatment given by van de Hulst (1964) and the interested reader is referred to this reference for further details. The code was checked against the concentric-sphere calculations of Kerker et al. (1962) with excellent numerical agreement.

For large particles, such that $2\pi a/\lambda >> 1$, a geometrical optics model may be used. Although the Mie program will work for large particles, it is unnecessary and wasteful of computer time since the time required per problem is proportional to $2\pi a/\lambda$. Hence, for most types of rain we can use the geometrical optics model as outline below.

The visibility or, more precisely, meteorological range as used in this study is defined by Koschmieder's relation

$$R_m = \frac{1}{\beta_{sc}} \ln \frac{1}{0.02} = \frac{3.912}{\beta_{sc}} \qquad (1)$$

where β_{sc} is the aerosol scattering coefficient at 0.55 μm, chosen because the peak sensitivity of the human eye occurs at this wavelength. The use of β_{sc} instead of β_{ex} (extinction coefficient) implies that the absorption coefficient (β_a) is small enough to neglect at visual wavelengths, a good assumption except for polluted air. From the foregoing relation, it is evident that the transmittance for a pth length equal to R_m is 0.02. Table 1.2-3 gives values of the meteorological range and scattering coefficient for the indicated meteorological

Table 1.2-3. International visibility code, meteorological range, and spectrally weighted scattering coefficient [McCartney (1977)].

Code no.	Weather condition	Meteorological range, R_m		Scattering coefficient, β_m (km^{-1})
		metric	English	
0	Dense fog	< 50 m	< 50 yd	> 78.2
1	Thick fog	50 m	50 yd	78.2
		200 m	219 yd	19.6
2	Moderate fog	200 m	219 yd	19.6
		500 m	547 yd	7.82
3	Light fog	500 m	547 yd	7.82
		1000 m	1095 yd	3.91
4	Thin fog	1 km	1095 yd	3.91
		2 km	1.1 nmi	1.96
5	Haze	2 km	1.1 nmi	1.96
		4 km	2.2 nmi	0.954
6	Light haze	4 km	2.2 nmi	0.954
		10 km	5.4 nmi	0.391
7	Clear	10 km	5.4 nmi	0.391
		20 km	11 nmi	0.196
8	Very clear	20 km	11 nmi	0.196
		50 km	27 nmi	0.078
9	Exceptionally clear	> 50 km	> 27 nmi	0.078
—	Pure air	277 km	149 nmi	0.0141 (β_m)

conditions. Also listed are the corresponding numbers of the International Visibility Code. The entries on the bottom line are for aerosol-free air and represent the effects of molecular scattering only. For earth's atmosphere, this represents an irreducible restriction on visibility. The corresponding value of β_m refers to air at standard conditions and is spectrally weighted for daylight within the visual spectrum.

Haze

The atmospheric transmission efficiency for hazy conditions was calculated using representative aerosol models selected from the work of Shettle and Fenn (1975). The vertical distribution of the aerosol extinction coefficient at 0.55 μm for the different models is shown in Figure 1.2-1. Between 2 and 30 km, where a distinction is made on a seasonal bases, the spring-summer conditions

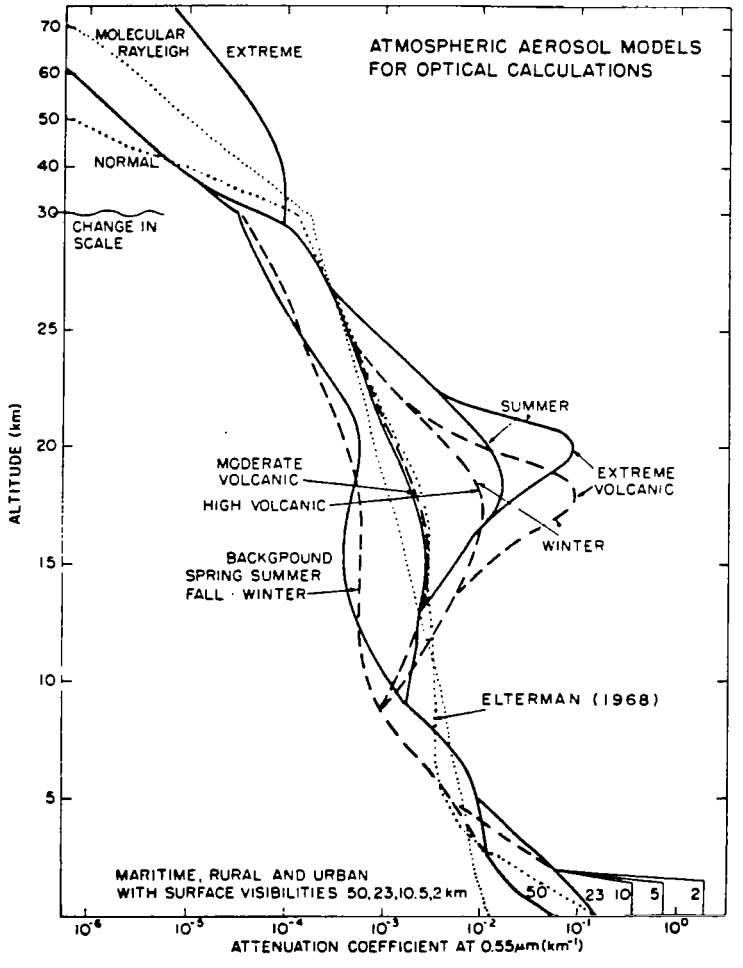

Figure 1.2-1. The vertical distribution of the aerosol extinction coefficients (at 0.55 μm) for the different models of Shettle and Fenn (1975).

are indicated by a solid line and fall-winter conditions by a dashed line. A computer code was written to calculate transmission efficiency for space-to-earth propagation to an elevation h given the wavelength λ, zenith angle θ, and surface visibility R_m. Calculations were performed for clear conditions (R_m = 23 km) and hazy conditions (R_m = 5 km) as shown in Figures 1.2-2 and 1.2-3, respectively. The solid curves denote $\theta = 0°$ and dashed curves are for $\theta = 50°$. The actual aerosol models employed for each atmospheric layer are given in the figure inserts. These curves show little fine structure as would be expected, since molecular absorption has been neglected. We can conclude that selection of a laser wavelength shorter than about 2 μm is undesirable for propagation through haze. Furthermore, Rayleigh (molecular) scattering becomes

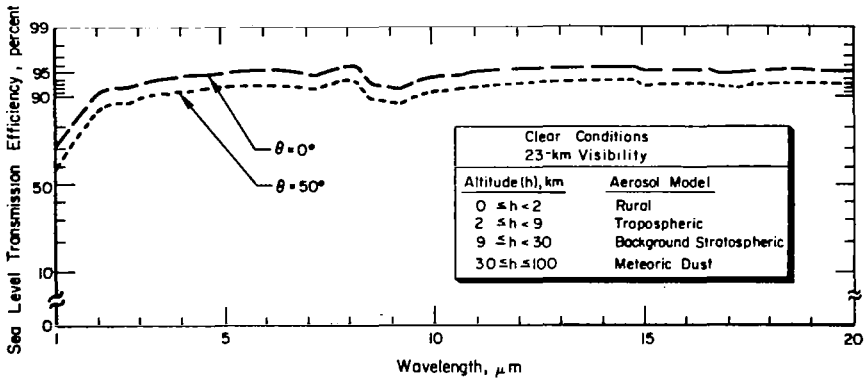

Figure 1.2-2. Transmission efficiency for space-to-earth propagation to sea level under clear atmospheric conditions (R_m = 23 km). Molecular absorption is omitted to permit consideration of aerosol extinction alone.

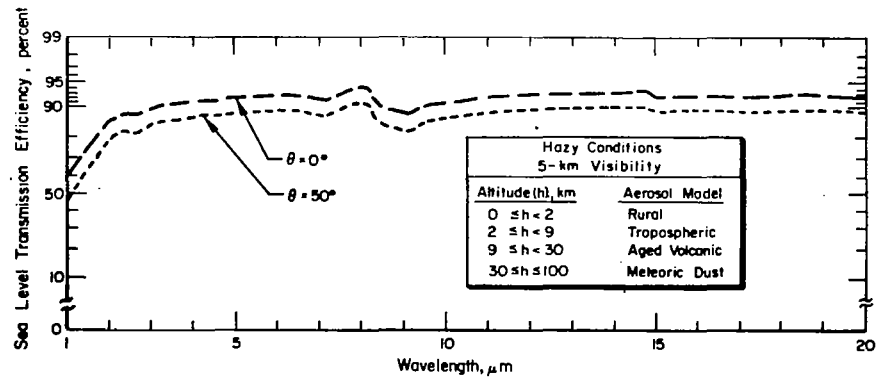

Figure 1.2-3. Transmission efficiency for space-to-earth propagation to sea level under hazy atmospheric conditions (R_m = 5 km). Molecular absorption is omitted to permit consideration of aerosol extinction alone.

significant at shorter wavelengths, scaling as λ^{-4}, and visible lasers would suffer attenuation due to this mechanism as well as because of haze aerosol extinction.

The transmission efficiency as a function of altitude for propagation at a zenith angle of 50° under clear and hazy conditions is shown in Figure 1.2-4. Clearly, receptor siting at elevations $h \gtrsim 1$ km is desirable to partially mitigate the effects of haze. Thus, siting in basin or valley areas subject to weather inversions is undesirable, especially if the site is subject to urban pollution.

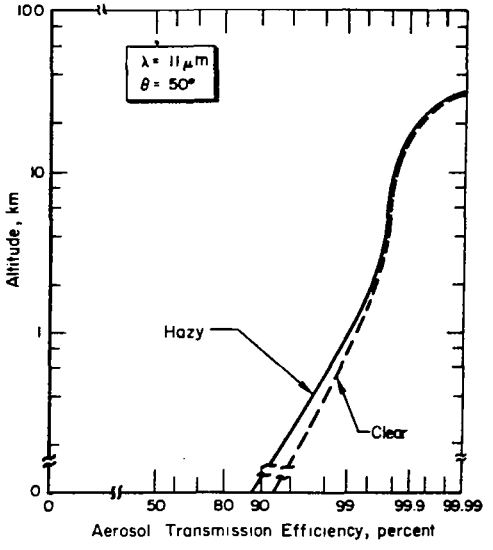

Figure 1.2-4. Space-to-earth transmission efficiency at 11 μm as a function of elevation for a 50° zenith angle (aerosol extinction only).

Fog

It has been recently shown [Chýlek (1978); Pinnick et al. (1979)] that a linear relationship, independent of the form of the size distribution, exists between infrared extinction and liquid water content of fogs under many conditions. The relation is given by

$$\beta_{ex} = \frac{3\pi c}{2\rho\lambda} W, \tag{2}$$

where W is the liquid water content, ρ is the density of water, and c is the slope of a straight line that approximates the Mie extinction efficiency curve $Q_{ex}(\chi,\lambda)$ by

$$Q_{ex}(\chi,\lambda) \simeq c(\lambda) \tag{3}$$

where $\chi = 2\pi a/\lambda$ is the size parameter. The approximately linear relation between Q_{ex} and χ holds below some cutoff value χ_m, and as long as a significant fraction of the particle distribution curve has $\chi \leq \chi_m$, then relation (2) is a good approximation. Now χ_m is largest for λ = 10-11 μm and, thus, many

fog distributions obey relation (2) using $c \simeq 0.3$ with good accuracy. The largest χ_m corresponds to a_m = 14 μm; either above or below λ = 10-11 μm, χ_m and, hence, a_m are smaller, placing greater restrictions on the fog distributions for which relation (2) is applicable. In a similar manner, the absorption coefficient β_a can be related to liquid water content, although the numerical values of c and χ_m are different.

Rather than using Eq. (2) in the present study, we have taken the Mie calculations of Pinnick et al. (1979) for four liquid water contents and replotted the extinction and absorption data as functions of wavelength. The fog measurements judged to be reliable were chosen to represent a wide range of conditions ranging from maritime and continental advection fogs [Kumai (1973); Kunkel (1971); and part of Garland's (1971) work] to inland radiation fogs [Garland (1971); Garland et al. (1973); Roach et al. (1976); Pinnick et al. (1978)]. These calculations are shown in Figures 1.2-5 through 1.2-8. Error bars, if used, simply denoted the range of calculated β_{ex} and β_a for the various size distributions given by the respective authors.

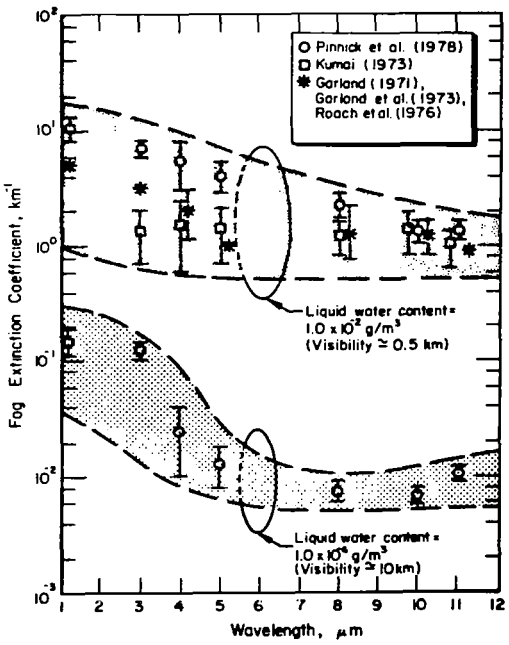

Figure 1.2-5. Calculated extinction coefficients for Code 2 and Code 6 fogs.

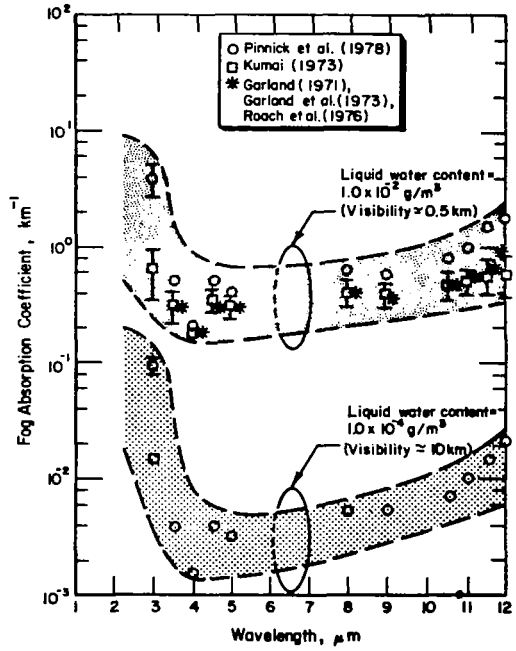

Figure 1.2-6. Calculated absorption coefficients for Code 2 and Code 6 fogs.

These figures show that laser operation at a wavelength around 11 μm may be effective in partially mitigating the effects of light fog as has been confirmed experimentally [Chu and Hogg (1968); Rensch and Long (1970)]. The minimum scatter in these data around 11 μm is in conformance with the fact that χ_m is largest in this vicinity and the explicit details of the size distributions have less influence on β_{ex}. As the water content increases, accompanied

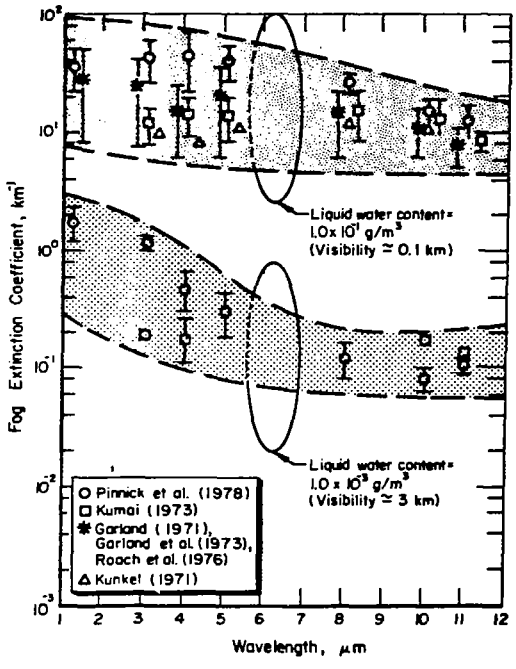

Figure 1.2-7. Calculated extinction coefficient for Code 1 and Code 5 fogs.

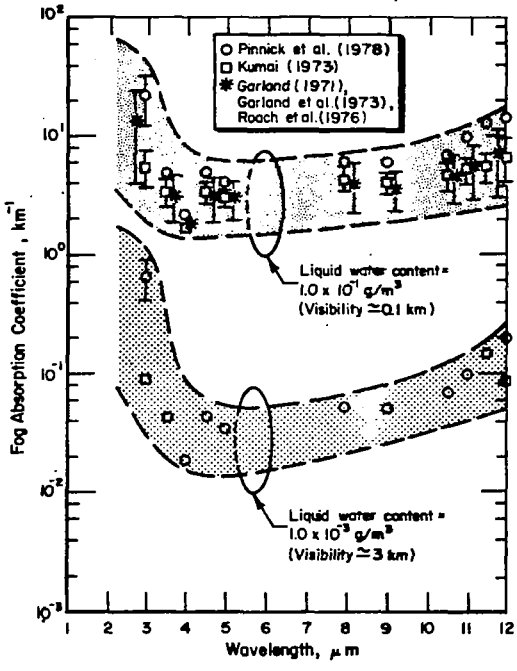

Figure 1.2-8. Calculated absorption coefficients for Code 1 and Code 5 fogs.

by a decrease in visibility, the minimum in β_{ex} near 11 μm disappears and the extinction coefficient is nearly flat with wavelength. Note that before transmission efficiency calculations can be performed for various fog conditions, forward scattering corrections must be made to the extinction coefficients. Hence, use of the present coefficients in the Beer-Lambert transmission law would result in an over-estimation of the beam attenuation.

In addition, fog banks are not homogeneous and may display considerable vertical structure. The trend toward increasing concentration of larger droplets with increasing altitude found by Pinnick et al. (1978) for inland radiation fogs near Grafenwöhr, West Germany is in agreement with measurements of advection fogs over San Francisco by Goodman (1977) for fogs in the Chemung River Valley in New York, show directly contradictory behavior. Clearly, average fog bank properties must be adopted for the present study.

Clouds

Because many of the candidate receptor sites are subject to extended periods of cloudiness, these meteorological formations may be responsible for the greatest decrease in power availability. The wide variety of cloud types (Table 1.2-4), taken with the difficulties inherent in determining statistical information related to cloud thickness and receptor obscuration frequency, make any calculation of transmission efficiency and power availability subject to a large error. Guidelines for this evaluation are developed in the section describing the power availability model; for the present purpose, however, we

Table 2.1-4. Principal classes and descriptions of clouds [McCartney (1971)].

Cloud type	Abbreviation	Description	In temperate regions: Height range	In temperate regions: Temperature range	Type of vertical air motion
		I. Stratiform or layer clouds			
High-level clouds					
Cirrus	Ci	Detached clouds composed of delicate white fibers and appearing in tufts, streaks, trails, feather plumes, or bands	Above 20,000 ft	Below −25 °C	Widespread, prolonged and regular ascent with vertical velocities of typically 5–10 cm sec^{-1}
Cirrocumulus	Cc	A dappled layer or patch of cloud forming among cirrus. Composed of small white flakes or very small globules arranged more or less regularly in groups or lines, or more often as ripples resembling those of sand on the seashore			
Cirrostratus	Cs	A fused sheet of cirrus cloud which does not obscure the sun or moon, but gives rise to halos. Sometimes it appears as a diffuse white veil across the sky			
Medium-level clouds					
Altostratus	As	A grey striated or fibrous veil, like thick Cs but without halo phenomena, through which the sun is seen only as a diffuse bright patch or not at all	7000–20,000 ft	0 to −25 °C	
Altocumulus	Ac	A dappled layer or patch of cloud composed of flattened globules which may be arranged in groups, lines, or waves collectively known as billows			

Table 1.2-4 (Continued)

Cloud type	Abbreviation	Description	In temperate regions: Height range	In temperate regions: Temperature range	Type of vertical air motion
Low-level clouds					
Stratocumulus	Sc	A layer of patches composed of laminae or globular masses arranged in groups, lines, or waves and having a soft, grey appearance. Very often the rolls are so close together that their edges join and give the undersurface a wavy character. Stratocumulus (cumulogenesis) is formed by the spreading out of the tops of cumulus clouds, the latter having disappeared	Below 7000 ft	Usually warmer than −5 °C	Widespread irregular stirring with vertical velocities usually less than 10 cm sec^{-1}
Stratus	St	A uniform, featureless layer of cloud resembling fog but not resting on the ground. When this very low layer is broken up into irregular shreds it is designated fractostratus	Usually within 1000 or 2000 ft of the ground	—	Widespread irregular stirring and lifting of a shallow layer of cool, damp air formed near the ground
Nimbostratus	Ns	An amorphous, dark gray, rainy cloud layer reaching almost to the ground		As for St	Widespread regular ascent with vertical velocities of 20 cm sec^{-1}
		II. Cumuliform or heap clouds			
Clouds with marked vertical development					
Cumulus	Cu	Detached, dense, clouds with marked vertical development; the upper surface is dome-shaped with sharp-edged rounded protuberances, while the base is nearly horizontal	Extend from 2000 to 20,000 ft or more	—	Convective motion in which large bubbles of warm air rise with vertical speeds of 1–5 m sec^{-1}

Table 1.2-4 (Concluded)

Cumulonimbus	Cb	Heavy masses of dense cloud, with great vertical development, whose cumuliform summits rise in the forms of towers, the upper parts having a fibrous texture and often spreading out into the shape of an anvil. These clouds generally produce showers of rain and sometimes of snow, hail or soft hail, and often develop into thunderstorms	May extend up to 40,000 ft	Summits may be as cold as −50 °C	Strong convective motions with vertical upcurrents of 3 to more than 30 m sec^{-1}
		III. Special types of cloud			
Fracto clouds: fracto-cumulus, fractostratus, fractonimbus		Fragments of low cloud associated with cumulus, stratus, or nimbostratus, as the case may be	—	—	Indeterminate
Castellanus	Ac-cas	Miniature turreted heap clouds forming at medium levels usually in lines. In summer they are symptomatic of the approach of thundery weather		As for Ac	Convective motions released at middle levels by the slow lifting of unstable air often ahead of cold fronts
Orographic clouds: Lenticular and wave clouds		When air is forced to ascend a hill or mountain barrier, a smooth, lens-shaped cloud with well-defined edges may form over the summit. This is a lenticular cloud. If the air flow is set into oscillation by the hill, a succession of such clouds may form in the crests of the stationary waves produced in the lee of the mountain. These are designated wave clouds	—	—	The upcurrents in these clouds are usually quite strong—of order 1–10 m sec^{-1}

wish to examine the effects of the choice of wavelength on the absorption and scattering coefficients.

Using size distribution data given by the references in Table 1.2-1 as input to the Mie scattering code HSPHR, β_a, β_{sc}, and β_{ex}, and the forward and backward angular scattering coefficients, k_f and k_b, were calculated for all of the middle- and low-level cloud types in Table 1.2-4. Two particle compositions were modeled: (1) homogeneous particle polydispersions of pure water, and (2) heterogenerous particle polydispersions consisting of nuclei of fixed radius a_o surrounded concentrically by liquid water. Hence, the thickness of the liquid water shell varies according to the particle size distribution while the diameter of the nuclei remains constant. Nuclei models used in the heterogeneous aerosol calculations were taken from Nilsson (1979) and their parameters are given in Table 1.2-5. There are many different processes which generate the aerosol particles comprising cloud nuclei. Each generating process, called a "mode," produces particles of a certain chemical composition within a limited size range. Continental air masses are seldom characterized by a single mode but, because of mixing, different air masses have different proportions of the various modes. Each mode type can be described by a long-normal particle size distribution; because of the paucity of definitive data on cloud-nuclei size distributions, however, we adopted the simpler approach of a constant-radius nucleus specified by the representative mode radius given by Nilsson (1979).

Table 1.2-5. Nuclei models used in the heterogeneous aerosol calculations.

Aerosol description	Type*	Nuclei radius (a_o), μm	Mass fractions	
			Water soluble	Water insoluble
Nuclei mode	1	0.015	0.8	0.2
Accumulation mode				
Rural, average	2	0.05	0.7	0.3
Normal, mode average	3	0.1	0.8	0.2
Coarse particle mode				
Normal, mode average	5	2.0	0.4	0.6

*According to the classification proposed by Nilsson (1979).

Comparisons were made between homogeneous (water mode) and heterogeneous particle models for two cloud types, cumulus and cumulonimbus, which are representative of cloud distributions having only small particles ($a < 20$ μm) and those having a significant fraction of larger particles with $a > 20$ μm. The wavelength dependencies of the absorption and extinction coefficients for the various modes are shown in Figures 1.2-9 through 1.2-12 and Figures 1.2-13 through 1.2-15 for the cumulus and cumulonimbus distributions, respectively. The presence of nuclei strongly influences the behavior at shorter wavelengths, whereas negligible differences exist between calculated coefficients at wavelengths longer than about 5 μm. The extinction coefficient as a function of wavelength for $\lambda \lesssim 9$ μm is relatively constant for homogeneous (water mode) particle calculations. For particle distributions with small-diameter nuclei,

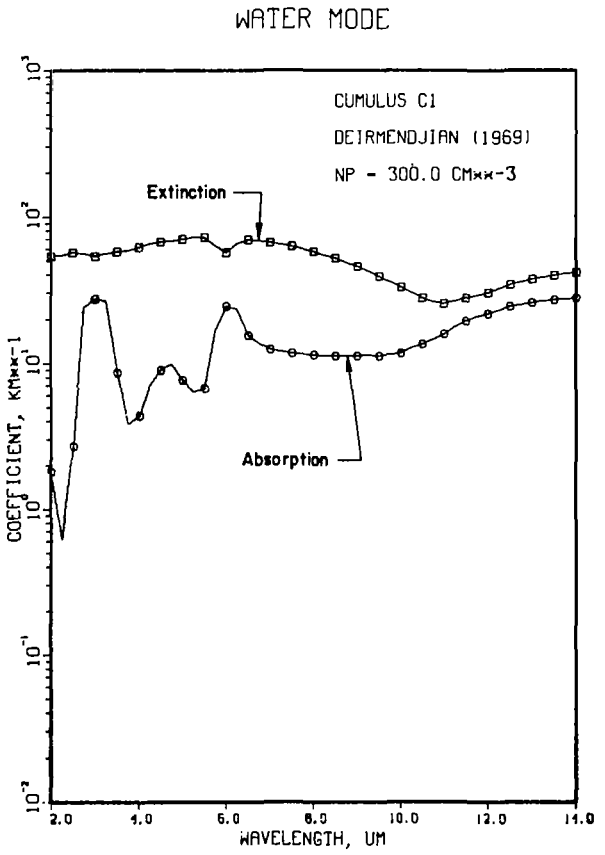

Figure 1.2-9. Cumulus C1 extinction and absorption coefficients calculated using the water mode particle model.

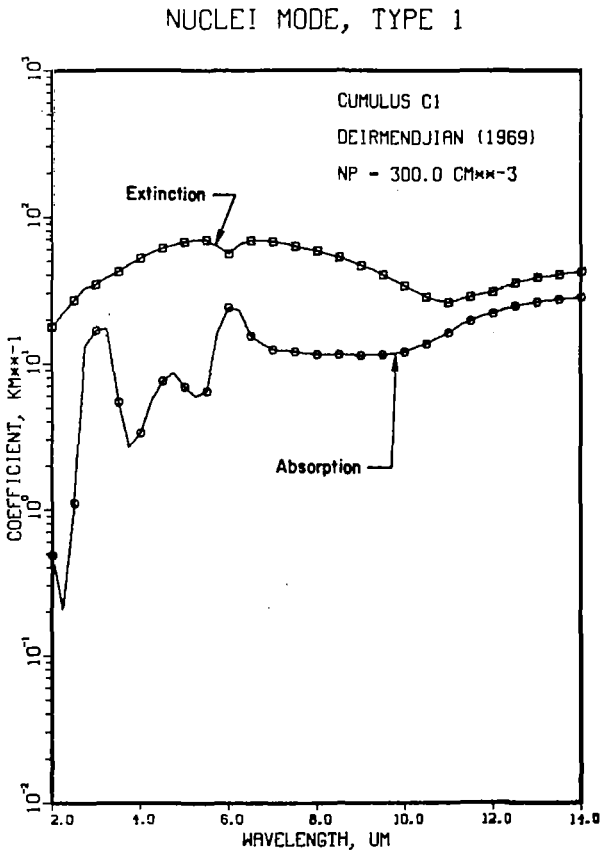

Figure 1.2-10. Cumulus C1 extinction and absorption coefficients calculated using the nuclei mode (Type 1) particle model.

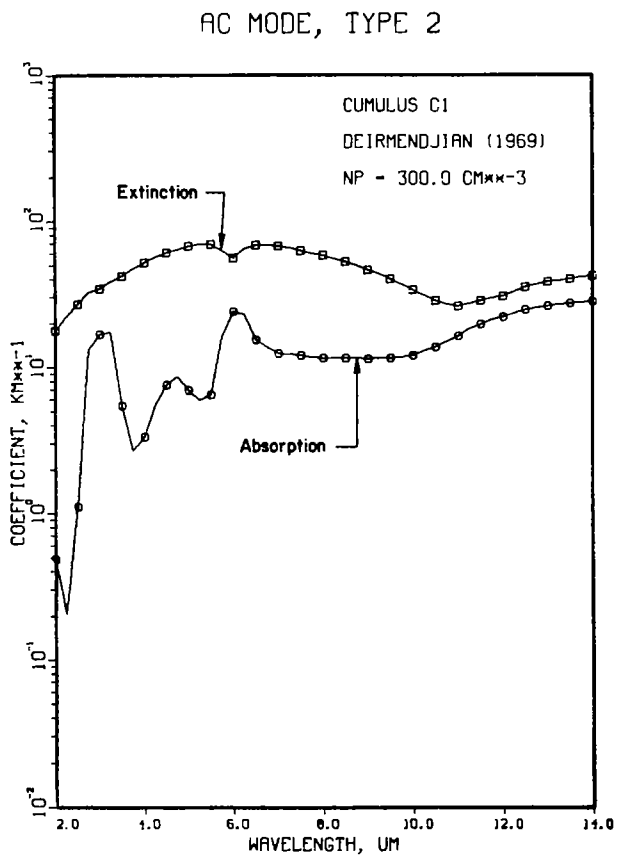

Figure 1.2-11. Cumulus C1 extinction and absorption coefficients calculated using the accumulation mode (Type 2) particle model.

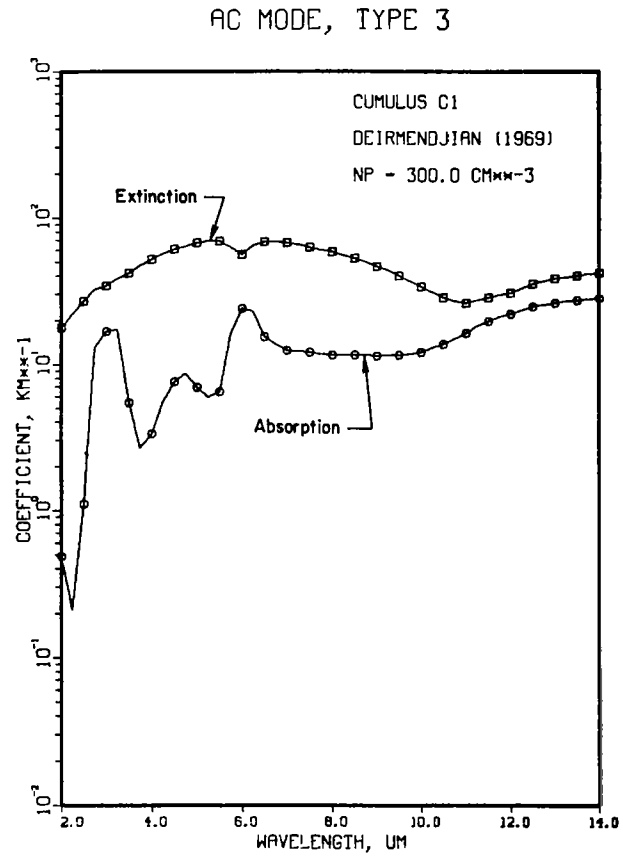

Figure 1.2-12. Cumulus C1 extinction and absorption coefficients calculated using the accumulation mode (Type 3) particle model.

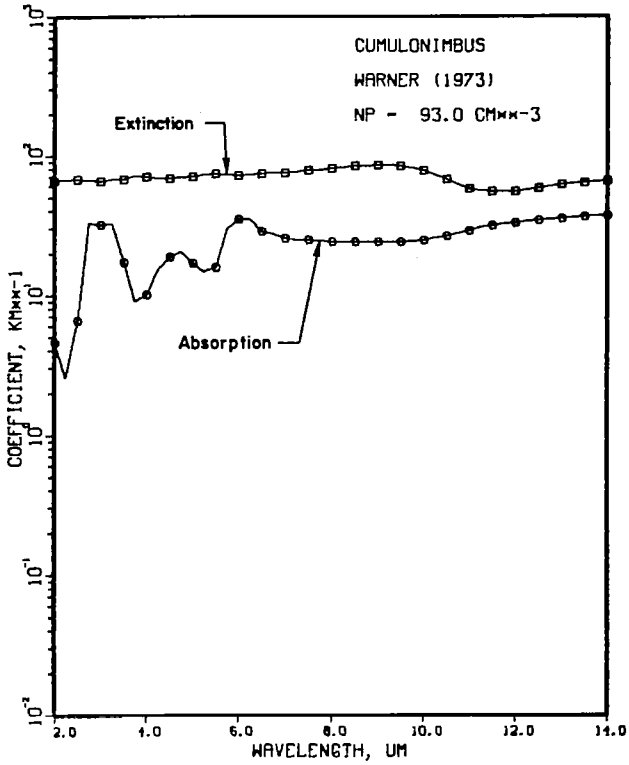

Figure 1.2-13. Cumulonimbus extinction and absorption coefficients calculated using the water mode (Type 1) particle model.

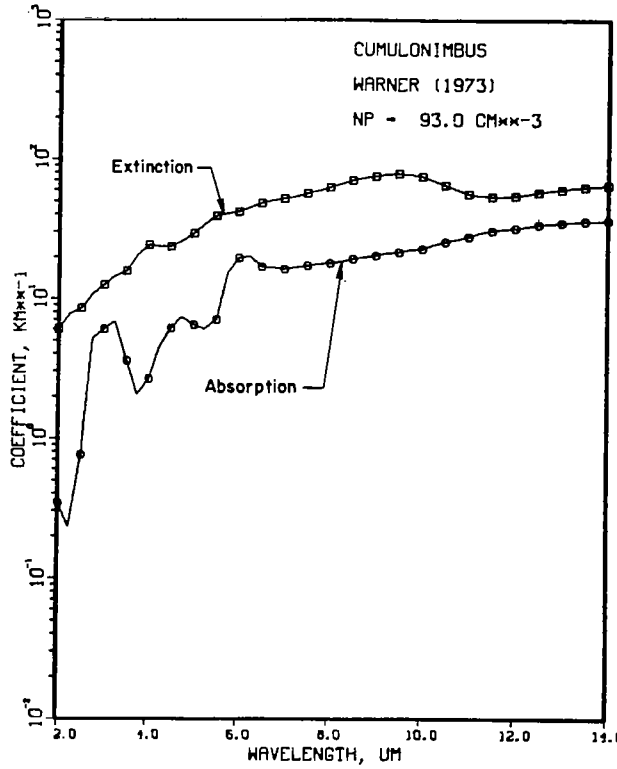

Figure 1.2-14. Cumulonimbus extinction and absorption coefficients calculated using the accumulation mode (Type 3) particle model.

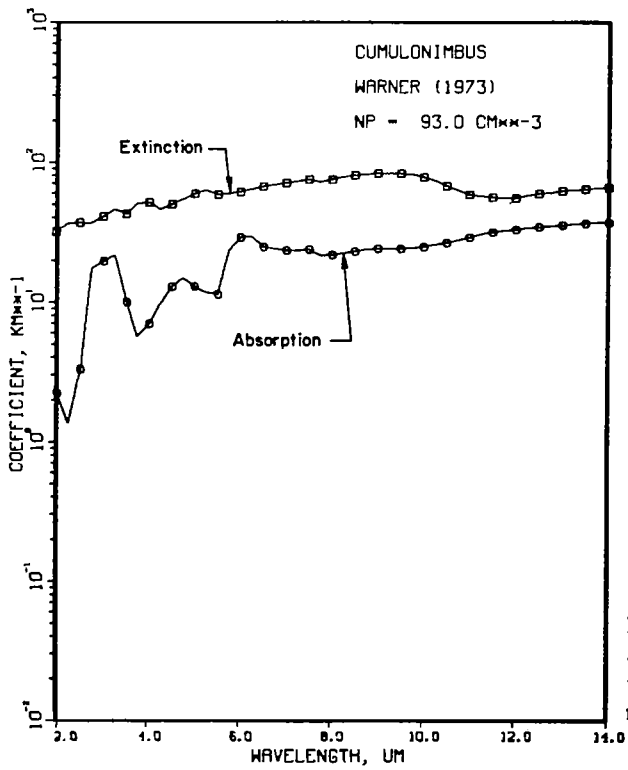

Figure 1.2-15. Cumulonimbus extinction and absorption coefficients calculated using the coarse particle mode (Type 5) model.

however, the extinction coefficient decreases with decreasing wavelength for $\lambda < 5$ μm. When the nuclei diameter increases, as with the coarse particle mode, the extinction coefficients at these shorter wavelengths increase in magnitude. Comparison of these results with other published Mie calculations of heterogeneous aerosols is impossible because others [Nilsson (1979); Prishivalko and Astaf'yeva (1974)] did not consider specific cloud distributions. We note that observational measurements do not show a decrease in β_{ex} with decreasing wavelength as predicted by the accumulation mode, which may result from certain experimental anomalies or, more likely, from the assumption in the present models, e.g., use of constant-diameter nuclei. In particular, the particle size distribution for $a < 2$ μm is not well defined due to the lack of adequate *in situ* measurement techniques. Since such small particles largely determine the absorption/scattering behavior at shorter wavelengths, calculational errors may be significant.

Because of the uncertainties inherent in the heterogeneous particle models (especially at shorter wavelengths), we have performed calculations for all remaining low- and medium-level clouds using the water mode. The assumption that cloud particles are homogeneous and composed entirely of pure water is perfectly acceptable in the middle- and far-infrared spectral regions and is subject to error only for UV, visible, and near-infrared wavelengths.

Particle size distributions taken from the work of Carrier (1967), representative of many of the cloud types modeled here, are shown in Figure 1.2-16.

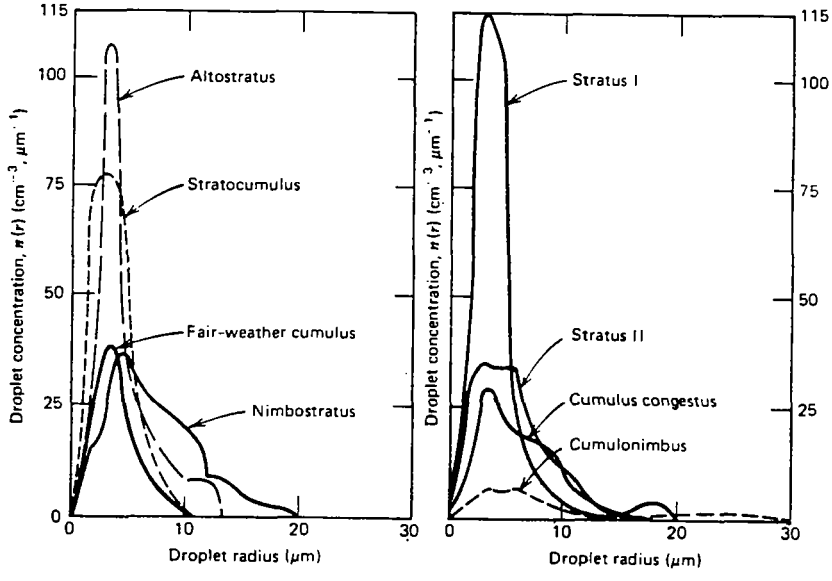

Figure 1.2-16. Representative particle size distribution for various cloud types [Carrier (1967)].

All distirbutions were divided into as many as 20 bins for numerical input to the code, and the wavelength interval from 2 μm to 14 μm was spanned in 0.25-μm increments. Calculational results for all cloud types are shown in Figures 2.1-17 through 2.1-28. Water mode calculations were checked for numerical

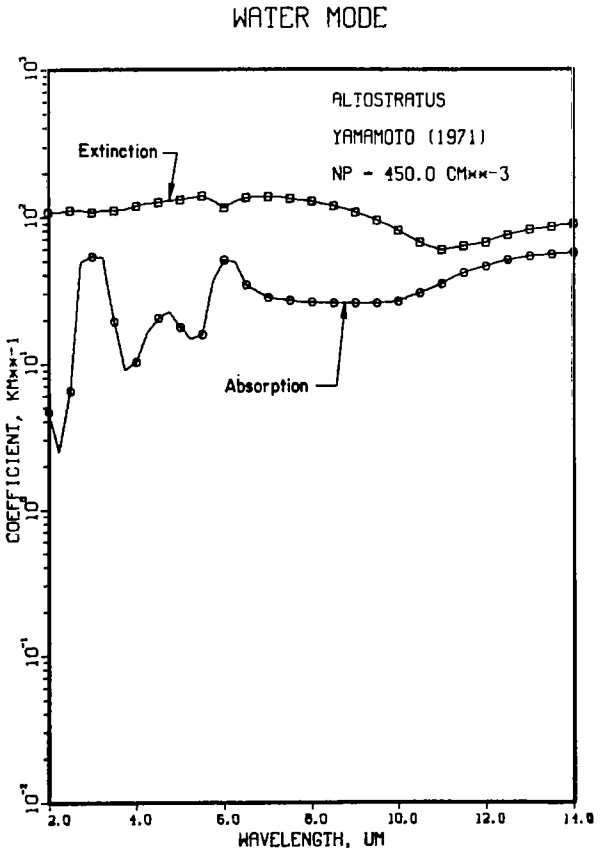

Figure 1.2-17. Altostratus extinction and absorption coefficients.

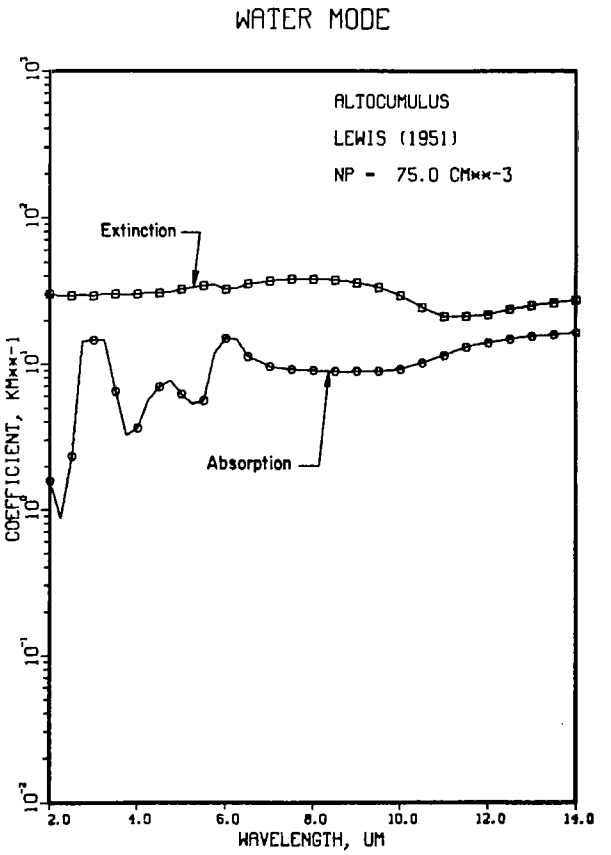

Figure 1.2-18. Altocumulus extinction and absorption coefficients.

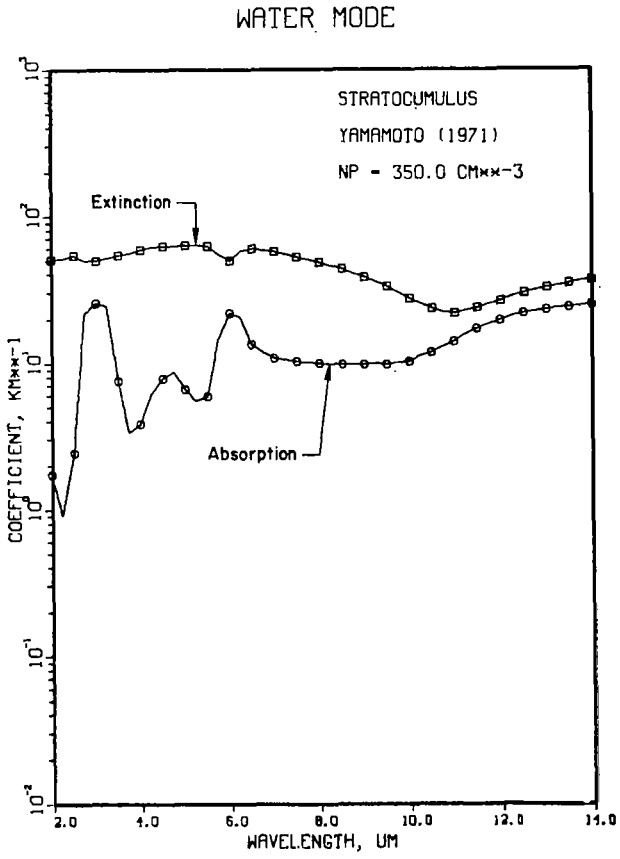

Figure 1.2-19. Stratocumulus extinction and absorption coefficients.

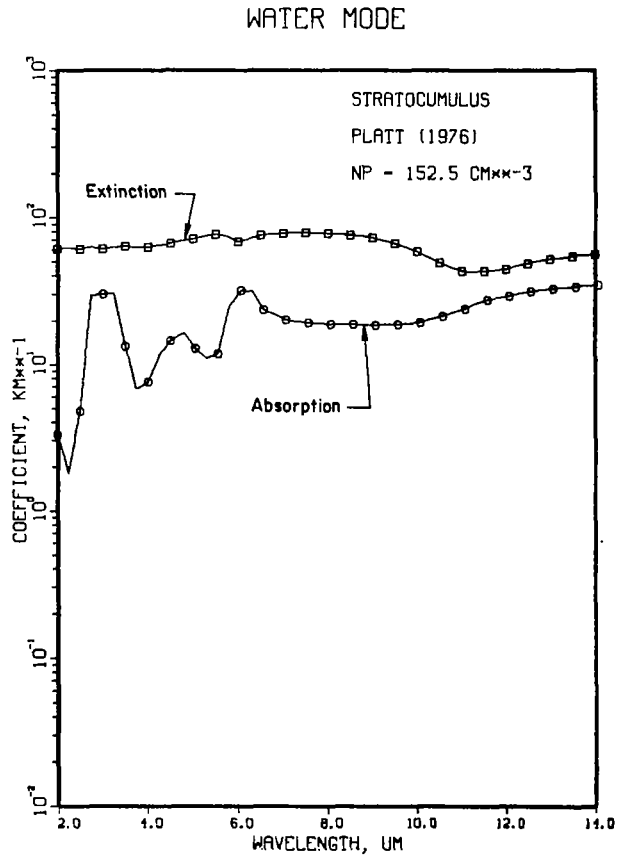

Figure 1.2-20. Stratocumulus extinction and absorption coefficients.

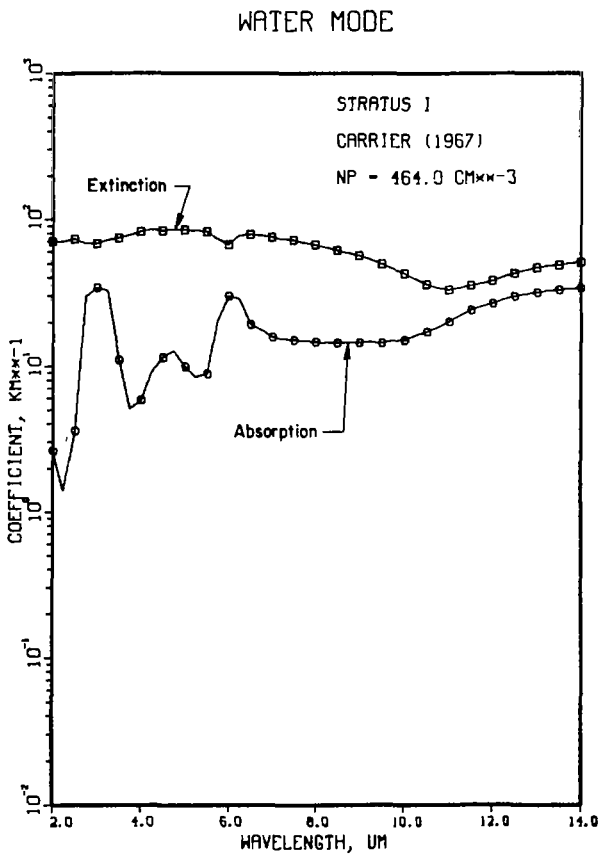

Figure 1.2-21. Stratus (Distribution 1) extinction and absorption coefficients.

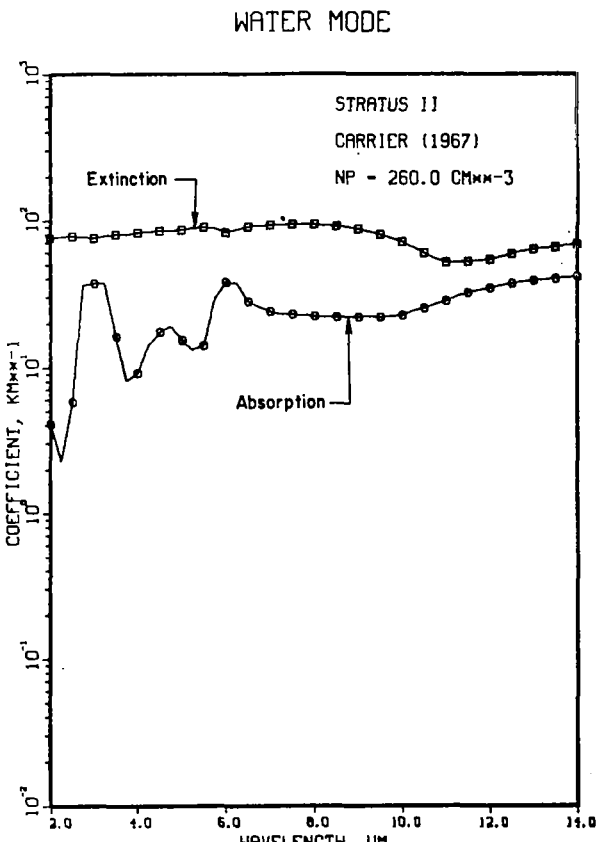

Figure 1.2-22. Stratus (Distribution 2) extinction and absorption coefficients.

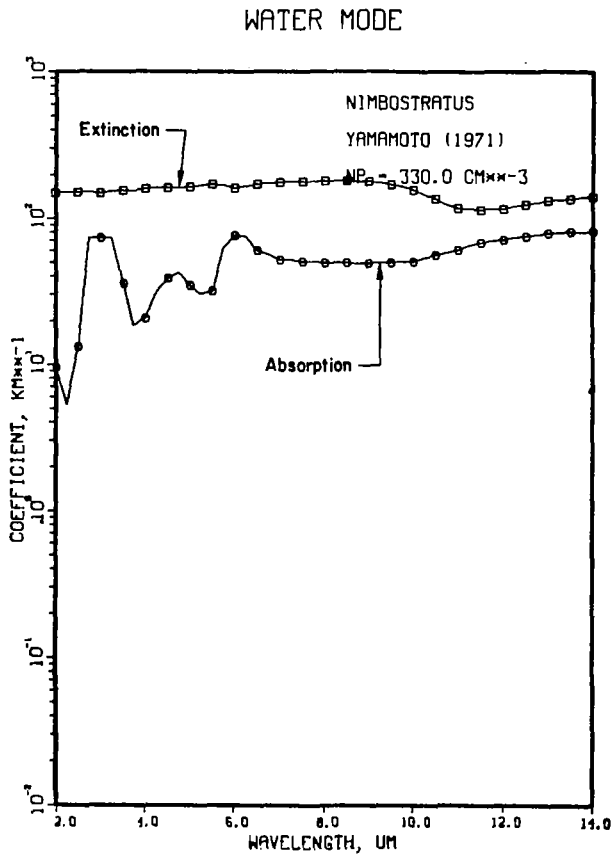

Figure 1.2-23. Nimbostratus extinction and absorption coefficients.

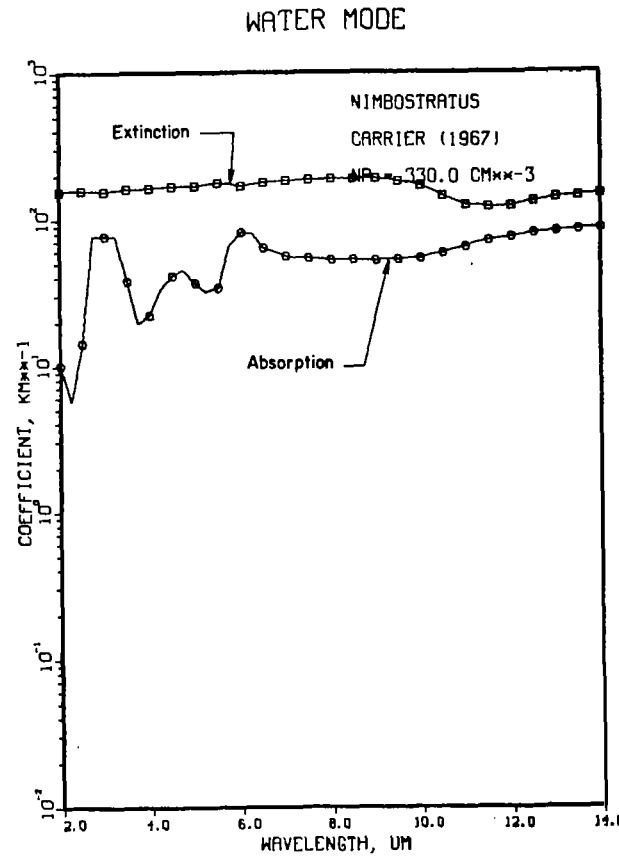

Figure 1.2-24. Nimbostratus extinction and absorption coefficients.

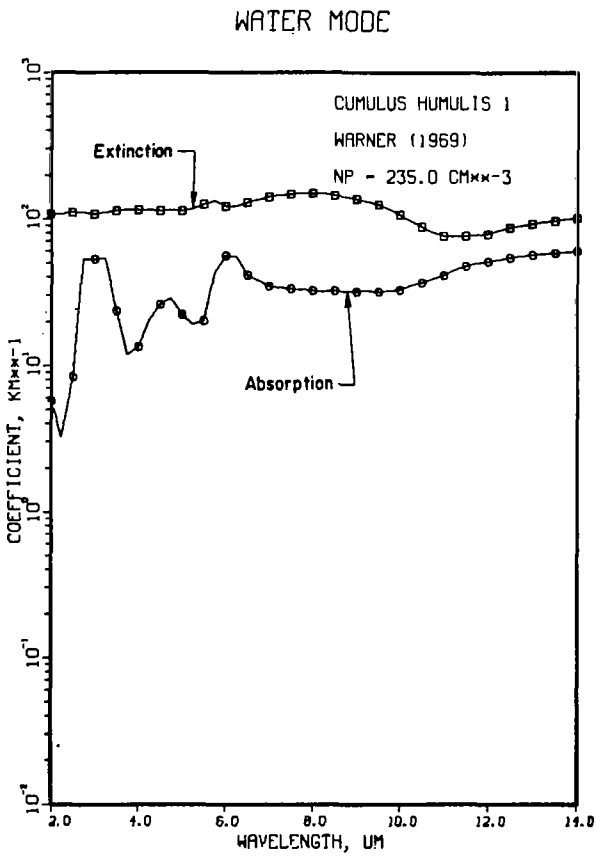

Figure 1.2-25. Cumulus humulis (Distribution 1) extinction and absorption coefficients.

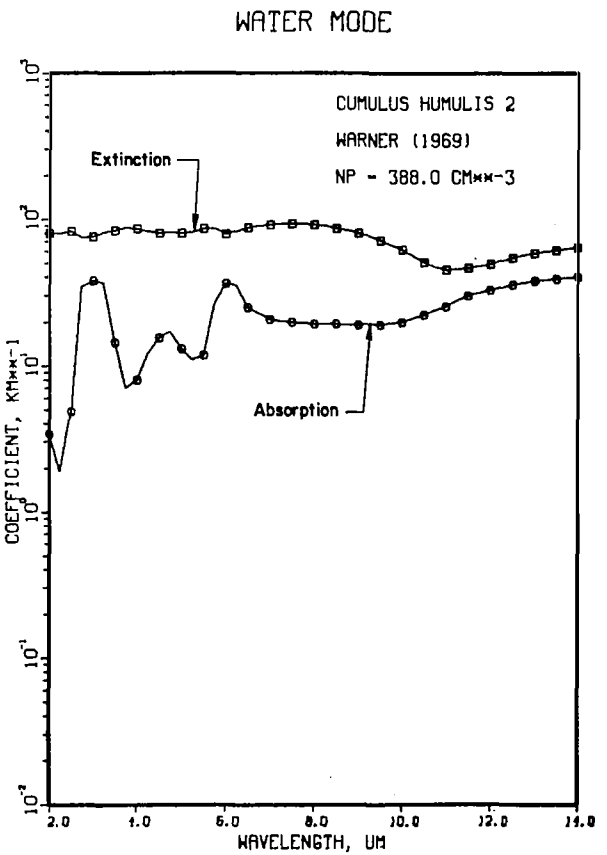

Figure 1.2-26. Cumulus humulis (Distribution 1) extinction and absorption coefficients.

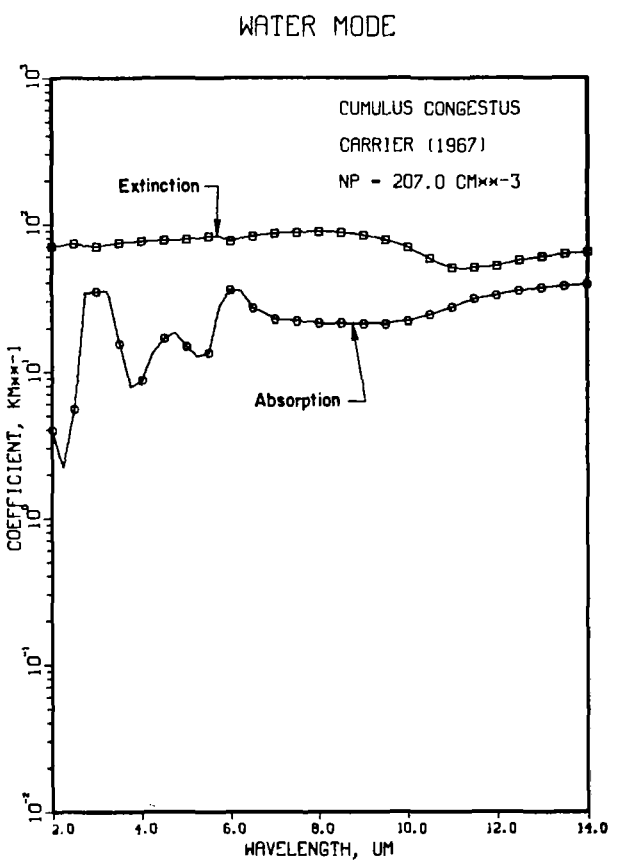

Figure 1.2-27. Cumulus congestus extinction and absorption coefficients.

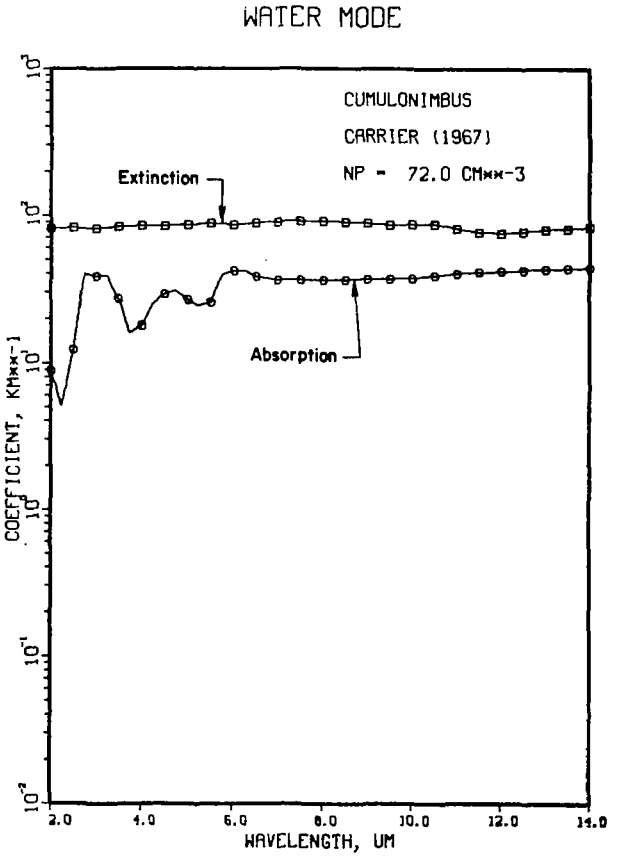

Figure 1.2-28. Cumulus congestus extinction and absorption coefficients

accuracy by using the particle distributions of Yamamoto et al. (1971), as shown in Figure 1.2-29, and comparing our results (Figures 1.2-17, 1.2-19, and 1.2-23) with published results (Figure 1.2-30). The agreement is excellent.

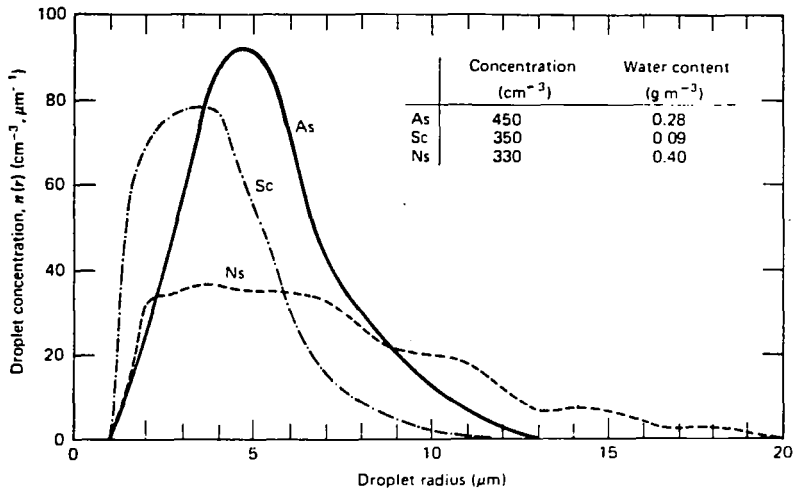

Figure 1.2-29. Altostratus, stratocumulus, and nimbostratus particle size distributions used by Yamamoto et al. (1971).

As noted by Ruppersberg et al. (1975), a significant reduction in β_{ex} occurs around 11 μm for clouds in which the large-particle distribution decays more rapidly than a^{-2}. This effect is particularly noticeable in calculations for altostratus, stratocumulus, and stratus clouds (Figures 1.2-17, 1.2-19, and 1.2-21). Clouds characterized by a greater proportion of larger particles, e.g., nimbostratus and cumulonimbus (Figures 1.2-13, 1.2-23, 1.2-24, and 1.2-28) show little improvement in β_{ex} at 11 μm. Alternately, operation at a laser wavelength near 2.25 μm may offer improved transmission through thin clouds because of the minimum in β_a. Operation at even shorter wavelengths is undesirable because of the increased attenuation due to haze and molecular scattering. Tabulated absorption and extinction coefficients for the two spectral windows of interest are given in Table 1.2-6. Calculated coefficients for different particle size distributions of the same cloud type are denoted by a range of values. Although these coefficients are representative for the various cloud types, statistical variations in the particle distributions and concentrations can result in up to a factor of 3 difference in the predicted value. For example, particle concentrations for cumulus clouds range from about 100 cm^{-3} to greater than 400 cm^{-3}.

All of the thicker cloud types (especially cumuliform types) are highly attenuating and are impenetrable unless hole boring at very high intensities is employed. Those cloud types which are characteristically thinner, such as middle and stratiform types, can be partially transparent, as shown by the observational measurements cited in Table 1.2-7.

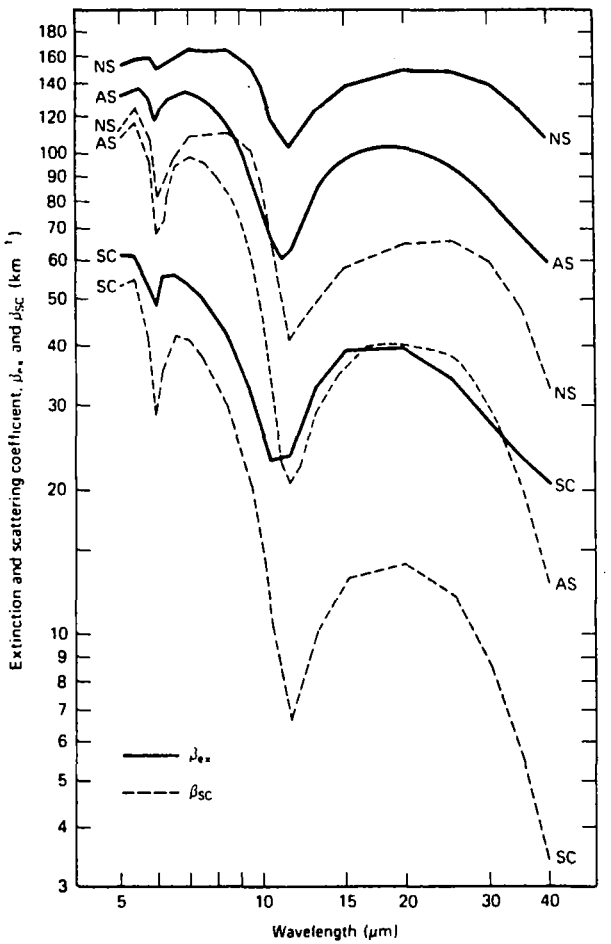

Figure 1.2-30. Calculated extinction and scattering coefficients for altostratus, stratocumulus, and nimbostratus clouds [Yamamoto et al. (1971)].

Table 1.2-6. Calculated absorption (β_a) and extinction (β_{ex}) coefficients for middle- and low-level clouds.

	λ = 2.25 μm		λ = 11.0 μm	
Cloud type	β_a, km^{-1}	β_{ex}, km^{-1}	β_a, km^{-1}	β_{ex}, km^{-1}
As	2.47×10^{0}	1.07×10^{2}	3.49×10^{1}	5.97×10^{1}
Ac	8.59×10^{-1}	2.91×10^{1}	1.13×10^{1}	2.12×10^{1}
Sc	$(0.89\text{-}1.80)\times10^{0}$	$(5.11\text{-}6.20)\times10^{1}$	$(1.38\text{-}2.33)\times10^{1}$	$(2.19\text{-}4.30)\times10^{1}$
St	$(1.38\text{-}2.26)\times10^{0}$	$(7.03\text{-}7.70)\times10^{1}$	$(2.01\text{-}2.84)\times10^{1}$	$(3.32\text{-}5.24)\times10^{1}$
Ns	$(5.28\text{-}5.63)\times10^{0}$	$(1.52\text{-}1.57)\times10^{2}$	$(6.12\text{-}6.46)\times10^{1}$	$(1.18\text{-}1.26)\times10^{2}$
Cu humulis	$(0.63\text{-}3.21)\times10^{0}$	$(0.55\text{-}1.07)\times10^{2}$	$(1.62\text{-}4.50)\times10^{1}$	$(2.51\text{-}7.67)\times10^{1}$
Cu congestus	2.16×10^{0}	7.15×10^{1}	2.71×10^{1}	5.06×10^{1}
Cb	$(2.54\text{-}5.03)\times10^{0}$	$(6.67\text{-}8.17)\times10^{1}$	$(2.89\text{-}4.02)\times10^{1}$	$(5.77\text{-}8.19)\times10^{1}$

Table 1.2-7. Observed 2- and 11-μm transmissivities for selected optically thin clouds at lower altitudes.

Cloud category	Type	Thickness	Transmissivity		Reference
			λ ≈ 2 μm	λ ≈ 11 μm	
Middle	As	1.8 km	--	0.14	Platt and Bartusek (1974)
	As translucidus	unknown	≈ 0.45	≈ 0.40	Guzzi et al. (1974)
	Ac	0.25-1.6 km	--	0.14-0.97	Platt and Bartusek (1974)
	Ac floccus	thin (?)	≈ 0.85	--	Guzzi et al. (1974)
Stratiform	St translucidus	unknown	≈ 0.50	≈ 0.45	Guzzi et al. (1974)
	St fractus	unknown	≈ 0.65	≈ 0.75	Guzzi et al. (1974)

Calculation of the transmission efficiency through such formations should use forward-scattering corrections since Mie scattering from cloud particles is predominately in a forward direction. While this correction may result in a change in the transmission efficiency of perhaps 20%, this effect is unimportant compared with statistical uncertainties inherent in the power availability model. Because the cloud transmission models described later bound the range of expected behavior by estimating average cloud transmissivities as a function of total sky cover, such detailed propagation calculations are unwarranted.

For completeness, illustrative forward and backward scattering coefficients as functions of wavelength are shown in Figures 1.2-31 and 1.2-32. Differential scattering coefficients for the cumulus C1 distribution are shown in Figure 1.2-33 for a wavelength of 11 μm. Scattering is strongly peaked in the forward direction for all cloud types modeled. Tabulated data for wavelengths of 2.25 μm and 11.0 μm are given in Table 1.2-8.

Ice Clouds

Ice clouds forming at high altitudes contain predominantly non-spherical crystals and, hence, the Mie scattering code HSPHR is unsuitable for calculating extinction and absorption coefficients. For example, cirriform clouds are composed mainly of hexagonal-column crystals several hundred micrometers long at a concentration of 0.1 to 1 cm^{-3}. To estimate the transmissivity through these cloud types, we relied upon existing observational measurements and the rather limited number of theoretical treatments as listed in Table 1.2-9. A number of these authors have measured the transmissivity of various cloud types at different wavelengths. Few, however, have simultaneously measured the cloud thickness so that β_{ex} can be estimated.

For those instances where the cloud thickness is known, we have plotted the transmissivity at 11 μm as a function of cloud thickness for various cirriform clouds in Figure 1.2-34. The upper curve is a least-squares fit to the measurements of Kuhn and Weickmann (1969) for cirrus clouds. Cirrus-cloud measurements of other references are in close agreement with this curve. The

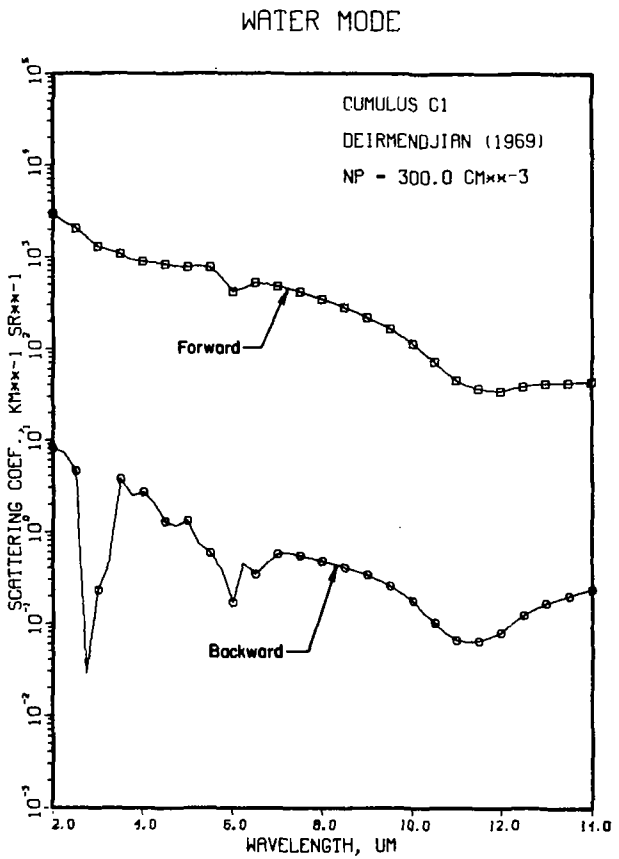

Figure 1.2-31. Cumulus C1 forward and backward scattering coefficients.

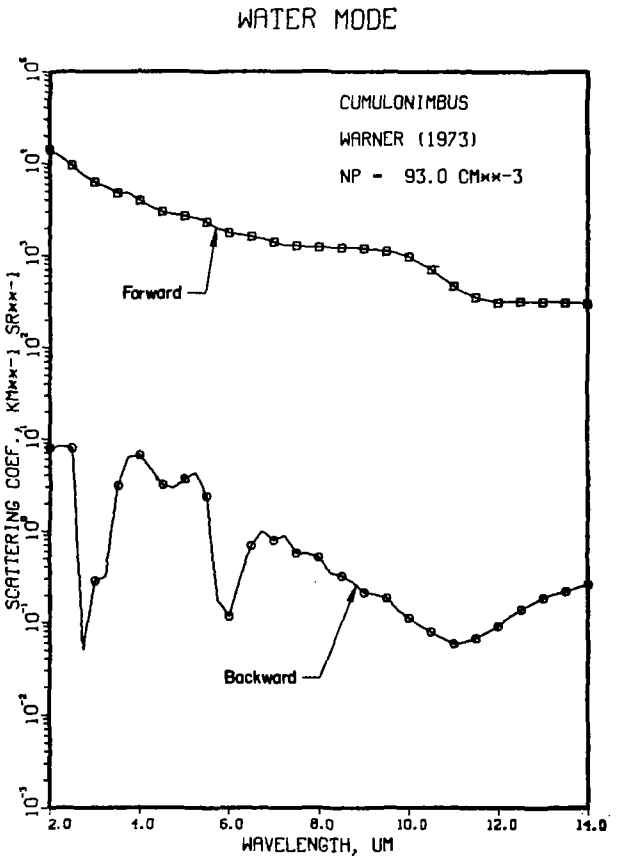

Figure 1.2-32. Cumulonimbus forward and backward scattering coefficients.

Table 1.2-8. Calculated forward (k_f) and backward (k_b) scattering coefficients for middle- and low-level clouds.

	λ = 2.25 μm		λ = 11.0 μm	
Cloud type	k_f, $km^{-1}sr^{-1}$	k_b, $km^{-1}sr^{-1}$	k_f, $km^{-1}sr^{-1}$	k_b, $km^{-1}sr^{-1}$
As	6.59×10^{3}	1.48×10^{1}	1.62×10^{2}	1.18×10^{-1}
Ac	2.98×10^{3}	5.72×10^{0}	1.04×10^{2}	2.52×10^{-2}
Sc	$(2.00\text{-}6.32) \times 10^{3}$	$(5.85\text{-}7.65) \times 10^{0}$	$(0.38\text{-}2.13) \times 10^{2}$	$(5.72\text{-}6.29) \times 10^{-2}$
St	$(3.65\text{-}7.82) \times 10^{3}$	$(0.75\text{-}1.07) \times 10^{1}$	$(0.98\text{-}2.66) \times 10^{2}$	$(1.10\text{-}1.14) \times 10^{-1}$
Ns	$(2.26\text{-}2.40) \times 10^{4}$	$(1.84\text{-}2.16) \times 10^{1}$	$(8.91\text{-}9.60) \times 10^{2}$	$(1.42\text{-}2.14) \times 10^{-1}$
Cu humulis	$(0.25\text{-}1.00) \times 10^{4}$	$(0.73\text{-}2.15) \times 10^{1}$	$(0.50\text{-}3.01) \times 10^{2}$	$(0.66\text{-}1.08) \times 10^{-1}$
Cu congestus	7.51×10^{3}	9.29×10^{0}	2.60×10^{2}	7.00×10^{-2}
Cb	$(1.17\text{-}4.13) \times 10^{4}$	$(0.75\text{-}1.07) \times 10^{1}$	$(0.47\text{-}2.03) \times 10^{3}$	$(5.89\text{-}7.06) \times 10^{-2}$

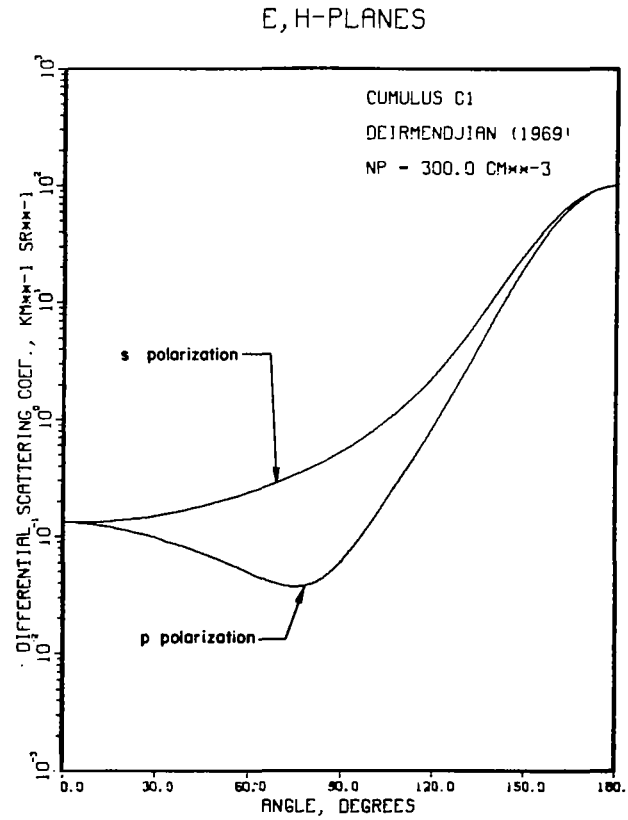

Figure 1.2-33. Differential scattering coefficients for the Cumulus C1 particle distribution at λ = μm.

Table 1.2-9. References for observational measurements and/or theoretical studies of infrared light transmission through ice clouds.

Breene et al. (1969)
Brewer and Houghton (1956)
Dugin et al. (1976)
Fritz and Rao (1967)
Gates and Shaw (1960)
Georgiyevskii and Shukurov (1974)
Guzzi et al. (1974)
Hall (1968)
Hobbs et al. (1974)
Kuhn and Weickmann (1969)
Kuhn et al. (1974)
Liou (1972, 1974, 1977)
Liou and Wittman (1979)
Volkovitskii et al. (1974)

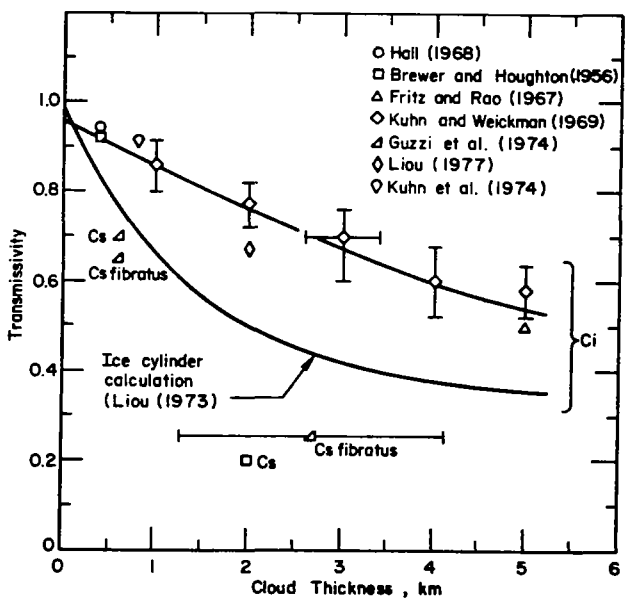

Figure 1.2-34. Measured and calculated transmissivities of cirriform clouds for $\lambda \simeq 11$ μm.

theoretical calculation of Liou (1973) is for randomly oriented ice cylinders having a mean length of 200 μm, a mean radius of 30 μm, and a mean concentration of 0.05 cm^{-3}. This gives a frozen water density of 0.0283 g/m^3. Because Liou (1973) did not attempt to incorporate a size distribution model into his calculations, this theoretical estimate must be taken only as a rough approximation to the transmissivity properties of an actual cirrus cloud. Denser cirriform clouds, such as cirrostratus, are more opaque to infrared radiation

even though their average thickness is generally less than for cirrus clouds. Unlike many water-based cloud types occurring at lower altitudes, dense cirriform clouds may attenuate more strongly at 11 μm than at shorter wavelengths [Guzzi et al. (1974); Georgiyevskii and Shukurov (1974); Hall (1968)], although this effect amounts to a difference in transmissivity of perhaps 20% at most.

Rain

For large, homogeneous, and spherical droplets such as rain, light absorption and extinction can be approximated by geometrical optics. Van de Hulst (1964) obtained the following approximation formula for the extinction efficiency factor:

$$Q_{ex} = [2 - 4\exp(-\varepsilon \tan\delta)(\cos\delta/\varepsilon)\sin(\varepsilon - \delta) - 4\exp(-\varepsilon\tan\delta)(\cos\delta/\varepsilon)^2\cos(\varepsilon - 2\delta) + 4(\cos\delta/\varepsilon)^2\cos(2\delta)], \quad (4)$$

where the complex refractive index is

$$n = n' - ik, \quad (5)$$

and the other factors are

$$\varepsilon = (4\pi a/\lambda)(n' - 1), \quad (6)$$

$$\tan\delta = k/(n' - 1). \quad (7)$$

Equation (4) was derived assuming $2\pi a/\lambda >> 1$ and $(n' - 1) << 1$, which holds for most rains with the exception of fine mists. The absorption efficiency factor is likewise given by

$$Q_a = [1 + \frac{\exp(-4xk)}{2xk} + \frac{\exp(-4xk)}{8x^2k^2}], \quad (8)$$

where $\chi = 2\pi a/\lambda$. The extinction and absorption coefficients are

$$\beta_{ex} = \pi\int_{a_1}^{a_2} Q_{ex}(\lambda,n)N(a)a^2da, \quad (9)$$

$$\beta_a = \pi\int_{a_1}^{a_2} Q_a(\lambda,n)N(a)a^2da, \quad (10)$$

where N(a) is the scatterer size distribution with lower and upper radius limits a_1 and a_2, respectively. Chut and Hogg (1968) and Rensch and Long (1970) have taken normalized rain particle distributions, such as those of Laws and Parsons (1943), and calculated β_{ex} and β_a as functions of the rainfall rate, R. For the present study, we have employed the Marshall-Palmer distribution given by

$$N(D) = N_o \exp(-\Lambda D), \tag{11}$$

where D is the drop diameter (mm) and N(D)dD is the number of drops per unit volume in the size increment from D to D + dD ($m^{-3} mm^{-1}$). Three separate distributions, taken from the work of Joss et al. (1968) and representative of different types of precipitation, were used in the numerical calculations. The distribution parameters are as follows:

- Drizzle

$$N_o = 30{,}000 \ m^{-3} \ mm^{-1}$$

$$\Lambda = 5.7 \ R^{-0.21} \ mm^{-1}$$

$$D_o = 0.64 \ R^{0.21} \ mm$$

- Continuous

$$N_o = 7{,}000 \ m^{-3} \ mm^{-1}$$

$$\Lambda = 4.1 \ R^{-0.21} \ mm^{-1}$$

$$D_o = 0.90 \ R^{0.21} \ mm$$

- Thunderstorm

$$N_o = 1{,}400 \ m^{-3} \ mm^{-1}$$

$$\Lambda = 3.0 \ R^{-0.21} \ mm^{-1}$$

$$D_o = 1.22 \ R^{0.21} \ mm$$

where R is the rainfall rate (mm/hr), N_o is the value of N(D) where the curve crosses the D = 0 axis, Λ is a parameter which depends on the type and intensity of the precipitation, and D_o is the median volume diameter. A computer code (RAIN) was written to evaluate Equations (9) and (10) using these distributions and assuming that rain is composed entirely of pure water with index of refraction data given in Table 1.2-2. The presence of condensation nuclei may be neglected because of the small size and mass of the nuclei compared with the raindrop as a whole.

Calculational results for a wavelength of 11 μm are shown in Figure 1.2-35. Because of the large particle diameters in the rain distributions, Q_{ex} and Q_a rapidly converge to values of 2 and 1, respectively, as we integrate from a_1 to a_2. For R > 0.1 mm/hr, therefore, the present results are effectively independent of wavelength for wavelengths in the infrared, and depend only upon the explicit details of the particle distribution. Observational

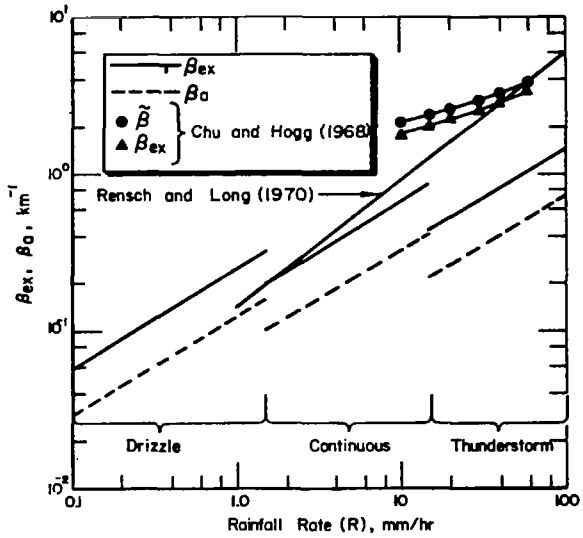

Figure 1.2-35. Calculated and measured extinction and absorption coefficients for rain.

measurements, however, show distinct differences between the total attenuation coefficient for different wavelengths, partly due to differences in molecular absorption. Few measurements of the attenuation of laser radiation due to rain have been performed; Chu and Hogg (1968) made observations at 0.63 μm, 3.5 μm, and 10.6 μm during periods of rainfall largley free of accompanying fog. They observed greater attenuation at 10.6 μm than at the shorter wavelengths, and we have plotted their data in Figure 1.2-35. The curve labeled $\tilde{\beta}$ is a least-squares fit to their experimental data and represents total attenuation due to all processes. The curve labeled β_{ex} is the estimated extinction coefficient, found by subtracting the molecular absorption and clear-air background aerosol attenuation from $\tilde{\beta}$. Because the relative humidity during the summer showers reported by Chu and Hogg approaches 100%, the molecular absorption coefficient was calculated at 10.6 μm using the code LASER and the Tropical Summer atmospheric model. We notice that the corrected extinction curve thus obtained is in good agreement with theoretical predictions using the continuous rainfall particle distribution. Wilson and Penzias (1966) found values of $\tilde{\beta}/R$ in the range $2.3\text{-}2.8 \times 10^{-2}\,km^{-1}\,mm^{-1}$ hr for $R < 50$ mm/hr, in good agreement with our theoretical predictions without any correction. Obviously, the range of β_{ex} and β_a observed at a particular rainfall rate is due to variations in the particle distribution.

Snow

Little theoretical or observational data of laser propagation in snow exists. Observational measurements taken by Wilson and Penzias (1966), Chu and Hogg (1968), Sokolov (1970), and Nakajima et al. (1973) show severe attenuation for moderate precipitation rates, and preliminary measurements indicate that the attenuation at 10.6 μm is significantly greater than at 0.63 μm and 3.5 μm.

We have estimated the values of β_{ex} and β_a as functions of the snowfall rate R using two models. In the equivalent liquid-drop model, Sekhon and Srivastava (1970) found that the particle distribution of melted snow crystals is given by

$$N(D) = 2500\ R^{-0.94} \exp(-\Lambda D),\ m^{-3}\ mm^{-1} \quad (12)$$

where

$$\Lambda = 2.29\ R^{-0.45},\ mm^{-1} \quad (13)$$

Here, D is the liquid drop diameter (mm), and R is the melted snowfall rate (mm/hr). In the second model, called the aggregate snowflake model, we use the actual particle size distribution which can also be represented in the Marshall-Palmer functional form. To obtain the snowflake diameter, the relationship between particle masses in the liquid and ice-crystal forms is used:

$$\rho_L D_L^3 = \rho_i D_i^3 , \quad (14)$$

where ρ is the density, D is the particle diameter and the subscripts L and i denote liquid and ice forms, respectively. Passarelli (1978) found that $\rho_i = 0.09\ g/cm^3$, from which we obtain

$$D_i/D_L = 2.23 . \quad (15)$$

If the liquid-drop particle distribution given in Equation (12) is modified by Equation (15), we have an approximate relation giving the actual snowflake particle size distribution.

These two distribution models were combined with the geometrical optics model and a computer code (SNOW) was written to solve for β_{ex} and β_a. We expect that the equivalent liquid-drop model will underestimate these coefficients because the particle diameters are too small, whereas the aggregate snowflake model will overestimate β_{ex} and β_a because the actual snowflake distribution is approximated by spherical particles composed of liquid density water. The results of these calculations are shown in Figure 1.2-36 for a wavelength of 11 μm. These calculations bound the experimental measurement of Chu and Hogg (1968) and Sokolov (1970) as would be intuitively expected. At low snowfall rates, the aggregate snowflake model more closely estimates the measured extinction coefficients of Sokolov (1970), whereas at higher snowfall rates, the aggregate snowflake model clearly overpredicts observed behavior and the equivalent liquid-drop model establishes a lower bound for the estimates. As with their measurement of the attenuation of rain at several wavelengths, these researchers found

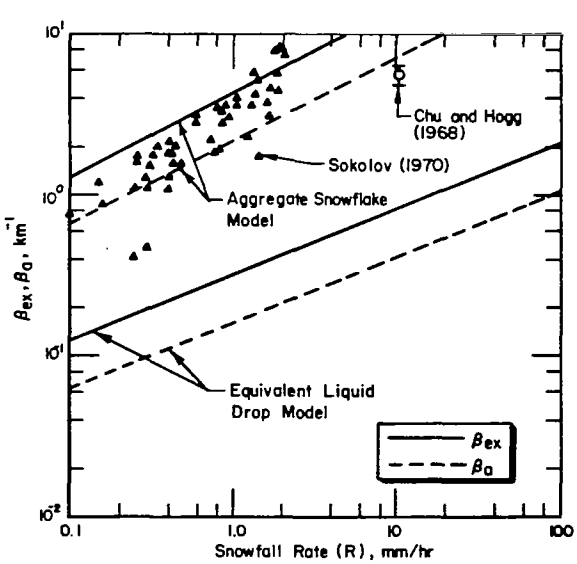

Figure 1.2-36. Calculated and measured extinction and absorption coefficients for snow.

more severe attenuation at 10.6 μm than at the shorter wavelengths and, in general, the attenuation and forward scattering properties of snow appear to be in between those of rain and dense fog. At present, there is no satisfactory theoretical method for calculating the scattering properties of snowflake crystals, although Monte Carlo techniques have been applied with some degree of success [Nakajima et al. (1973)].

1.2.4 PROPAGATION CALCULATIONS—MOLECULAR ABSORPTION

Calculational Models

Molecular absorption is calculated for a given laser wavelength λ by the computer code LASER [McClatchey and D'Agati (1978)]. Absorption line parameters for atmospheric molecular species are taken from the AFGL line-parameter compilation [McClatchey et al. (1973)]. The average molecular absorption coefficient for each of 32 atmospheric layers is calculated for the following atmospheric models: U.S. Standard, Tropical, Midlatitude Summer, Midlatitude Winter, Subarctic Summer, and Subarctic Winter. In addition, several of the aerosol models of Shettle and Fenn (1975) are included, and the code also calculates aerosol absorption and scattering coefficients for each atmospheric layer. The results given here consider molecular absorption only to permit better understanding of the roles of the various attenuation mechanisms. Molecular (Rayleigh) scattering is important only at $\lambda \lesssim 1$ μm.

Transmission Efficiencies

The transmission efficiency for space-to-earth propagation was calculated for a number of laser lines in the 2-μm, 9-μm, and 11-μm regions. The 2-μm and 11-μm regions were chosen because they may afford an improvement in transmission through various meteorological aerosols. The 9-μm region was chosen because the laser lines of certain isotopic species of CO_2 may offer higher transmission efficiencies than their naturally occurring counterpart, $^{12}C^{16}O_2$; $^{12}C^{16}O_2$ is uniformly distributed in the atmosphere and its strong absorption lines should be avoided by selection of alternate laser wavelengths. All calculations are for propagation to receptor site elevations of 0.0, 0.5, and 3.0 km for a zenith angle of 50°.

The spectral region from 2.100 μm to 2.315 μm offers an excellent high-transparency window with relatively few strong absorption features. Calculated transmission efficiencies of three sample lines, as given in Table 1.2-10 exceed 99.9% for all site elevations and are insensitive to seasonal variations. Since the individual windows between absorption features are wide (in many cases > 10 cm^{-1}), there is hope that a scalable, high-power laser operating at a wavelength in one of these windows can be developed.

The transmission efficiency of several midrotational P- and R-branch laser lines of the isotopic-species $^{12}C^{18}O_2$ laser operating on the $10°0 \rightarrow 02°0$ band are given in Table 1.2-11. Operation of a CO_2 laser in this mode results in a significant improvement in the transmission efficiency compared with operation on "standard" lines of the $00°1 \rightarrow 10°0$ band of $^{12}C^{16}O_2$; seasonal variations, however, are pronounced and the highest annual transmission efficiency to typical receptor sites (h = 0.5 km) is only 87.7% for the 9.124-μm line.

Table 1.2-10. Space-to-earth transmission efficiencies of selected laser lines in the 2.100-2.315-μm window region for molecular absorption and (Rayleigh) scattering only and a zenith angle of 50°.

			Transmission efficiency to elevation h					
			Midlatitude Summer			Midlatitude Winter		
Transition	ν, cm^{-1}	λ, μm	0.0 km	0.5 km	3.0 km	0.0 km	0.5 km	3.0 km
--	4444.444	2.250	0.99947	0.99950	0.99964	0.99949	0.99952	0.99965
--	4484.000	2.230	0.99945	0.99948	0.99963	0.99947	0.99950	0.99964
--	4666.000	2.143	0.99901	0.99912	0.99949	0.99922	0.99928	0.99952

Table 1.2-11. Space to earth transmission efficiencies for $^{12}C^{18}O_2$-laser transitions in the $00°1 \rightarrow 02°0$ band including molecular absorption only and for a zenith angle of 50°.

			Transmission efficiency to elevation h					
			Midlatitude Summer			Midlatitude Winter		
Transition	ν, cm^{-1}	λ, μm	0.0 km	0.5 km	3.0 km	0.0 km	0.5 km	3.0 km
P(22)	1067.3589	9.369	0.388	0.434	0.859	0.799	0.814	0.863
P(20)	1068.9425	9.355	0.487	0.551	0.774	0.698	0.721	0.809
P(18)	1070.5071	9.341	0.431	0.496	0.775	0.666	0.696	0.827
R(18)	1095.9645	9.124	0.725	0.792	0.975	0.952	0.962	0.991
R(20)	1097.1507	9.115	0.720	0.788	0.971	0.947	0.958	0.987
R(22)	1098.3174	9.105	0.708	0.777	0.968	0.942	0.953	0.984

Because of the potential importance of the 11-μm region, the interval from 10 μm to 12 μm was closely examined for high transparency windows. This spectral region is characterized by a profuse number of absorption lines which are highly pressure broadened in the lower troposphere.

Windows which were at least 1.0 cm^{-1} wide with edges at least 1.0 cm^{-1} from a major absorption line were selected for detailed calculations. The HITRAN spectral plots of McClatchey and Selby (1974) were particularly useful in this earch, although their transmission efficiencies cannot be used in the present study because they are for 10-km horizontal paths. If a known (high-power) laser line exists within a window, this wavelength was used in the LASER-code calculation; for those windows for which no laser line could be identified, the central wavelength was used. The transmission efficiencies for all windows identified in this manner are given in Table 1.2-12. For comparison, calculations are also shown for the "standard" 10.6-μm CO_2 laser line, which is totally unsuitable for space-to-earth power beaming. Most of the absorption occurs in the lower troposphere and seasonal variations in the

Table 1.2-12. Space-to-earth transmission efficiencies of selected laser lines in the 11-μm window region for molecular absorption only and a zenith angle of 50°.

Transition	ν, cm^{-1}	λ, μm	Transmission efficiency to elevation h					
			Midlatitude Summer			Midlatitude Winter		
			0.0 km	0.5 km	3.0 km	0.0 km	0.5 km	3.0 km
--	875.000	11.429	0.553	0.653	0.960	0.921	0.939	0.991
$^{13}C^{16}O_2$ $P_I(24)$*	893.372	11.194	0.571	0.665	0.952	0.918	0.935	0.985
$^{13}C^{16}O_2$ $P_I(16)$	900.369	11.107	0.572	0.664	0.943	0.912	0.929	0.978
$^{13}C^{16}O_2$ $P_I(12)$	903.750	11.065	0.581	0.673	0.948	0.915	0.932	0.979
N_2O $P_I(30)$	912.359	10.961	0.600	0.691	0.964	0.930	0.946	0.992
N_2O $P_I(26)$	916.065	10.916	0.607	0.697	0.965	0.933	0.948	0.992
$^{12}C^{16}O_2$ $P_I(20)$	944.195	10.591	0.192	0.232	0.412	0.439	0.463	0.570
$^{13}C^{16}O_2$ $P_{II}(26)$	994.986	10.050	0.472	0.526	0.681	0.660	0.669	0.697

*Subscript denotes vibrational-rotational band: I = 00°1 → 10°0; II = 00°1 → 02°0.

transmission efficiency are again pronounced. The highest annual transmission efficiency to typical receptor sites is 82.3% for the 10.916-μm line. High-elevation operation (h = 3.0 km) increases this value to 96.3%. Indeed, power transmission in the 9-μm and 11-μm regions is probably limited to high-elevation sites. The examination of the 10-μm to 12-μm spectral region was exhaustive and we believe that no high-transparency window was overlooked. Therefore, laser operation at any other wavelength in this region or pressure detuning of "standard" high-power laser lines will not result in transmission efficiencies greater than those given here.

1.3 RECEPTOR SITING CRITERIA

Laser receptor siting criteria are far less restrictive than their microwave rectenna counterparts, due primarily to the smaller land area requirement. Estimates [Beverly (1980)] predict a necessary land area of only a few square kilometers, roughly two orders of magnitude smaller than necessary for the microwave rectenna. In addition, siting criteria are less restrictive in terms of topological acceptability, permitting siting in closer proximity to load centers and/or existing power transmission lines. Many of the exclusion areas for receptor siting as listed in Table 1.3-1 are identical to those involved in microwave-rectenna siting. Because of the proposed power density for laser transmission (~1-100 W/cm^2), however, it is unlikely that any site will be subject to multiple land use.

Because the purpose of this research is to bound cogent power-availability parameters for the various regions of the United States and to develop mitigation techniques and siting criteria which will diminish the deleterious effects of inclimate weather, detailed land tract evaluations were not performed.

Table 1.3-1. Receptor siting exclusion areas.

Absolute exclusion areas:
Military and DOE reservations
National and state parks
National wildlife preserves
Indian reservations
Lakes and navigable waterways
Off-shore locations
Marshlands
Metropolitan areas
Metropolitan and county airports, including approach corridors
Interstate highways
Preferentially flooded lands
Wild and scenic rivers
Probable exclusion areas:
High-quality agricultural land
Coastal regions, river valleys, and other locations subject to persistent fog
Topographically unacceptable land
Area of unknown impact:
Migratory pathways of birds

Furthermore, siting criteria based on projected electrical power demand are beyond the scope of this study, and no attempt was made to identify planned transmission line additions or to project future expansion of any grid.

Since detailed statistical meteorological data are required by the power availability model, the sites selected are identified by their associated weather station. If the actual site tract is in close proximity to the weather station, the assumption of identical statistics is usually good for most mid-latitude climates. For our purposes, sites were chosen which were within 100 miles of an existing extra-high-voltage (EHV) transmission line, consistent with the exclusion areas listed in Table 1.3-1. No closely spaced sites were chosen and attempts were made to distribute the sites throughout the contiguous United States. Because the layout of the EHV grid is strongly correlated with existing load-demand centers, the number of sites selected was not evently proportioned by geographical region. Difficulties in obtaining the necessary statistical meteorological data also precluded selection of the "best" sites for certain geographical regions. However, the number of sites selected (22) is statistically significant enough so that patterns of expected performance for the different regions can be gleaned, especially considering the climatic similarity of many sites within the same region.

1.4 POWER AVAILABILITY

1.4.1 INTRODUCTION AND SOURCES OF STATISTICAL CLIMATIC DATA

Calculation of the power availability at any given site requires statistical climatic data in much greater detail than is routinely accumulated by the U.S. Weather Service for any of their stations. For instance, an extensive model will require information not only concerning sky cover but regarding

cloud type, thickness, and frequency of occurrence, which is not available for civilian stations [Nybro (1980)]. In this section, sources of such data are reviewed and their applicability in formulating a power-availability model for space-to-earth laser power transmission is discussed.

Considerable work has been performed in developing empirical global cloud-cover models and representative theoretical statistical distributions [see, for example, Falls (1974) and references therein]. This work was motivated principally by earth-viewing space missions, such as NASA's Skylab program. Although a substantial amount of data was accumulated during the course of these studies, the various statistical distributions are unsuitable for modeling space-to-earth power availability for the following reasons. First, the models are representative of large areas and assume homogeneous cloud-cover distributions within each region. The earth's surface is divided into 29 regions of different areas, which is too coarse for present purposes. Furthermore, such models give the probability of a specific type of cloud cover within a 55.6-km-diameter circle, which can be quite different from the cloud-cover probability within the small area typified by a laser beam. Second, only five sky cover categories were employed rather than the customary 11 categories (0 to 10 tenths sky cover). This lack of detail would hamper our ability to estimate transmission efficiencies through clouds on the basis of their types and thicknesses as statistical functions of cloud cover.

A large number of models exists which relate laser attenuation at a specific wavelength to the meteorological visibility. Some authors have integrated these relations with statistical climatological data and developed transmission probability distributions [see, for example, Warner and Bichard (1979)]. These models are suitable only for horizontal or near-horizontal laser propagation where the beam is attenuated by haze, fog, or precipitation. Such models are completely useless for space-to-earth propagation where the most frequently encountered obscurring media are clouds.

A three-dimensional nephanalysis program [Coburn (1971)] was developed at the Air Force Global Weather Center (AFGWC) to process the tremendous quantity of satellite-sensed cloud data and conventionally sensed meteorological parameters into a three-dimensional cloud model of the atmosphere. The horizontal resolution is defined by a grid array projected onto a polar stereographic map; at 60° latitude, the distance between grid points is 40 km. The vertical resolution is defined by 15 atmospheric layers ranging from ground level to 55,000 feet (16.8 km) above mean sea level. Data available at each point include cloud amounts, types, maximum tops and minimum bases, the total cloud cover, and the current weather. Civilian satellites used for such observations include the Synchronous Meteorological Satellite (SMS)/Geostationary Operational Environmental Satellite (GEOS) series, and the Improved TIROS (ITOS) polar-orbiting series. These satellites use scanning radiometers with one channel each of visible and IR data. To this author's knowledge, a statistical data base which incorporates these variables into an analyzed format and which could be referenced to particular receptor locations does not exist.

More advanced instrumentation, such as the high-resolution multichannel IR sounder on board the NIMBUS VI satellite, can be used to infer more detail regarding the cloud type and composition, including water content, from

measurements of upwelling radiance at different wavelengths [Feddes and Liou (1977]. Such observations, however, are not continually available and no statistical data base exists.

The most useful climatic data for present purposes are the frequencies of total sky cover (0-10 tenths), which are observational data gathered at almost all military air bases. The power availability model developed here considers laser transmission under two conditions, i.e., when a cloud-free line-of-sight (CFLOS) exists between the satellite transmitter and the receptor site and when clouds obscure the beam. The probability of a CFLOS is a function of the observed frequencies of sky cover and the propagation zenith angle. Statistical data needed to estimate this probability were obtained from the work of Lund at the Air Force Geophysics Laboratory. The transmission efficiency through cloud cover is calculated using three schemes. The first cloud-cover transmission model gives the worst-case behavior and is believed to establish a lower bound on the calculated power availability by assuming zero transmission through all cloud types except for thin cirriform, middle, and stratiform types. The second model is our best estimate which, admittedly, represents a large amount of subjective judgment. The third and most optimistic model assumes considerable transmission through certain cloud types by virtue of substantial hole boring. These models are believed to accurately bound the expected performance of space-to-earth laser energy transmission. The statistical distribution of cloud types is estimated using Lund's data for midlatitude sites and is a function of total sky cover.

1.4.2 POWER AVAILABILITY MODEL

The average transmission efficiency for each total sky cover j is

$$T_j = C_j + (1 - C_j)\tau_j, \quad j = 0, 1, \ldots, 10 \tag{16}$$

where C_j is the probability of a CFLOS as a function of total sky cover j and zenith angle θ, and τ_j is the weighted cloud transmissivity is the weighted cloud transmissivity if a cloud obscures the beam for each total sky cover j. The second term on the right-hand side of Equation (16) gives the probability of a cloudy line-of-sight multiplied by the weighted cloud transmissivity through that line-of-sight. This term accounts for those instances where some penetration through cloud cover is possible. Three different modes for τ_j are given in the sections below. The cumulative frequency, i.e., the frequency that the transmission efficiency equals or exceeds T_j, is

$$f_j = \sum_{i=0}^{j} K_i \ , \tag{17}$$

where K_j is the frequency of occurrence of each total sky cover. By definition,

$$\sum_{j=0}^{10} K_j \equiv 1. \tag{18}$$

Observational values of K_j were obtained for each receptor site from Part D (Sky Cover) of the U.S. Air Force/U.S. Navy Revised Uniform Summary of Surface Weather Observations, which is available from the National Climatic Center (NOAA) in Ashville, North Carolina. Statistical data are tabulated by month for standard daily three-hour intervals and by month and annually for all hours. The number of observations ranged from about 1000 to over 15,000, spanning from 6 to over 30 years of data gathering. The power availability for a given receptor site is then

$$P = \sum_{j=0}^{10} T_j K_j \quad . \tag{19}$$

The power availability is simply the temporally averaged transmission efficiency assuming that power is constantly beamed from space to the receptor site.

C_j probabilities were determined by Lund and Shanklin (1973) for all the cloud-form categories listed in Table 1.4-1. Because sky cover observations (K_j's) are not reported with regard to cloud form, we must use the weighted C_j probabilities for all cloud forms given in tabular form by Lund and Shanklin (1973) and shown graphically in Figure 1.4-1 as functions of the elevation angle ϕ, where $\theta = 90 - \phi$. According to comparisons made by these authors, the total probability of a CFLOS when cloud forms are considered and when weighted C_j probabilities are employed are almost identical, differing by $\lesssim 1\%$ which is statistically insignificant. The use of weighted C_j probabilities, independent of cloud form, should be valid for all U.S. midlatitude sites chosen for this study.

The most important statistical parameter in laser power transmission is not the frequency that the transmission efficiency exceeds some useful value, but rather the frequency that the transmission efficiency exceeds some useful value and persists for a reasonable time. It is senseless to continue power beaming to a site when the transmission efficiency falls below some acceptable value and remains low; instead, the beam can be switched to an alternate receptor site. If we consider the persistence time, the transmission efficiency is then

$$T_j = E_j C_j + (1 - C_j)\tau_j \quad , \tag{20}$$

where E_j is the probability that once a CFLOS is established it will persist for a specified time. E_j is a function of total sky cover and persistence time. Tabulated values were taken from Lund (1973b) and are shown in graphical from in Figure 1.4-2. The results of Lund (1973b) for longer periods were parameterized so that persistence times greater than one hour can be considered. The frequency that the transmission efficiency equals or exceeds T_j and persists for a time t is

$$f_j = \sum_{i=0}^{j} K_i \tag{21}$$

Note that the occurrence of meteorological phenomena other than clouds is implicitly included in the model. For instance, snow and rain originate within

Table 1.4-1. Cloud-form categories.

Category	Cloud type	Form
Cirriform	Cirrocumulus	--
	Cirrostratus	--
		fibratus
	Cirrus	fibratus
		fibratus floccus
		spissatus
		uncinus
Middle	Altocumulus	translucidus
		lenticularis
		cumulogenitus
		cumulonimbogenitus
		duplicatus
		opacus
		floccus
		castellanus
	Altostratus	translucidus
		opacus
Cumuliform	Cumulonimbus	calvus
		mammatus
		capillatus
	Cumulus	humulis
		congestus
		fractus
Stratiform	Stratus	---
		fractus
	Nimbostratus	--
	Stratocumulus	--
		cumulogenitus
Mixed	Mixtures of more than one form	

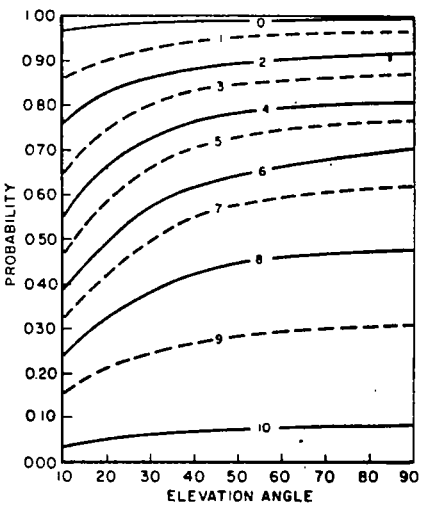

Figure 1.4-1. Probabilities of a cloud-free line-of-sight (C_j), as a function of elevation angle (ϕ) and observed total sky cover (j), for all cloud types [Lund and Shanklin (1973)].

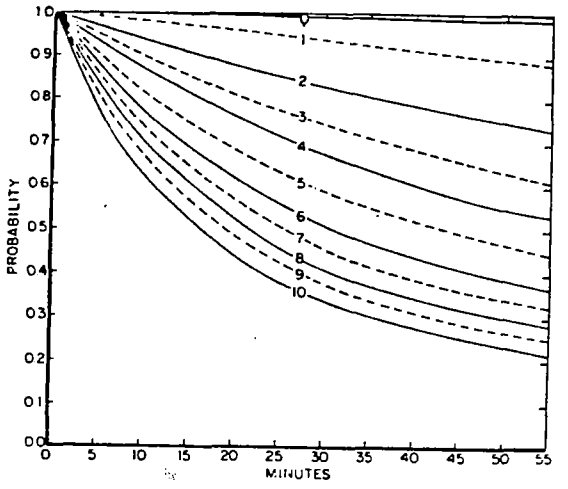

Figure 1.4-2. Cloud-free line-of-sight persistence probabilities (E_j) as a function of total sky cover (j) and time (t) [Lund (1973b)].

clouds and we have generally assumed zero transmission through precipitating cloud types. Likewise, heavy haze or fog, although not as statistically important as clouds, are reported as sky cover if they obscure visibility in a vertical direction. We have not included any attenuation due to molecular absorption, however, and have assumed that a high transparency window is available.

A computer code (PAVAIL) was written to manipulate observational data for the various receptor sites and to calculate the parameters given above. An Aitken interpolation and extrapolation scheme was employed so that the parameters of interest appear as smooth, continuous functions.

The following statistical parameters were calculated on a seasonal and annual basis for each site using the computer code PAVAIL:

1. The frequency for which the transmission efficiency exceeds a given value (calculated in tabular form for transmissivities of 0.1 to 0.9 inclusive)

2. The power availability (average yearly or seasonal transmission efficiency assuming constant power beaming)

3. The frequency for which the transmission efficiency exceeds a given value for a specified persistence time [tabular form as in (1)]

In addition, the code is set up to statistically reduce data for multiple sites within a geographical region. Diurnal variations in the calculated parameters can also be analyzed, although this was not done routinely.

Cloud Transmission Model 1

The first cloud transmission model is the most conservative and is utilized to establish a lower bound on the calculated power availability. We

assume that only thin cirriform, middle, and stratiform clouds are partially transmissive when they are observed at total sky covers less than or equal to 6 tenths. Furthermore, we are implicitly assuming that the thickness of these cloud forms increases in a manner directly proportional to sky cover so that the cloud-form transmission efficiency decreases with increasing sky cover. Numerically, Model 1 specifies (1) zero transmission efficiency for cumuliform or mixed-form clouds, (2) zero transmission efficiency for all cloud forms observed at total sky covers greater than 6 tenths, (3) the cirriform transmission efficiency decreases from 90% to 30% as the total sky cover increases from 0 to 6 tenths, in correlation with the lower range of observations in Figure 1.2-34, and (4) the transmission efficiency of middle and stratiform clouds decreases from 40% to 10% and 60% to 20%, respectively, in the same sky cover range (see Table 1.2-7). Also, to account for statistical variations in the persistence probabilities, E_j values used in Model 1 were reduced by 8%, consistent with the observational results of Lund (1973b) and the conservative nature of this model.

Cloud Transmission Model 2

The second model represents the best estimate for cloud transmission under conditions not involving hole boring. The model is based largely on subjective judgments and some comments and observations on the sensitivity of the power availability model to the estimated cloud-form transmission efficiencies will be presented in a later section. Specifically, Model 2 assumes (1) zero transmission efficiency through cumuliform clouds, (2) the cirriform transmission efficiency decreases from 90% to 35% as the total sky cover increases from 0 to 10 tenths, in correlation with the Kuhn-Weickmann curve in Figure 1.2-34, (3) the transmission efficiency of middle and stratiform clouds decreases from 40% to 10% and 60% to 20%, respectively, over the same sky cover limits (see Table 1.2-7), and (4) the transmission efficiency for mixed cloud forms decreases from 30% to 0% as the total sky cover increases from 0 to 10 tenths. Therefore, compared with the first model, Model 2 allows partial transmission during certain overcast conditions and through mixed cloud forms if they are observed during periods of lesser sky cover. Cumuliform clouds are again assumed to be completely opaque.

Cloud Transmission Model 3

To complete the power-availability model, a third cloud transmission model is proposed which assumes substantial penetration of certain cloud types by hole boring. We have limited the laser-beam power density by safety and environmental constraints so that not all cloud types are penetrable. Because the laser parameters required to affect boring are different for the 2-μm and 11-μm spectral windows, a description of the hole-boring calculations precedes the definition of cloud transmission Model 3.

For a laser beam to penetrate an aerosol layer of thickness Δz_c moving with a lateral wind velocity v, Harney (1977) showed that the aerosol vaporization time t_v must satisfy the following inequality as a minimum requirement:

$$vt_v(1 + \beta_a \Delta z_c) < d \ , \tag{22}$$

where d is the beam diameter, and the absorption coefficient β_a and water content W are related by

$$\beta_a \simeq \langle Q_a N_p \pi a_c^2 \rangle = \frac{3W}{4\rho} \langle Q_a / a_c \rangle \tag{23}$$

Q_a is the Mie absorption factor, N_p is the total particle concentration, ρ is the droplet density, and a_c is the mode radius, i.e., the radius corresponding to the maximum number of particles. Numerical solution of the approximate equation for the evaporation rate was obtained by Kuzikovskii and Khmelevitsov (1968) allowing for the nonlinear dependence of the temperature on water-vapor concentration for laser intensities $I \sim 10^2 - 10^4$ W/cm^2. The parameterized relationship of the vaporization time t_v and instantaneous droplet radius a was expressed as

$$t_v = \frac{a_c - a}{0.494\ qI^{1.102}}, \quad pa_c >> 1 \tag{24}$$

and

$$t_v = \frac{\ell n(a/a_c)}{0.494\ pqI^{1.102}}, \quad pa_c << 1 \tag{25}$$

where

$$p = 8\pi k/\lambda \tag{26}$$

$$q = \exp[-0.2(|n| - 1)]. \tag{27}$$

In Equations (24) and (25), t_v is in sec, I is in W/cm , and λ and a_c are in μm. The complex index of refraction is $n = n' - ik$. For the droplet to be ineffectual in attenuating the beam, we require that the particle be reduced in size until $a = 0.01\ \lambda$.

Before proceeding, it is more convenient to specify meteorological aerosols in terms of their liquid-water/ice path lengths, μ (g/cm^2), so that

$$\mu = 0.1\ W\ \Delta z_c, \tag{28}$$

where W is in g/m^3 and Δz_c is in km. Substituting Equations (24) and (25) into (22) and solving for the minimum intensity to affect hole boring gives

$$I > \left[\frac{v(a_c - 0.01\ \lambda)}{0.494\ qd}\left(1 + 7500\ \frac{\mu}{\rho}\langle Q_a/a_c\rangle\right)\right]^{0.907}, \quad pa_c >> 1 \tag{29}$$

$$I > \left[\frac{v\ \ell n\left(\frac{a_c}{0.01\ \lambda}\right)}{0.494\ pqd}\left(1 + 7500\ \frac{\mu}{\rho}\langle Q_a/a_c\rangle\right)\right]^{0.907}, \quad pa_c << 1 \tag{30}$$

where v is in m/sec, d is in m, a_c and λ are in μm, μ is in g/cm^2, ρ is in g/cm^3, and I is in W/cm^2. Q_a, given previously by Equation (8) for the large-radius approximation, is not valid for cloud and fog droplets. As an analytic convenience, we use the Shifrin approximation [see Gordin and Strelkov (1975] given by

$$Q_a \simeq q[1 - \exp(-pa_c)]. \tag{31}$$

Using Equations (29) and (30), the minimum intensities to penetrate atmospheric aerosols were calculated for the cloud and fog parameters listed in Table 1.4-2. The results are given in Table 1.4-3 for a beam diameter of 100 m and wind velocities typical for the altitudes at which the various formations

Table 1.4-2. Representative liquid water/ice content values for various commonly occurring clouds and fog.

Category	Cloud type	a_c, μm	Δz_c, km	W, g/m^3	μ, g/cm^2
Cirriform	Cc, Cs, Ci	65*	0.3	0.05	0.002
Middle	Ac	6.0	0.5	0.1	0.005
	As	4.5	1.0	0.3	0.03
Cumuliform	Cb	5.0	7.6	2.5	1.9
	Cu humulis	3.5	1.4	1.0	0.14
	Cu congestus	3.5	3.1	2.0	0.62
Stratiform	St	4.0	0.4	0.3	0.012
	Ns	3.5	3.6	0.4	0.14
	Sc	3.5	0.5	0.2	0.010
Dense (Code 1) fog	--	12	0.25	0.1	0.003

*Radius of sphere with equivalent volume as ice crystal.

Table 1.4-3. Minimum intensities for hole boring through commonly occurring clouds and fog.

			I, W/cm^2	
Category	Cloud type	v, m/sec	λ = 2.0 μm	λ = 11.0 μm
Cirriform	Cc, Cs, Ci	20	170	24
Middle	Ac	10	83	6
	As	10	190	71
Cumuliform	Cb	10	6300	960
	Cu humulis	10	600	290
	Cu congestus	10	2200	1100
Stratiform	St	5	58	17
	Ns	5	320	154
	Sc	5	52	15
Dense (Code 1) fog	--	3	27	2

occur. The minimum intensity will only barely penetrate the aerosol layer and the hole will be in constant danger of closure due to convective effects. To maintain a properly cleared channel characterized by a high transmission efficiency, roughly three to five times as much intensity will be required [Sutton (1978)].

From an environmental and safety standpoint, the maximum cw laser intensity is probably limited to 100-200 W/cm^2. For 11-μm operation, therefore, all fogs, cirriform clouds with $\mu \lesssim 0.005$ g/cm^2, middle clouds with $\mu \lesssim 0.02$ g/cm^2, and stratiform clouds with $\mu \lesssim 0.03$ g/cm^2 can be bored at these intensities. All cumuliform cloud types and nimbostratus clouds are impenetrable except with weapon-quality ($I \gtrsim 1$ kW/cm^2) beams. Although the environmental consequences of laser-power transmission at these intensities are probably negligible, the transmission air-zone associated with each receptor must be restricted to all aircraft due to potential ocular hazards posed by the randomly pointing and highly reflective aluminum aircraft skins [Beverly (1979, 1980)].

For 2-μm operation, however, substantially higher cw intensities are necessary to affect hole boring because the aerosol absorption coefficient (β_a) is much smaller at 2 μm than an 11 μm. A potentially viable and attractive solution is to combine cw laser-power transmission with pulsed laser hole boring. At $I \sim 10^5$ W/cm^2, the internal heat generation in an aerosol droplet is so violent that shock waves form which explosively shatter the droplet [see, for instance, Kuzikovskii et al. (1971); Sutton (1978)]. Thus, a train of intense, short-duration pulses can be superimposed on the main cw beam allowing a reduction in average power density. A repetitively pulsed laser producing ~100 pulses/sec with a pulsewidth ~ 1 μsec and an energy density ~0.1 J/cm^2 gives an average power density ~10 W/cm^2. Now if the cw power-transmission component is reduced to $I \sim 1 - 10$ W/cm^2, the ocular hazards from quasi-specular reflection are greatly reduced and the transmission air zone would no longer be restricted to aircraft. Note that the pulse train can be turned off for clear periods and that the relative power densities of the beam components can be adjusted according to prevailing meteorological conditions to maintain a constant total average power density at the receptor. More theoretical and experimental research is needed to demonstrate the feasibility of this technique since the laser parameters suggested here are only rough estimates.

Numerically, the third cloud transmission model assumes (1) zero transmission efficiency for cumuliform clouds, (2) the transmission efficiency for cirriform and middle clouds decreases from 95% to 80% as the total sky cover increases from 0 to 10 tenths, i.e., 5% to 20% of the transmitted power is lost to aerosol vaporization, (3) the transmission efficiency for stratiform clouds decreases from 90% to 60% over the same sky-cover range, and (4) for mixed cloud forms, the transmission efficiency decreases from 80% to 30% as the total sky cover increases from 0 to 8 tenths; overcast conditions (9-10 tenths sky cover) with mixed-form clouds are impenetrable. Also, to account for statistical variations in the persistence probabilities, E_j values used in Model 3 were increased by 9%, consistent with the observational results of Lund (1973b) and the optimistic nature of the model.

The weighted cloud transmissivity for a given sky cover is calculated by multiplying the probability of occurrence of a cloud form if a cloud is present

by the respective transmission efficiency and summing over all cloud-form categories. This procedure is shown in Table 1.4-4, where the occurrence

Table 1.4-4. Calculation of weighted cloud transmissivities.

Sky cover, tenths	Cloud-form: Category	Probability of occurrence if cloud is present[a]	Transmission efficiency for model: 1	2	3	Weighted cloud transmissivity, τ: Model 1	2	3
0	Cirriform	0.31	0.90	0.90	0.95			
	Middle	0.14	0.40	0.40	0.95			
	Cumuliform	0.40	0.00	0.00	0.00	0.40	0.41	0.56
	Stratiform	0.10	0.60	0.60	0.90			
	Mixed	0.05	0.00	0.30	0.80			
1	Cirriform	0.47	0.60	0.80	0.95			
	Middle	0.09	0.40	0.40	0.95			
	Cumuliform	0.28	0.00	0.00	0.00	0.37	0.49	0.67
	Stratiform	0.09	0.60	0.60	0.90			
	Mixed	0.07	0.00	0.30	0.80			
2	Cirriform	0.37	0.50	0.70	0.95			
	Middle	0.06	0.20	0.40	0.95			
	Cumuliform	0.30	0.00	0.00	0.00	0.21	0.38	0.63
	Stratiform	0.04	0.40	0.60	0.90			
	Mixed	0.23	0.00	0.30	0.80			
3	Cirriform	0.38	0.45	0.60	0.90			
	Middle	0.06	0.20	0.40	0.90			
	Cumuliform	0.30	0.00	0.00	0.00	0.22	0.36	0.57
	Stratiform	0.10	0.40	0.60	0.80			
	Mixed	0.16	0.00	0.30	0.60			
4	Cirriform	0.22	0.40	0.55	0.90			
	Middle	0.05	0.10	0.20	0.90			
	Cumuliform	0.32	0.00	0.00	0.00	0.11	0.20	0.51
	Stratiform	0.09	0.20	0.40	0.80			
	Mixed	0.32	0.00	0.10	0.60			
5	Cirriform	0.15	0.35	0.50	0.90			
	Middle	0.01	0.10	0.20	0.90			
	Cumuliform	0.28	0.00	0.00	0.00	0.07	0.16	0.50
	Stratiform	0.09	0.20	0.40	0.80			
	Mixed	0.47	0.00	0.10	0.60			
6	Cirriform	0.27	0.30	0.45	0.85			
	Middle	0.02	0.10	0.20	0.85			
	Cumuliform	0.29	0.00	0.00	0.00	0.11	0.20	0.42
	Stratiform	0.11	0.20	0.40	0.70			
	Mixed	0.31	0.00	0.10	0.30			
7	Cirriform	0.25	0.00	0.45	0.85			
	Middle	0.03	0.00	0.10	0.85			
	Cumuliform	0.16	0.00	0.00	0.00	0.00	0.13	0.44
	Stratiform	0.09	0.00	0.20	0.70			
	Mixed	0.47	0.00	0.00	0.30			
8	Cirriform	0.23	0.00	0.40	0.85			
	Middle	0.06	0.00	0.10	0.85			
	Cumuliform	0.05	0.00	0.00	0.00	0.00	0.12	0.48
	Stratiform	0.09	0.00	0.20	0.70			
	Mixed	0.57	0.00	0.00	0.30			
9	Cirriform	0.15	0.00	0.40	0.80			
	Middle	0.09	0.00	0.10	0.80			
	Cumuliform	0.04	0.00	0.00	0.00	0.00	0.09	0.26
	Stratiform	0.12	0.00	0.20	0.60			
	Mixed	0.60	0.00	0.00	0.00			
10	Cirriform	0.09	0.00	0.35	0.80			
	Middle	0.07	0.00	0.10	0.80			
	Cumuliform	0.01	0.00	0.00	0.00	0.00	0.13	0.40
	Stratiform	0.46	0.00	0.20	0.60			
	Mixed	0.37	0.00	0.00	0.00			

[a] Derived from the observational data of Lund and Shanklin (1973).

probabilities of the various cloud forms as a function of sky cover were inferred from data of Lund and Shanklin (1973). These data are observational results for Columbia, Missouri, although Lund and Shanklin suggest that they can be generalized to other continental midlatitude sites without substantial error. Occurrence probabilities for each site should be used but, as discussed previously, such statistical data are not routinely available. Histograms of the weighted cloud transmissivity τ_j as a function of total sky cover j for the three models are shown in Figure 1.4-3.

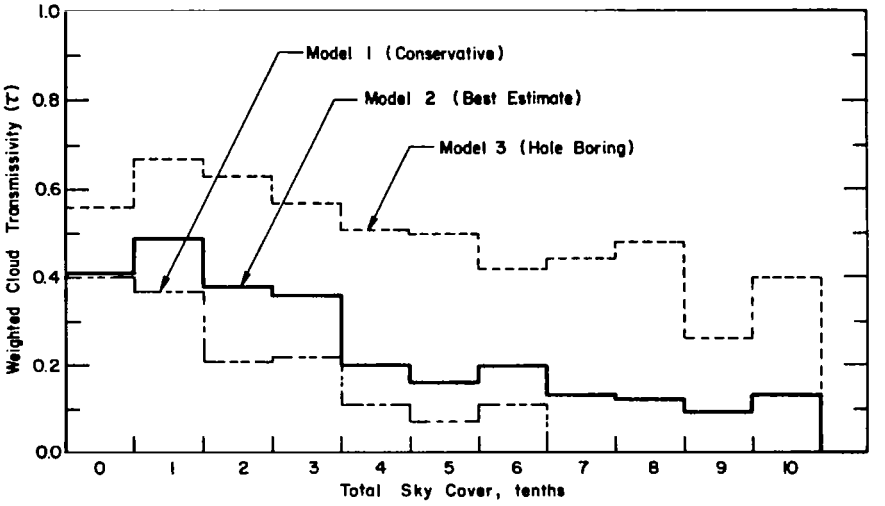

Figure 1.4-3. Cloud transmissivity models.

1.4.3 STATISTICAL RESULTS AND ANALYSIS

Statistical calculations of the seasonal and annual power availabilities, transmission frequencies, and persistence frequencies were performed for each of the sites designated in Table 1.4-5 and computer generated tabular data are presented in the appendix. The calculational results clearly demonstrate the marked influence meteorological conditions have on laser propagation. Indeed, operational procedures and siting criteria must be much different for power transmission employing laser radiation rather than microwaves. This analysis leads to a reformulation of these requirements so that laser power transmission can achieve power-availability levels at the commercial grid equivalent to those for the microwave-SPS concept and conventional electric-power plants. This performance is believed to be feasible within constraints imposed by safety and environmental considerations.

A comparison of the annual power availability for the various U.S. regions is shown in Figure 1.4-4. The low end of the range corresponds to average results for Model 1, while the high end corresponds to the improved conditions affected by hole boring (Model 3). Average results for Model 2 usually fall close to the low end of the range and are only slightly better than for Model 1. Seasonal variations for all models are highly region-dependent, as would be expected intuitively, and are often pronounced. Hole boring affords and improvement in the annual power availability of from 9% to 33% compared with Model 2; significantly larger improvements are not possible without utilizing weapon-quality beams. Seasonal improvements can exceed 50%.

Table 1.4-5. Receptor sites and associated sources of statistical climatological data.

Geographical region	Site number	Weather station
Southeast	SE-1	Huntsville, Alabama
	SE-2	MacDill AFB (Tampa), Florida
	SE-3	Dobbins AFB (Marietta), Georgia
	SE-4	Columbus AFB, Mississippi
	SE-5	Fort Bragg (Fayetteville), North Carolina
South Central	SC-1	Little Rock AFB, Arkansas
	SC-2	Barksdale AFB (Shreveport), Louisiana
	SC-3	Kirtland AFB (Albuquerque), New Mexico
	SC-4	Sheppard AFB (Wichita Falls), Texas
	SC-5	Connally AFB (Waco), Texas
Southwest	SW-1	Luke AFB (Phoenix), Arizona
	SW-2	McClellan AFB (Sacramento), California
	SW-3	Nellis AFB (Las Vegas), Nevada
Atlantic	AT-1	Griffis AFB (Rome), New York
	AT-2	Quantico, Virginia
New England	NE-1	Pease AFB (Portsmouth), New Hampshire
Midwest	MW-1	Chanute AFB (Rantoul), Illinois
	MW-2	Wright-Patterson AFB (Dayton), Ohio
Central	CN-1	Whiteman AFB, Missouri
North Central	NC-1	Ellsworth AFB (Rapid City), South Dakota
	NC-2	Hill AFB (Ogden), Utah
Northwest	NW-1	Fort Lewis (Gray), Washington

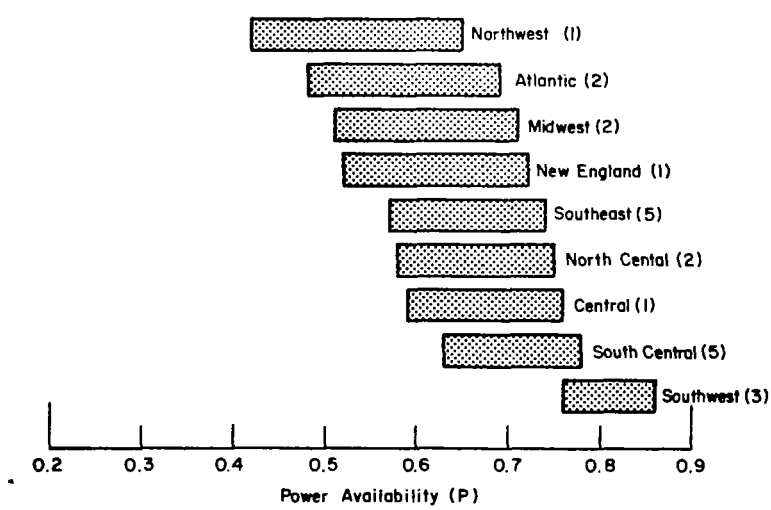

Figure 1.4-4. Annual power availability for the various U.S. regions. The number in parentheses is the number of sites analyzed in the region.

Differences in the prevailing meteorological conditions within the regions are more readily apparent when transmission frequencies are compared, as in Figure 1.4-5. The poor performance of sites in the northwest, Atlantic, midwest, and New England regions is particularly noticeable. Only sites in the southwest region offer a power availability in excess of 80% and a frequency for acceptable transmission efficiency ($T \geq 0.80$) suitable for commercial interest. To remedy this situation, it is obvious that the laser-SPS concept must rely upon multiple receptor sites for each transmitted beam.

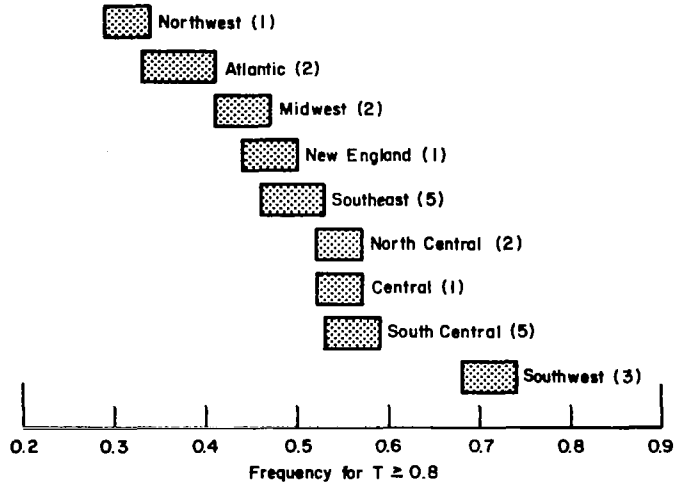

Figure 1.4-5. Annual frequency for which the transmission efficiency equals or exceeds 80% for the various U.S. regions.

To establish receptor placement criteria and beam-switching scenarios, a knowledge of the persistence times for an acceptable transmission efficiency is needed. Persistence frequencies for a persistence time of eight hours are tab ulated in the appendix for all sites. To illustrate the wide range of behavior, the seasonal persistence frequency for $T \geq 0.8$ is plotted as a function of persistance time in Figure 1.4-6 for sites having the best and worst meteorological conditions. Again, the pessimistic lower curves correspond to Model 1 and the optimistic upper curves correspond to Model 3. Attempted hole boring is of no use for sites plagued by frequent and heavy overcasts. For the "better" sites, hole boring is significantly beneficial at later times, being able to penetrate thin, high clouds which often precede the passage of a warm front. We have observed cases where the use of hole boring extends the period of acceptable transmission efficiency by factors of 2 to 3. For sites having intermediate meteorological conditions, hole boring offers an improvement in the persistence frequency at slightly earlier persistence times, but increases in the period of acceptable transmission efficiency are not as dramatic. Only the southwestern sites given persistence frequencies exceeding 50% for eight-hour persistence times. Even so, no site attains this level of performance for all seasons.

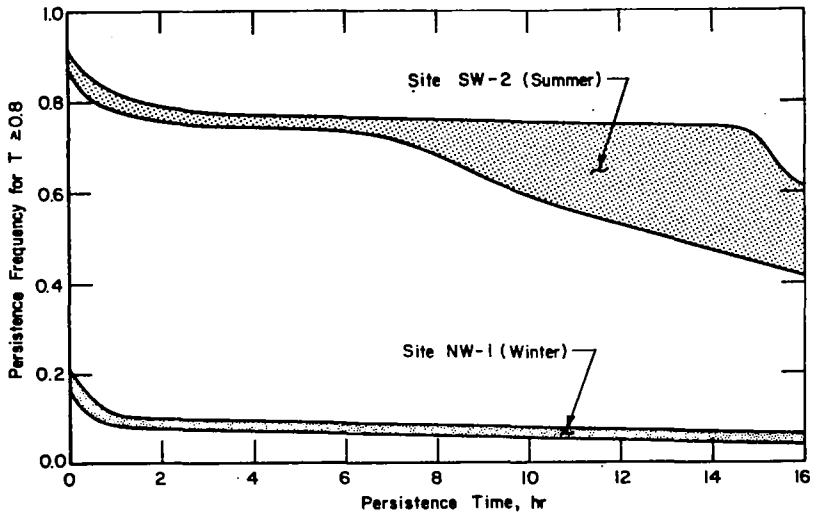

Figure 1.4-6. Frequency for which the transmission efficiency remains equal to or greater than 80% as a function of persistence time for the best and worst conditions encountered.

As alluded earlier, the calculational results are particularly insensitive to the assumed values of cloud transmission efficiency, especially for Models 1 and 2. Because the probability of a CFLOS, C_j, is close to unity during periods of negligible or scattered cloud cover (j = 0 to 3), the $(1 - C_j)\tau_j$ term in Equation (16) is small and less significant than the first term, C_j. Since the sky-cover occurrence-frequency curve is usually U-shaped, as illustrated by the solid histogram in Figure 1.4-7, differences in the numerical results of

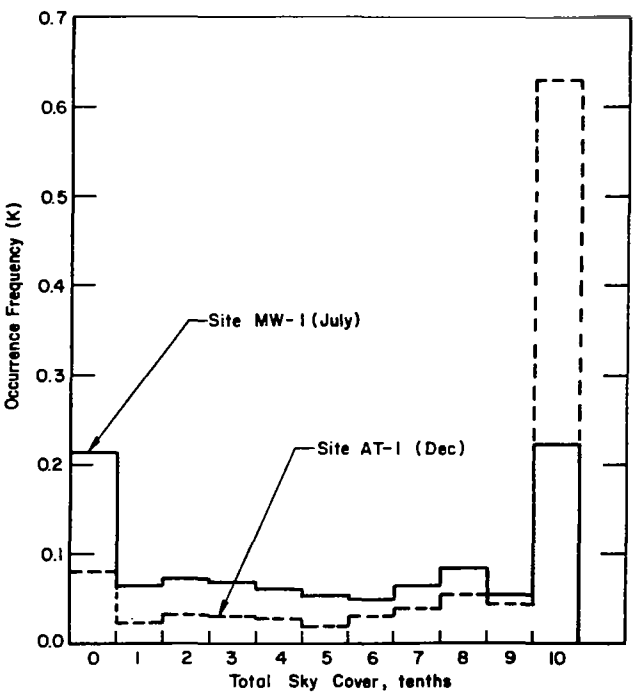

Figure 1.4-7. Representative sky-cover occurrence frequency histograms.

various cloud-transmissivity models are small if the τ_j curve decreases rapidly with increasing sky cover (e.g., Models 1 and 2). If partial transmission is assumed during periods of overcast conditions (j = 8 to 10), the $(1 - C_j)\tau_j$ term in Equation (16) dominates. The calculated T_j is then statistically significant because of the magnitude of K_{8-10}. Hence, Model 3, which assumes a slower decrease in τ_j with increasing sky cover, shows markedly different behavior when compared with the first two models and is subject to greater possible error. Because $(1 - C_j)\tau_j \ll C_j$ in Model 1, potentially large errors in the model can only be due to errors in the probabilities of a CFLOS and not to details of the τ_j dependence. The statistical sample size of Lund and Shanklin's C_j data is large and they have reportedly checked the applicability of their model to other midlatitude sites, so we reassert the belief that Model 1 places a lower bound on the expected performance of space-to-earth transmission using lasers. For a few climatic conditions, the sky-cover occurrence-frequency curve appears as a reclining J as shown by the dashed histogram in Figure 1.4-7. If the intermediate values of K_j are statistically significant, i.e., $K_{2-6} \gtrsim 0.1$, then observable differences between the predictions of Models 1 and 2 will develop under these conditions. Most of the sky-cover data, however, are U-shaped and large differences between the first two models never occur.

Laser power transmission to a single, dedicated site cannot achieve the power availability and persistence time necessary for commercial viability of the laser-SPS concept. Multiple receptor sites must be available for each transmitted beam, and rapid-switching capability is essential. The development of a power-availability model for multiple sites requires an estimate of the joint probability of a CFLOS for at least 1 of N available sites ($\hat{P}$) which, in turn, requires a climatic record of aky-cover observations taken simultaneously from each of the N sites [Lund (1973a)]. Climatic summaries of sky-cover occurrence frequencies, as used previously, will not suffice. Such simultaneous data are scarce, and we can only project estimates of the number of sites N and average separation $\hat{r}$ necessary to achieve viable performance levels.

If we neglect the contribution of partial transmission through certain cloud types, then our calculated power availability (P) and Lund's joint CFLOS probability are identical for N = 1. Obtaining commercially acceptable transmission frequencies, e.g., $f \geq 0.8$ for $T \geq 0.80$, is highly correlated with power availability such that $\overline{P} \gtrsim 0.9$. Hence, if we plot curves of $\hat{P}$(1 of N) versus N for several different sites separations, $\hat{r}$, we can roughly estimate the receptor criteria for multiple sites. Using data for three sites in North Dakota taken for the month and hours when the CFLOS probabilities are the lowest, we have attempted to parameterize the dependence of $\hat{P}$ on N and $\hat{r}$. Figure 1.4-8 gives Lund's data, connected by solid lines, and estimates of $\hat{P}$ for larger and smaller average site separations, shown by dotted lines. The average site separation is defined by the centroid radius

$$\hat{r} = \frac{1}{N}\left[\sum_{i=1}^{N-1}\left(\sum_{j=i+1}^{N} \ell_{ij}^2\right)\right]^{1/2} , \qquad (32)$$

where ℓ_{ij} is the distance between sites i and j.

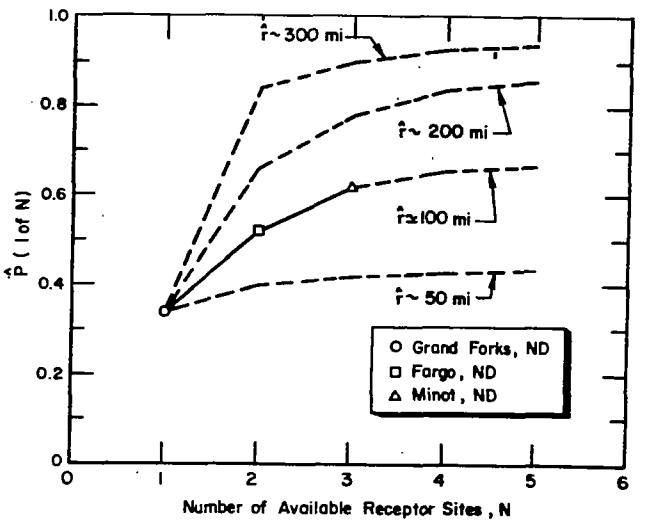

Figure 1.4-8. Probability of a CFLOS for at least one site given that N are available.

The behavior depicted in Figure 1.4-8 is probably representative of other regions giving poor single-site power availabilities, such as the northwest region in winter. To meet our criteria of $f \geq 0.8$ for $T \geq 0.80$ under these conditions, three receptor sites must be available separated by $\hat{r} \sim 300$ miles. For the majority of other regions, for which P ranges from about 0.4 to 0.7, the centroid radius may be reduced to $\hat{r} \sim 200$ miles. Only for the southwest region can the number of mandatory receptor sites be reduced to N = 2. Under these conditions, the average site separation could be as close as 100 miles. The average persistence time, defined as the average time for which the beam remains at a given receptor before the transmission efficiency becomes unacceptable ($T < 0.8$) and the beam must be switched to an alternate site, ranges from greater than 24 hours for southwestern sites to less than 4 hours for the least favorable sites. Obviously, the receptor device, laser transmitter, and electric-power grid must be capable of accommodating these switching demands.

1.5 CONCLUSIONS AND RECOMMENDATIONS

This study has examined potential mitigation techniques which can minimize the deleterious effects of inclimate weather on space-to-earth power transmission using lasers. We have investigated the choice of laser wavelength, propagation zenith angle, receptor-site elevation, and the potential of laser hole boring. An extensive series of propagation calculations have been performed to estimate the attenuation due to molecular absorption and aerosol absorption and scattering. All commonly encountered meteorological conditions have been modeled, including haze, fog, clouds, rain and snow, and compared with observational data when available.

Using these mitigation techniques as guidelines, preliminary receptor siting criteria were defined and 22 candidate sites in the contiguous United States were selected for detailed study. A power availability model has been developed which uses statistical meteorological data for each site to calculate the annual and seasonal power availability (average transmission efficiency assuming constant power beaming) and the frequency for which the transmission efficiency exceeds a given value for a specified persistence time. The results of this work enable us to redefine siting criteria and laser parameters such that the power availability is comparable to the microwave-SPS concept or to conventional electric-power plants.

Specific conclusions of this research are as follows:

- At high elevations, atmospheric transmission windows in the wavelength region around 11 μm provide the best combined propagation efficiency considering both molecular absorption and aerosol extinction. At low elevations, laser operation at a wavelength near 2.25 μm is preferable.

- If the laser wavelength is properly optimized, operation at a propagation zenith angle of 0° instead of 50° does not afford a significant improvement in the power availability and cannot be juctified in terms of the increased cost and complexity of the required space hardware.

- High-elevation receptor sites are desirable although not essential to the laser-SPS concept because of the reduction in attenuation due to haze and molecular absorption.

- Laser hole boring at $\lambda \simeq 11$ μm through certain types of haze, fogs, and clouds may be possible consistent with safety and environmental concerns and without the need for weapon-quality laser beams; in particular, all but the thickest cirriform and middle clouds and all stratiform clouds with the exception of nimbostratus can be penetrated with power densities of 100-200 W/cm^2. All other cloud types will require substantially higher power densities for penetration, which is unacceptable given the present safety margins.

- At $\lambda \simeq 2$ μm, hole boring is only feasible using combined repetitively pulsed/cw operation; this mode of operation may be preferable, however, since the average power density can be reduced to allow unrestricted transmission air-zone access.

- Power availabilities in excess of 80% are unattainable in most geographical regions of the United States if only a single receptor site is available for each transmitted laser beam (the exception is the southwestern United States).

- Hole boring, as defined above, will increase the annual power availability by 9 to 33% depending upon the cloud-form frequencies of the individual sites and can be particularly beneficial in extending the persistence time for an acceptable transmission efficiency.

- If an 80% frequency for the transmission efficiency to equal or exceed 80% is defined as the minimum requirement for commercial viability of the laser-SPS concept, then three receptor sites separated by a centroid radius of from 200 to 300 miles must be available for each transmitted laser beam for most regions of the United States; for the southwest region, however, only two sites separated by as little as 100 miles will be sufficient.

- The average persistence time, during which the prevailing meteorological conditions allow a high transmission efficiency, is considerably shorter than eight hours at many sites, so that any viable laser-SPS concept must be capable of frequent beam switching between sites with a minimum of downtime.

- Under the aforementioned circumstances, thermodynamic laser-energy conversion schemes may be unsuitable because of the long start-up times required by rotating turbomachinery.

Therefore, the laser-SPS concept must be based on the availability of multiple sites for each transmitted beam, accompanied by frequent beam-switching between sites. Obviously, this operational scenario is considerably different from that envisioned for the microwave-SPS concept, and the economic and engineering viability of the multiple-site concept must be further evaluated. Superficially, it seems that the smaller land area required for each laser-receptor site will outweight the additional cost of three times the number of sites and their associated hardware when compared with the microwave-SPS concept. An evaluation of the effects of frequent beam switching will require an analysis of the dynamic response of the electric-power grid. Additional recommendations of needed research include:

- Examination of potential short-wavelength transmission windows for aerosols

- Further theoretical and experimental research on combined repetitively pulsed/cw laser hole boring

- Development of efficient laser-energy conversion schemes not based on thermal cycles

- Development of a joint power-availability model for multiple sites including more sophisticated statistical cloud-cover models and the statistical effects of frontal passage over multiple-site clusters.

1.6 REFERENCES

Akhmanov, S. A. et al. (1968). "Thermal self-actions of laser beams," IEEE J. Quant. Electron. QE-4, 568.

Almayev, R. Kh. et al. (1978). "The temperature and water content in the cloud clearance zone," Izv. Acad. Sci. USSR Atmos. Oceanic Phys. 14, 208.

Bartlett, J. T. and Jones, P. R. (1972). "On the dispersion of the sizes of droplets growing by condensation in turbulent clouds," Quart. J. R. Met. Soc. 98, 150.

Bedair, S. M. and Aly, S. S. (1975). "Fog dissipation using 10.6 μm radiation," Infrared Phys. 15, 233.

Belyayev, V. P. et al. (1975). "Observational studies of the clearing of fog by laser radiation at λ = 10.6 μm," Izv. Acad. Sci. USSR Atmos. Oceanic Phys. 11, 678.

Beverly, R. E. III (1979). "SPS-laser environmental impact study," Final Report to Rockwell International Corporation, Space Systems Group on Contract No. M9M 8BNB-896662D.

Beverly, R. E. III (1980). "Laser-SPS systems analysis and environmental impact assessment," submitted to Space Solar Power Review.

Bisyarin, V. P. and Sokolov, A. V. (1974). "Theoretical estimation of the effect of the complex refractive index of water drops on the amount of attenuation of 10.6 μm laser radiation in fog," Radio Eng. Electron. Phys. (USSR) 19, 101.

Bisyarin, V. P. et al. (1978). "On the hydrometeor attenuation of laser radiation at 10.6 and 0.63 μm wavelength at mountain altitudes (in Russian)," Izv. Akad. Nauk Arm. SSR Fiz. 13, 324.

Breene, R. G. Jr. et al. (1969). "Interpretation of OV1-5 spectrometric observations," J. Quant. Spectrosc. Radiat. Transfer 9, 1239.

Brewer, A. W. and Houghton, J. T. (1956). "Some measurements of the flux of infrared radiation in the atmosphere," Proc. Roy. Soc. (London) 20, 175.

Bukatyi, V. I. and Pogodaev, V. A. (1970). "Evaporation of a water drop by ir radiation," Sov. Phys. J., No. 1, 119.

Bukatyi, V. I. et al. (1973). "Thermal defocusing of the optical radiation traveling in an absorbing disperse medium," Sov. J. Quant. Electron. 3, 37.

Bukatyi, V. I. et al. (1975). "Thermal effect of intense light beams on droplet aerosols," Sov. Phys. Dokl. 19, 425.

Caledonia, G. E. and Wray, K. L. (1974). "Aerosol propagation effects," Physical Sciences Inc. Final Report on Contract No. N00014-74-C-0254.

Carrier, L. W. et al. (1967). "The backscattering and extinction of visible and infrared radiation by selected major cloud models," Appl. Opt. 6, 1209.

Chu, T. S. and Hogg, D. C. (1968). "Effects of precipitation on propagation at 0.63, 3.5, and 10.6 microns," Bell Sys. Tech. J. 47, 723.

Chýlek, P. (1978). "Extinction and liquid water content of fogs and clouds," J. Atmos. Sci. 35, 296.

Coburn, A. R. (1971). "Improved three-dimensional nephanalysis model," Air Force Global Weather Center Tech. Memo. AFGWC-TM-71-2.

Cohen, A. (1975). "Cloud-base water content measurement using single wavelength laser-radar data," Appl. Opt. 14, 2873.

Deirmendjian, D. (1964). "Scattering and polarization properties of water clouds and haze in the visible and infrared," Appl. Opt. 3, 187.

Deirmendjian, D. (1969). Electromagnetic Scattering on Spherical Polydispersions, American Elsevier, New York.

Dugin, V. P. et al. (1976). "Spectral transmission of artificial crystalline cloud formations," Izv. Acad. Sci. USSR Atmos. Oceanic Phys. 12, 271.

Eldridge, R. G. (1966). "Haze and fog aerosol distributions," J. Atmos. Sci. 23, 605.

Eldridge, R. G. (1971). "The relationship between visibility and liquid water content in fog," J. Atmos. Sci. 28, 1183.

Elterman, L. (1968). "UV, visible, and ir attenuation for altitudes to 50 km, 1968," Air Force Geophysics Laboratory Report No. AFCRL-68-0153.

Falls, L. W. (1974). "The Beta distribution: A statistical model for world cloud cover," J. Geophys. Res. 79, 1261.

Feddes, R. G. and Liou, K.-N. (1977). "Cloud composition determination by satellite sensing using the Nimbus VI high resolution infrared sounder," Air Force Geophysics Laboratory Report No. AFGL-TR-77-0123.

Friedmann, D. et al. (1979). "Nonlinear transmission of fog for laser light," J. Appl. Phys. 50, 5998.

Fritz, S. and Rao, P. K. (1967). "On the infrared transmission through cirrus clouds and the estimation of relative humidity from satellites," J. Appl. Meteor. 6, 1088.

Galakhov, N. V. et al. (1976). "An observational study of intensity fluctuations of optical radiation propagating in the atmospheric surface layer during precipitation," Izv. Acad. Sci. USSR Atmos. Oceanic Phys. 12, 777.

Garland, J. A. (1971). "Some fog droplet size distributions obtained by an impaction method," Quart. J. R. Met. Soc. 97, 483.

Garland, J. A. et al. (1973). "A study of the contribution of pollution to visibility in a radiation fog," Atmos. Environ. 7, 1079.

Gates, D. M. and Shaw, C. C. (1960). "Infrared transmission of clouds," J. Opt. Soc. Am. 50, 876.

Gebhardt, F. G. (1976). "High power laser propagation," Appl. Opt. 15, 1479.

Georgiyevskii, Yu. S. and Shukurov, A. Kh. (1974). "Certain results of measurements of the transmission of thin clouds in the visible and infrared," Izv. Acad. Sci. USSR Atmos. Oceanic Phys. 10, 53.

Glicker, S. L. (1971). "Propagation of a 10.6-μ laser through a cloud including droplet vaporization," Appl. Opt. 10, 644.

Goodmann, J. (1977). "The microstructure of California coastal fog and stratus," J. Appl. Meteor. 16, 1056.

Gordin, M. P. and Strelkov, G. M. (1975a). "The passage of laser radiation through a fine-droplet water aerosol," Radio Eng. Electron. Phys. (USSR) 20, 1.

Gordin, M. P. and Strelkov, G. M. (1975b). "Supercondensation effect in diffusion evaporation of a water aerosol in radiation field," Sov. J. Quant. Electron. 5, 315.

Guzzi, R. et al. (1974). "Sun spectra through optically thin clouds," J. Atmos. Sci. 31, 251.

Hall, F. F. Jr. (1968). "The effect of cirrus clouds on 8-13 μm infrared sky radiance," Appl. Opt. 7, 891; "Physical model of cirrus 8-13 μm infrared radiance," Appl. Opt. 7, 2264.

Harney, R. C. (1977). "Hole-boring in clouds by high intensity laser beams: Theory," Appl. Opt. 16, 2974.

Hobbs, P. V. (1974). "The dimensions and aggregation of ice crystals in natural clouds," J. Geophys. Res. 79, 2199.

van de Hulst, H. (1964). Light Scattering by Small Particles, John Wiley and Sons, New York.

Joss, J. et al. (1968). "The variation of raindrop size distributions at Locarno," Proc. Int. Conf. on Cloud Phys., Am. Meteor. Soc., Boston, p. 369.

Kerker, M. et al. (1962). "Light scattering functions for concentric spheres. Total scattering coefficient, $m_1 = 2.1050$, $m_2 = 1.4821$," J. Opt. Soc. Am. 52, 551.

Kolosov, V. V. and Kuzikovskii, A. V. (1979). "Focusing and defocusing of light in an aerosol exploded by a laser beam," Sov. Phys. Tech. Phys. 24, 56.

Kuhn, P. M. and Weickmann, H. K. (1969). "High altitude radiometric measurements of cirrus," J. Appl. Meteor. 8, 147.

Kuhn, P. M. et al. (1974). "Transfer of infrared radiation through clouds," Appl. Opt. 13, 512.

Kumai, M. (1973). "Arctic fog droplet size distribution and its effect on light attenuation," J. Atmos. Sci. 30, 635.

Kunkel, B. A. (1971). "Fog drop-size distributions measured with a laser hologram camera," J. Appl. Meteor. 10, 482.

Kuzikovskii, A. V. (1970). "Dynamics of a spherical particle in an intense optical field," Sov. Phys. J., No. 5, 615.

Kuzikovskii, A. V. and Khmelevitsov, S. S. (1968). "Kinetics of the evaporation of an aqueous aerosol in an optical radiation field," Izv. Acad. Sci. USSR Atmos. Oceanic Phys. 4, 206.

Kuzikovskii, A. V. and Khmelevitsov, S. S. (1975). "Influence of overcondensation on the evaporation of a water aerosol in a radiation field," Izv. Acad. Sci. USSR Atmos. Oceanic Phys. 11, 219.

Kuzikovskii, A. V. et al. (1971). "Evaporation of a drop of water under the influence of a pulse of light," Sov. J. Engr. Phys. 20, 12.

Lamb, G. L. Jr. and Kinney, R. B. (1969). "Evaporation of mist by an intense light beam," J. Appl. Phys. 40, 416.

Laws, J. O. and Parsons, D. A. (1943). "The relation of rain drop size to intensity," Trans. Am. Geophys. Union 24, 452.

Lewis, W. (1951). "Meteorological aspects of aircraft icing," in Compendium of Meteorology, T. F. Malone, ed., Amer. Meteor. Soc., Boston.

Liou, K.-N. (1972). "Light scattering by ice clouds in the visible and infrared: A theoretical study," J. Atmos. Sci. 29, 524.

Liou, K.-N. (1974). "On the radiative properties of cirrus in the window region and their influence on remote sensing of the atmosphere," J. Atmos. Sci. 31, 522.

Liou, K.-N. (1977). "Remote sensing of the thickness and composition of cirrus clouds from satellites," J. Appl. Meteor. 16, 91.

Liou, K.-N. and Wittman, G. D. (1979). "Parameterization of the radiative properties of clouds," J. Atmos. Sci. 36, 1261.

List, R. and Gillespie, J. R. (1976). "Evolution of raindrop spectra with collision-induced breakup," J. Atmos. Sci. 33, 2007.

Lund, I. A. (1973a). "A model for estimating joint probabilities of cloud-free lines-of-sight through the atmosphere," J. Appl. Meteor. 12, 1040.

Lund, I. A. (1973b). "Persistence and recurrence probabilities of cloud-free and cloudy lines-of-sight through the atmosphere," J. Appl. Meteor. 12, 1222.

Lund, I. A. and Shanklin, M. D. (1973). "Universal methods for estimating probabilities of cloud-free lines-of-sight through the atmosphere," J. Appl. Meteor. 12, 28.

McCartney, E. J. (1976). Optics of the Atmosphere, Scattering by Molecules and Particles, John Wiley and Sons, New York.

McClatchey, R. A. and D'Agati, A. P. (1978). "Atmospheric transmission of laser radiation: Computer code LASER," Air Force Geophysics Laboratory Report No. AFGL-TR-78-0029.

McClatchey, R. A. and Selby, J. E. A. (1974). "Atmospheric attenuation of laser radiation from 0.76 to 31.25 μm," Air Force Geophysics Laboratory Report No. AFCRL-TR-74-0003.

McClatchey, R. A. et al. (1973). "AFCRL atmospheric line parameters compilation," Air Force Geophysics Laboratory Report No. AFCRL-TR-73-0096. The latest version of the computer tape (October, 1978) was used in these calculations.

McTaggart-Cowan, J. D. and List, R. (1975). "Collision and breakup of water drops at terminal velocity," J. Atmos. Sci. 32, 1401.

Mullaney, G. J. et al. (1968). "Fog dissipation using a CO_2 laser," Appl. Phys. Lett. 13, 145.

Nakajima, S. et al. (1973). "Propagation of the laser light in snowfall," Electron. Commun. Japan 56B, 79.

Nerushev, A. F. and Semenov, L. P. (1976). "Propagation of a light beam in an evaporating liquid-drop medium in the presence of wind refraction," Sov. J. Quant. Electron. 6, 665.

Nilsson, B. (1979). "Meteorological influence on aerosol extinction in the 0.2-40-μm wavelength range," Appl. Opt. 18, 3457.

Nybro, R. (1980). Private communication, National Climatic Center, NOAA (Ashville, NC).

Orlov, A. P. et al. (1976). "Aircraft studies of vertical infrared extinction profiles in the 10-12 μm window," Izv. Acad. Sci. USSR Atmos. Oceanic Phys. 12, 433.

Passarelli, R. E. Jr. (1978). "Theoretical and observational study of snow-size spectra and snowflake aggregation efficiencies," J. Atmos. Sci. 35, 882.

Pilié, R. J. et al. (1975). "The life cycle of valley fog. Part II; Fog microphysics," J. Appl. Meteor. 14, 364.

Pinnick, R. G. et al. (1978). "Vertical structure in atmospheric fog and haze and its effects on visible and infrared extinction," J. Atmos. Sci. 35, 2020-2032; see also U.S. Army Atmospheric Sciences Laboratory Report No.ASL-TR-0010.

Pinnick, R. G. et al. (1979). "Verification of a linear relation between ir extinction, absorption and liquid water content of fogs," J. Atmos. Sci. 36, 1577-1586; see also U.S. Army Atmospheric Sciences Laboratory Report No. ASL-TR-0037.

Platt, C. M. R. and Bartusek, K. (1974). "Structure and optical properties of some middle-level clouds," J. Atmos. Sci. 31, 1079.

Platt, C. M. R. (1976). "Infrared absorption and liquid water content in stratocumulus clouds," Quart. J. R. Met. Soc. 102, 553.

Prishivalko, A. P. and L. G. Astaf'yeva, (1974). "Absorption, scattering and extinction of light by water-coated atmospheric particles," Izv. Acad. Sci. USSR Atmos. Oceanic Phys. 10, 815.

Rensch, D. B. and Long, R. K. (1970). "Comparative studies of extinction and backscattering by aerosols, fog, and rain at 10.6 μ and 0.63 μ," Appl. Opt. 9, 1563.

Roach, W. T. et al. (1976). "The physics of radiation fog: I -- a field study," Quart. J. R. Met. Soc. 102, 313.

Romanov, G. S. and Pustovalov, V. K. (1973). "Transillumination of a water-droplet-containing cloudy atmosphere with an intensive monochromatic radiation," J. Appl. Spectrosc. 19, 1072.

Ruck, G. T. (1980). Personal communication.

Ruppersberg, G. H. et al. (1975). "Calculations about the transmittance window of clouds and fog at about 10.5 μm wavelength," Atmos Environ. 9, 723.

Schickel, K. P. (1972). "Datensammlung über die Größenverteilung von Nebel- und Wolkentropfen," DFVLR-Institut für Physik der Atmosphäre, Internal Report.

Semenov, L. P. and Svirkunov, P. N. (1971). "Evaporation of a drop in the presence of a considerable internal heat release (in Russian)," Tr. Inst. Eksp. Meteorol., No. 23, 91.

Sekhon, R. S. and Srivastava, R. C. (1970). "Snow size spectra and radar reflectivity," J. Atmos. Sci. 27, 299.

Shettle, E. P. and Fenn, R. W. (1975). "Models of atmospheric aerosols and their optical properties," AGARD Conf. Proc. 183, Optical Propagation in the Atmosphere. Available from NTIS, Springfield, VA.

Shifrin, K. S. and Zolotova, Zh. K. (1966). "Kinetics of the evaporation of drops in a radiation field," Izv. Acad. Sci. USSR Atmos. Oceanic Phys. 2, 800.

Sokolov, A. V. (1970). "Attenuation of visible and infrared radiation in rain and snow," Radio Eng. Electron. Phys. (USSR) 15, 2175.

Sukhorukov, A. P. and Shumilov, É. N. (1973). "Brightening of a polydisperse fog," Sov. Phys. Tech. Phys. 18, 650.

Sukhorukov, A. P. et al. (1971). "Dynamics of clearing clouds with a laser beam," JETP Lett. 14, 161.

Sutton, G. W. (1970). "Fog dispersal by high-power lasers," AIAA J. 8, 1907.

Sutton, G. W. (1978). "Fog hole boring with pulsed high-energy lasers: An exact solution including scattering and absorption," Appl. Opt. 17, 3424.

Svirkunov, P. N. (1978). "Possibility of self-focusing in the evaporation of a cloud medium by CO_2 laser radiation," Sov. J. Quant. Electron. 8, 509.

Takahashi, T. (1978). "Raindrop size distribution with collision breakup in an axisymmetric warm cloud model," J. Atmos. Sci. 35, 1549.

Tampieri, F. and Tomasi, C. (1976). "Size distribution models of fogs and cloud droplets in terms of the modified gamma function," Tellus 28, 333.

Tomasi, C. and Tampieri, F. (1976). "Size distribution models of small water droplets in mist and their volume extinction coefficients at visible and infrared wavelengths," Atmos. Environ. 10, 1005.

Volkovitskii, O. A. (1977). "Experimental studies of the effect of CO_2-laser emission upon the cloud droplet medium (in Russian)," Meteor. Hydrol. (USSR) 9, 9.

Volkovitskii, O. A. et al. (1974). "Some data on the propagation of CO_2 laser radiation in an ice cloud," Izv. Acad. Sci. USSR Atmos. Oceanic Phys. 10, 715.

Volkovitskii, O. V. et al. (1975). "'Turbidizing' effect of CO_2 laser radiation on crystalline clouds," Izv. Acad. Sci. USSR Atmos. Oceanic Phys. 11, 543.

Volkovitskii, O. A. et al. (1976). "Optical 'dimming' of cloud medium due to interaction with CO_2 laser radiation," Sov. J. Quant. Electron. 6, 215.

Vorob'yev, V. V. and Shemetov, V. V. (1975). "Forced convection in the atmosphere due to absorption of luminous radiation," Izv. Acad. Sci. USSR Atmos. Oceanic Phys. 11, 186.

Wang, T.-I. et al. (1979). "Path-averaged measurements of rain rate and raindrop size distribution using a fast-response optical sensor," J. Appl. Meteor. 18, 654.

Warner, J. (1969). "The microstructure of cumulus cloud. Part I. General features of the droplet spectrum," J. Atmos. Sci. 26, 1049.

Warner, J. (1973). "The microstructure of cumulus cloud. Part V. Changes in droplet size distribution with cloud age," J. Atmos. Sci. 30, 1724.

Warner, J. and Bichard, V. M. (1979). "The statistics of atmospheric extinction at the CO_2 laser wavelength derived from meteorological office records," Infrared Phys. 19, 15.

Wilson, R. W. and A. A. Penzias (1966). "Effect of precipitation on transmission through the atmosphere at 10 microns," Nature 211, 1081.

Yamamoto, G. et al. (1971). "Table of scattering function of infrared radiation for water clouds," NOAA Report No. COM-71-50312.

Zuev, V. E. et al. (1973). "Effect of heating water droplets by optical radiation," Sov. Phys. Dokl. 17, 765.

2.0 DIRECT SOLAR PUMPED LASERS FOR THE SATELLITE POWER SYSTEM

2.1 INTRODUCTION

Power transmission from satellites in earth orbit to terrestrial receptor sites using either microwave or laser beams is being investigated by NASA and the DOE as a possible commercial electric-power source. Although laser power transmission has the advantages of negligible environmental damage and small land requirements associated with the receptor sites,[1] meteorological conditions influence the transmission efficiency to a much greater extent than with microwaves, and no viable and substantiated laser concept exists which can compete with the microwave concept in terms of overall efficiency and specific mass (mass per unit of radiated power). The specific mass is of crucial importance because of the large cost of space transportation to high earth orbit. The influence of meteorological conditions on laser beam propagation is investigated in detail by the present author in Reference (2); the present study is concerned with a limited examination of advanced laser systems for the Satellite Power System (SPS).

Laser-SPS systems can be classified according to the method of solar power conversion and the type of laser. Specifically, the following combinations appear possible and have been investigated to various extents:

Solar-Power Conversion	Laser Type
Photovoltaic	Electric-Discharge Laser
Photovoltaic	Chemical
Photovoltaic	Free-Electron Laser
Thermal	Electric-Discharge Laser
Thermal	Chemical
Thermal	Free-Electron Laser
Thermal	Gas-Dynamic Laser
Thermal	Optically Pumped Laser
Quantum	Optically Pumped Laser
Quantum	Free-Electron Laser

The conversion efficiency of solar cells is $\lesssim 20\%$, and huge collector areas, oftentimes with solar concentrators, are required to achieve the desired power output. Thermal conversion is limited by the thermodynamic efficiency of the respective cycle. The high temperatures and exotic working fluids required for high efficiency operation may pose problems with system reliability. Furthermore, large-area space radiators are necessary to dispose of waste heat, thus adding to the satellite specific mass.

Quantum conversion relies upon excitation of discrete states in atomic or molecular systems via the solar flux. The conversion efficiency depends upon the fraction and wavelength interval of the solar spectrum which affect

excitation and the portion of the excited-state energy which is consumed in the lasing process. Solar concentration undoubtedly will be needed; to limit undue heating, the concentrators can be optically coated to pass that portion of the solar spectrum which is unusable and to reflect the useful portion into the lasing medium.

A detailed investigation of all of the laser systems listed above is not possible in conjunction with this limited study. Comparisons of some of the various possibilities were performed by Taussig et al.,[3] although their work was far from exhaustive. We have chosen to examine several candidate lasing schemes employing quantum conversion of the solar flux and optical pumping, i.e., "direct" solar pumped lasers. In particular, we have investigated optically pumped lasers employing electronic-vibrational energy transfer to triatomic molecules, atomic transitions in alkali metals, and atomic transitions in vapor-complex rare-earth-lanthanide ions.

2.2 PHOTOEXCITED E-V TRANSFER LASERS

Electronic-vibrational (E-V) transfer lasers operate by near-resonant energy transfer from an electronically excited atom (donor) to the lasing molecule (acceptor). The laser transition occurs between vibrational-rotational levels in the acceptor molecule. Two electronically excited atomic species which can be readily produced by optical pumping have been investigated and shown to achieve lasing in a number of molecular systems,[4,5] namely, $I(5^2P_{\frac{1}{2}})$ and $Br(4^2P_{\frac{1}{2}})$. $I(5^2P_{\frac{1}{2}})$ and $Br(4^2P_{\frac{1}{2}})$ are optically metastable, spin-orbit excited states with energies 7603 cm^{-1} and 3685 cm^{-1} above ground state. For solar photoexcitation, photodissociation of bromide compounds is preferred because a better spectral match exists between absorption features and the solar spectrum. Approximately 24% of the solar spectrum is useful in producing excited Br atoms, whereas only about 1% of the solar spectrum can produce excited I atoms since the photodissociation continuum lies in the soft-ultraviolet spectral region. Furthermore, if Br_2 is used as the photoytic source of excited Br atoms, then self-rejuvenation of the working gases will occur via recombination of ground-state Br atoms. Unfortunately, I_2 cannot be used as a photolytic source of excited I atoms since this molecule itself is the strongest quenching agent known. Other iodide compounds can be used, e.g., the perfluoroalkyl iodides, but the kinetics is more complicated and secondary byproducts quickly accumulate during the lasing process.[6] Complex chemical processing of the lasing gas mixture is required to rejuvenate the original iodide compound.[7]

To attain maximum laser efficiency, E-V energy transfer should be specific to the vibrational mode of the upper laser level. Energy transfer to competing modes should be avoided by selection of an appropriate acceptor molecule. The energy levels of several acceptor molecules made to lase in a $Br(4^2P_{\frac{1}{2}})$ E-V transfer laser are shown in Figure 2.2-1 and observed transitions are listed in Table 2.2-1. Energy transfer to N_2O, for example, involves levels (140) and (101) resulting in several kinetic paths for energy flow. Lasing on transitions in the 001→100 band has been observed, but complete energy channeling into the upper-level vibrational mode is impossible. For space-to-earth laser propagation, multiline laser operation characteristic of the heteronuclear

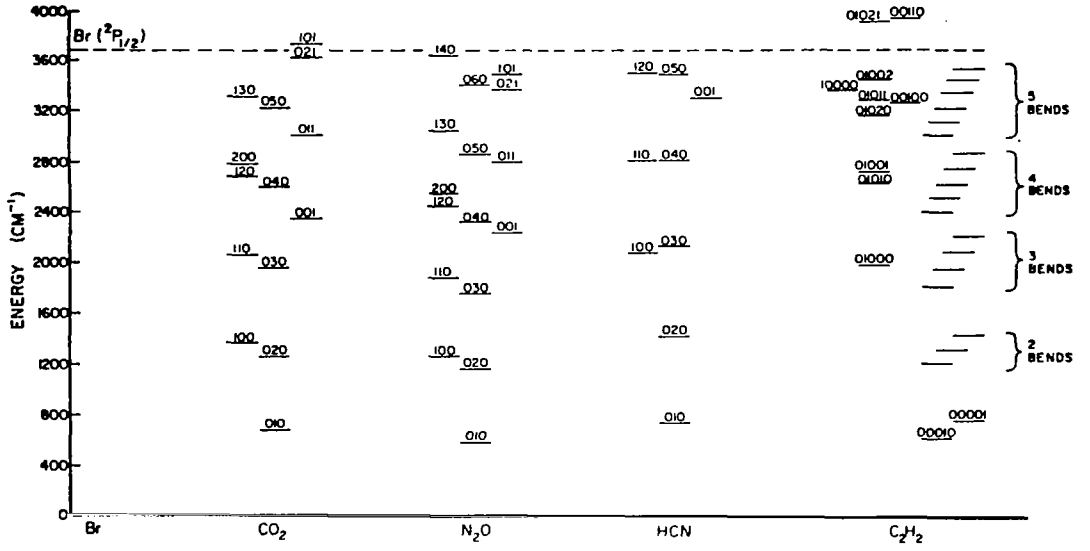

Figure 2.2-1. Molecular energy levels and $Br(4^2P_{\frac{1}{2}})$ excited-state energy.[4]

Table 2.2-1. E-V laser transitions pumped by $Br(4^2P_{\frac{1}{2}})$.

Molecule	Transition	Approximate wavelength, μm	Reference
CO_2	101→100	4.3	4,8,9,10,11
	001→020	9.6	
	001→100	10.6	
	101→011	14.1	
C_2H_2	00100→01000 (?)	7-8	4
HBr	v=1→0	3.9-4.2	12
(DBr)*	(v=1→0)	(5.4-5.7)	
HCl	v=1→0	3.5-3.8	12,13
(DCl)	(v=1→0)	(4.8-5.1)	
N_2O	001→100	10.9	4,14
HF	v=1→0	2.6-3.1	15
(DF)	(v=1→0)	(3.5-4.0)	
HCN	001→010	3.85	4,16
	001→100	8.48	
H_2O	020→010	7.1-7.7	14,17
NO	v=2→1	5.5	14

*Deuterated analogs are shown even though lasing with these molecules has not been attempted.

diatomic molecules is undesirable because of beam focusing and pointing difficulties and transmission inefficiencies. If atmospheric transmission efficiency is also considered, only tow of the molecular species listed in Table 2.2-1 remain as potentially viable candidates for a direct solar-pumped E-V transfer laser, namely, HCN (001→010) with $\lambda \simeq 3.9$ μm and the low-abundance isotopic-species $^{13}C^{16}O_2$ (001→100) with $\lambda \simeq 11$ μm. Because kinetic data are readily available for the CO_2 system, this laser was chosen for detailed modeling.

The lasing scheme is shown energetically in Figure 2.2-2. Optical pumping produces bromine atoms in both the excited $4^2P_{\frac{1}{2}}$ and ground $4^2P_{3/2}$ states. Collisions of excited Br atoms with CO_2 molecules in the ground state produce vibrational excitation of the (101) level which relaxes almost immediately into the (001) level via rapid intramode vibrational-vibrational (VV) processes. Stimulated emission (lasing) occurs between the asymmetric stretch (001) level and the symmetric stretch (100) level. Rapid intermode VV relaxation occurs between the (100) and (020) levels and, finally, the bending mode relaxes to the ground (000) state via vibrational-translational (VT) collisions. Because of the close proximity of the (010) level of the bending mode to the ground state, it is important that a buffer gas (e.g., He) be provided to affect

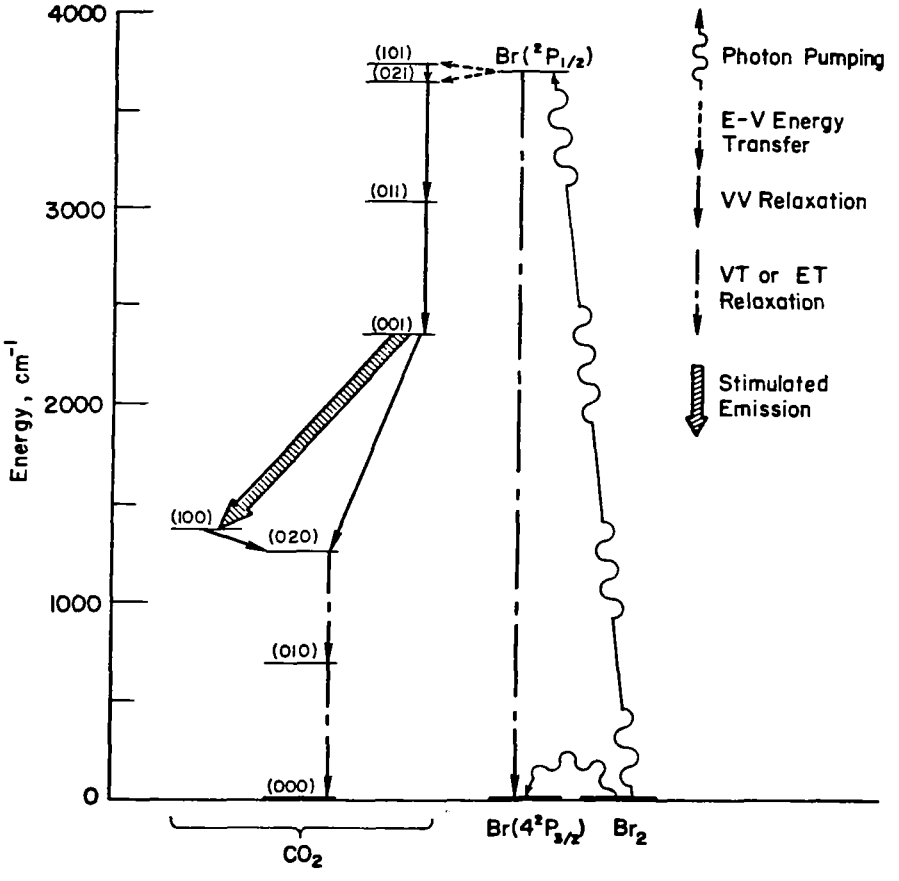

Figure 2.2-2. Br*-$^{13}C^{16}O_2$ solar-pumped E-V transfer laser.

collisional depopulation. Furthermore, the gas-kinetic temperature T cannot exceed approximately 400°K, otherwise significant thermal population of the (010) level will occur with subsequent "bottle-necking" of the laser inversion. Ground-state Br atoms recombine to form molecular bromine and the photoexcitation process can then be repeated. We now proceed to examine the kinetics of this lasing system. The P(16) line of the 001→100 band of $^{13}C^{16}O_2$ is employed to maximize the atmospheric transmission efficiency.[2]

Collision between excited bromine atoms, $Br(4^2P_{\frac{1}{2}})$, and CO_2 molecules in the ground state results in either E-V energy transfer or quenching:

$$Br^* + CO_2 \xrightarrow{f} CO_2\,(ASM) + Br \qquad (1)$$
$$Br^* + CO_2 \xrightarrow{(1-f)} CO_2 + Br$$

where we use the Notation Br* for the electronically excited state ($4^2P_{\frac{1}{2}}$) and Br for the ground state ($4^2P_{3/2}$), and ASM, SSM, and BM denote the asymmetric stretch, symmetric stretch, and bending vibrational modes of CO_2. The ground state $CO_2(000)$ is denoted simply as CO_2. The rate coefficient for Reaction (1) is $k_1 = (7.6\pm1.1) \times 10^{-12}$ cm^3 molecule^{-1} sec^{-1} if $^{13}C^{16}O_2$ is the acceptor species.[11] k_1 is approximately constant over the temperature range from 296°K to 600°K. f is the branching fraction, equal to 0.50 for $^{13}C^{16}O_2$. Br* can also be deactivated by bromine molecules:

$$Br^* + Br_2 \rightarrow Br + Br_2 \qquad (2)$$

The temperature dependence of the rate coefficient for Reaction (2) has not been determined; at 295°K, $k_2 = (0.3\pm1.9) \times 10^{-13}$ cm^3 molecule^{-1} sec^{-1}.[17] Deactivation of Br* by the buffer gas He proceeds very slowly and can be neglected.

Recombination of Br atoms proceeds via three-body collisons with the third bodies M = He, CO_2, and Br_2. The concentrations of other M species are substantially lower so that additional recombination mechanisms are insignificant. The dominant recombination reactions, therefore, are as follows:

$$Br + Br + He \rightarrow Br_2 + He \qquad (3)$$

$$\log k_3 = -(32.494\pm0.065) - (1.261\pm0.043)\log(T/300)$$

$$Br + Br + CO_2 \rightarrow Br_2 + CO_2 \qquad (4)$$

$$\log k_4 = -(32.179\pm0.055) - (2.287\pm0.125)\log(T/300) + (1.154\pm0.194)\log^2(T/300)$$

$$Br + Br + Br_2 \rightarrow 2\,Br_2 \qquad (5)$$

$$\log k_5 = -(30.67\pm2.40) - (3.01\pm0.28)\log(T/300)$$

where k_3 through k_5 were measured by Ip and Burns[18] and have units cm molecule^{-2} sec^{-1}. Reaction (4) is assumed to proceed at an analogous rate to that for M = Ar since CO_2 and Ar have about equal masses.

VT relaxation is important only for the CO_2 bending mode:

$$CO_2(BM) + CO_2 \rightarrow CO_2 + CO_2 \tag{6}$$

$$k_6 = 4.99 \times 10^{-5} x^2 \exp(-191x + 348x^2 + 480x^3)$$

$$CO_2(BM) + He \rightarrow CO_2 + He \tag{7}$$

$$k_7 = 2.67 \times 10^{-6} x^2 \exp(-121x + 149x^2 + 480x^3)$$

where $x = T^{-1/3}$. VT relaxation rates with Br_2 as a collision partner have not been measured. In the kinetic formulation we assume that the reaction

$$CO_2(BM) + Br_2 \rightarrow CO_2 + Br_2 \tag{6'}$$

is possible and assume $k_{6'} = k_6$.

VV relaxation between the SSM and BM and the ASM and BM of CO_2 are also included:

$$CO_2(SSM) + CO_2 \rightarrow CO_2(BM) + CO_2 \tag{8}$$

$$k_8 = 3.26x^2 \exp(-304x + 974x^2 + 74x^3)$$

$$CO_2(SSM) + He \rightarrow CO_2(BM) + He \tag{9}$$

$$k_9 = 1.76x^2 \exp(-304x + 974x^2 + 74x^3)$$

$$CO_2(ASM) + CO_2 \rightarrow CO_2(BM) + CO_2 \tag{10}$$

$$k_{10} = 1.45 \times 10^{-2} x^2 \exp(-298x + 830x^2 + 300x^3)$$

$$CO_2(ASM) + He \rightarrow CO_2(BM) + He \tag{11}$$

$$k_{11} = 3.24 \times 10^{-2} x^2 \exp(-300x + 952x^2 + 300x^3)$$

where values of k_6 through k_{11} were obtained from Reference (19). VV relaxation rates with Br_2 as a collision partner have not been measured with one exception. We assume that the reactions

$$CO_2(SSM) + Br_2 \rightarrow CO_2(BM) + Br_2 \tag{8'}$$

$$CO_2(ASM) + Br \rightarrow CO_2(BM) + Br_2 \tag{10'}$$

are possible and let $k_{8'} = k_8$ and $k_{10'} = k_{10}$. Hariri and Wittig[10] have investigated reaction (10') and found $k_{10'} = (7.9 \pm 0.6) \times 10^{-15}$ cm^3 molecule^{-1} sec^{-1} at 295°K. Since k_{10} for CO_2 and $k_{10'}$ for Br_2 are in close agreement at T = 295°K, we have arbitrarily taken $k_{6'} = k_6$, $k_{8'} = k_8$, and $k_{10'} = k_{10}$ and assumed identical temperature dependencies. Because the laser operating pressure is relatively low, errors in these rates should have only minor impact on the parameters of interest. Furthermore, we have assumed that the VV and VT rates involving CO_2 are independent of the CO_2 isotopic species since detailed measurements involving $^{13}C^{16}O_2$ are not generally available.

If we let brackets denote species concentrations in molecules or atoms per cm^3, then the spatially homogeneous kinetic rate equations can be written as follows:

$$\frac{d[Br^*]}{dt} = CP_{X\rightarrow B} - k_1[Br^*][C\theta_2] - k_2[Br^*][Br_2] \tag{12}$$

$$\frac{d[Br]}{dt} = C\{P_{X\rightarrow B} + 2(P_{X\rightarrow A} + P_{X\rightarrow \Pi})\} + k_2[Br^*][Br_2] - 2[Br]^2\{k_3[He] + k_4[CO_2] + k_5[Br_2]\} \tag{13}$$

$$\frac{d[CO_2(ASM)]}{dt} = fk_1[Br^*][CO_2] - [CO_2(ASM)]\{k_{10}([CO_2] + [Br_2]) + k_{11}[He]\} - \Gamma \tag{14}$$

$$\frac{d[CO_2(SSM)]}{dt} = \Gamma - [CO_2(SSM)]\{k_8([CO_2] + [Br_2]) + k_9[He]\} \tag{15}$$

$$\frac{d[CO_2(BM)]}{dt} = [CO_2(ASM)]\{k_{10}([CO_2] + [Br_2]) + k_{11}[He]\} + [CO_2(SSM)]\{k_8([CO_2] + [Br_2]) + k_9[He]\} - [CO_2(BM)]\{k_6([CO_2] + [Br_2]) + k_7[He]\} \tag{16}$$

where C is the solar concentration ratio and the P terms are the various solar pumped photodissociation rates of Br_2. Γ is the induced stimulated- plus spontaneous-transition rate for laser photons. Diffusion and flow effects, temperature gradients, and wall quenching of Br* have been neglected in the kinetic formulation.

For Br_2, three molecular transitions leading to photodissociation have been identified, namely,

$$X\,^1\Sigma_g^+ \rightarrow A\,^3\Pi_{1u} \quad ,$$

$$\rightarrow B\,^3\Pi_{0^+u} \quad ,$$

$$\rightarrow {}^1\Pi_{1u} \quad .$$

The dissociation of Br_2 following excitation of the X→B transition above the thermochemical threshold leads to production of one atom in the ground state (Br) and one in the optically metastable, spin-orbit excited state (Br*), which lies 3685 cm^{-1} above the ground state. The less strongly bound A $^3\Pi_{1u}$ state and the totally repulsive $^1\Pi_{1u}$ state correlate with two Br atoms only. The pumping rate (transitions cm^{-3} sec^{-1}) of a given photodissociation channel is

$$P_i = \int_{\lambda_c}^{0.62\ \mu m} \frac{\alpha_i(\lambda) I(\lambda) \lambda\, d\lambda}{hc} \quad , \tag{17}$$

where α_i is the absorption coefficient (cm^{-1}), I is the solar irradiance at earth orbit (W cm^{-2} μm^{-1}), λ is the wavelength (μm), and λ/hc is the photon energy (J). λ_c is the cutoff wavelength which is explained later. The solar irradiance as a function of wavelength was obtained from tables in Reference (20). Absorption coefficient data for the three transitions were obtained from References (21) and (22); absorption spectra are shown in Figure 2.2-3. Numerical integration of Eq. (17) was performed in 0.005-μm increments.

The steady-state (cw) behavior of the Br*-CO_2 transfer laser is determined by setting all time derivatives in Eqs. (12) through (16) equal to zero and solving for appropriate species concentrations. To simplify matters, we set Γ equal to zero in order to determine the parametric dependence of the small-signal gain (α_o) and stored power density in the lasing mode (Q_ℓ) on the temperature, lasing gas mixture, solar concentration, etc. These parameters are sufficient to assess laser performance without encumbering the calculation with resonator or amplifier extraction considerations. Furthermore, we assume that both the degree of Br_2 dissociation and the CO_2 vibrational-mode populations are small, so that $[Br_2]$ and $[CO_2]$ are constants. Under these conditions, Eqs. (12) through (16) can be solved algebraically to yield [Br*], [Br], $[CO_2(ASM)]$, $[CO_2(SSM)]$, and $[CO_2(BM)]$ directly. Because $\Gamma = 0$, we require that $[CO_2(SSM)] = 0$.

The stored power density in the lasing mode (W/cm^3) is approximately

$$Q_\ell = h\nu_{laser} fk_1 [Br^*][CO_2] \quad , \tag{18}$$

where $h\nu_{laser}$ is the energy per laser photon (1.79×10^{-20} J at λ = 11.1 μm) and $fk_1[Br^*][CO_2]$ is the pumping rate for CO_2 molecules into the ASM (upper laser level). A fraction of the absorbed solar flux produces atomic bromine in the ground state; the energy thus liberated cannot be channeled into lasing via E-V

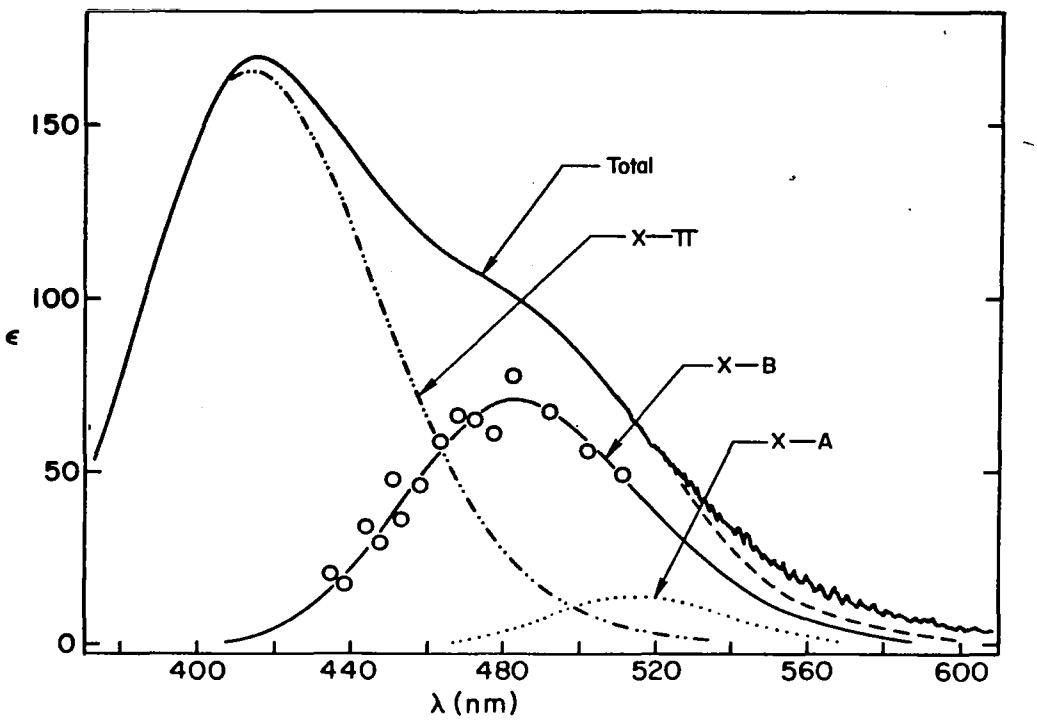

Figure 2.2-3. Absorption spectra of Br_2 showing total absorption and the three transition components.[21] ε is the molar absorptivity (liter $mole^{-1}$ cm^{-1}).

transfer and results ultimately in heating of the gas mixture. The thermal power density (W/cm^3) due to photoabsorption processes which produce only Br atoms is then

$$Q_{th} = \int_{\lambda_c}^{0.62\ \mu m} (0.5\ \alpha_{X\to B} + \alpha_{X\to A} + \alpha_{X\to \Pi}) I(\lambda) d\lambda \quad . \tag{19}$$

The small signal gain coefficient (cm^{-1}) is

$$\alpha_o = \sigma \Delta N \quad , \tag{20}$$

where σ is the stimulated emission cross section (cm^2) and ΔN is the population inversion (cm^{-3}). The stimulated emission cross section is

$$\sigma = \frac{g_o A}{8\pi c \nu_{laser}^2} \quad , \tag{21}$$

where A is the spontaneous transition rate ($\simeq 0.20\ sec^{-1}$) and the laser frequency, ν_{laser}, is 900.4 cm^{-1}. g_o is the line shape factor at line center. At the operating pressures of interest here, the laser transition is homogeneously pressure-broadened and the line shape is described by a Lorentzian linewidth $\Delta\nu_L$:

$$g_o = \frac{1}{\pi\Delta\nu_L} \tag{22}$$

The Lorentzian linewidth (cm^{-1}, HWHM) is given by

$$\Delta\nu_L = \sum_i P_i w_i \quad , \tag{23}$$

where P_i and w_i are the partial pressure (atm) and pressure-broadening coefficient ($cm^{-1}\ atm^{-1}$) for gas species i, and the summation is over all gas components. The pressure-broadening coefficients for CO_2,[23] He,[24] and Br_2[25] are

$$w_{CO_2} = 0.108(300/T)^{1/2}$$

$$w_{He} = 12.089/T + 0.03054 - 1.005 \times 10^{-5}T$$

$$w_{Br} = 0.1(300/T)^{1/2}.$$

The population inversion is

$$\Delta N = \psi_{J'}\,[CO_2(ASM)] - \psi_J\,[CO_2(SSM)], \tag{24}$$

where the rotational partition fraction is

$$\psi_J = 2(2J + 1)(\theta_r/T)\ \exp[-J(J + 1)\theta_r/T] \quad . \tag{25}$$

θ_r is the rotational temperature (0.556°K), which differs for the upper and lower laser levels by less than 1%, and J and J' are the rotational quantum numbers of the lower and upper levels, respectively (J' = J - 1 for P-branch transitions).

Only the X→B transition in Br_2 produces excited Br atoms, so we consider the use of specialized solar concentrators which reflect all of the solar flux having wavelengths greater than a cutoff value, λ_c, into the lasing medium and which transmit the unusable portion of the solar spectrum below λ_c. This technique is designed to minimize gas heating due to undesirable photoabsorption from other transitions which produce only ground-state Br atoms. The percentage of the total pumping rate due to the X→B photodissociation transition (69%) is maximized when λ_c = 0.48 μm. If the full, unmodified solar spectrum is employed, only 35% of the total pumping rate is due to the X→B transition.

The Br_2 partial pressure in the lasing gas must be optimized to affect adequate coupling of the incident solar flux while maintaining reasonable pumping homogeneity, necessary for efficient extraction of the stored laser power. For a uniformly illuminated 2-m-diameter cylindrical volume, the estimated Br_2 partial pressure is 6.8 Torr (STP). For optimum laser operation, the CO_2 and Br_2 partial pressures should be comparable, so we have taken an equal CO_2 partial pressure. The small-signal gain is proportional to (He pressure)$^{-1}$; to maintain adequate depopulation of the $CO_2(010)$ level in conjunction with a useful small-signal gain, the lowest He partial pressure which seems reasonable is 10 Torr (STP), which is the value adopted for these calculations.

Even with large solar concentration ratios, the stored power density in the lasing mode is several orders of magnitude smaller than obtained with electrical (gas-discharge) excitation, as shown in Figure 2.2-4. The extractable power density is less than Q_ℓ because of optical losses and limitations on

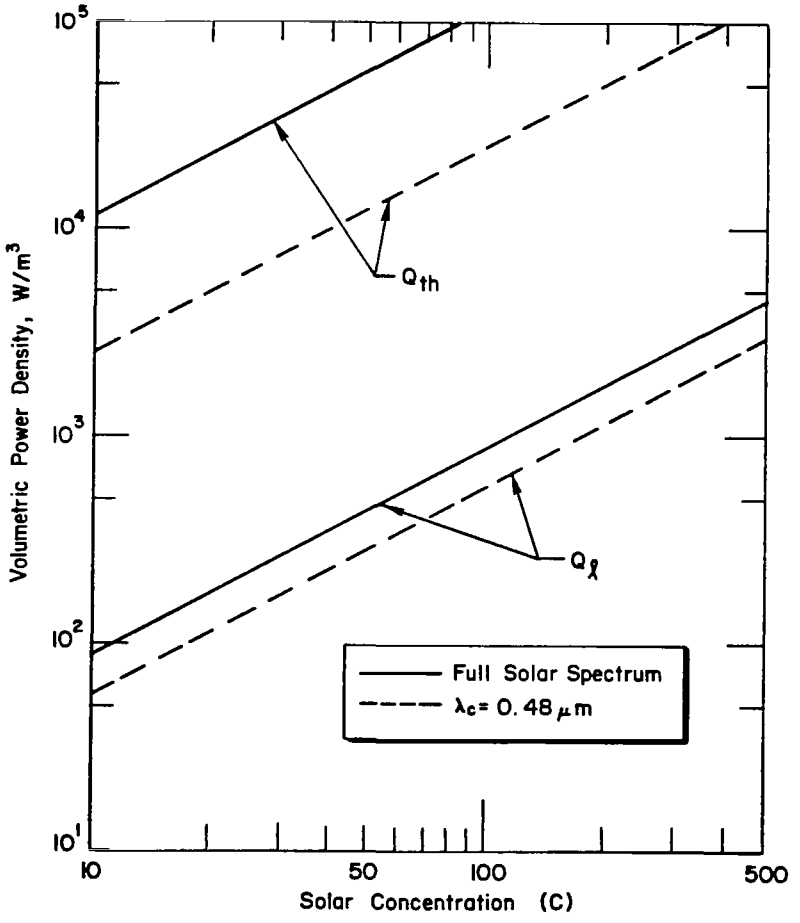

Figure 2.2-4. Stored power densities in the lasing mode (Q_ℓ) and due to nonproductive (thermal) photoabsorption processes (Q_{th}).

depopulation of the lower laser level imposed by VV equilibrium to the bending mode and subsequent VT relaxation. The thermal power density due to non-productive photoabsorption processes, Q_{th}, is 45 times greater than Q_{ℓ} if wavelength-selective solar concentrators are employed and 130 times greater if the full solar spectrum is used. Since this is only one source of thermal power, waste-heat management is a critical issue with this type of laser.

The small-signal gain coefficient and Br_2 dissociation fraction are shown in Figure 2.2-5 as functions of the solar concentration ratio for gas-kinetic temperatures of 300 and 400°K. Useful values of α_o are obtained only for large values of C and the deleterious effect of increasing temperature on α_o is readily apparent from the upper plots in Figure 2.2-5. The lower plots show that the Br_2 dissociation fraction is indeed small enough to justify the assumption of constant Br_2 concentration.

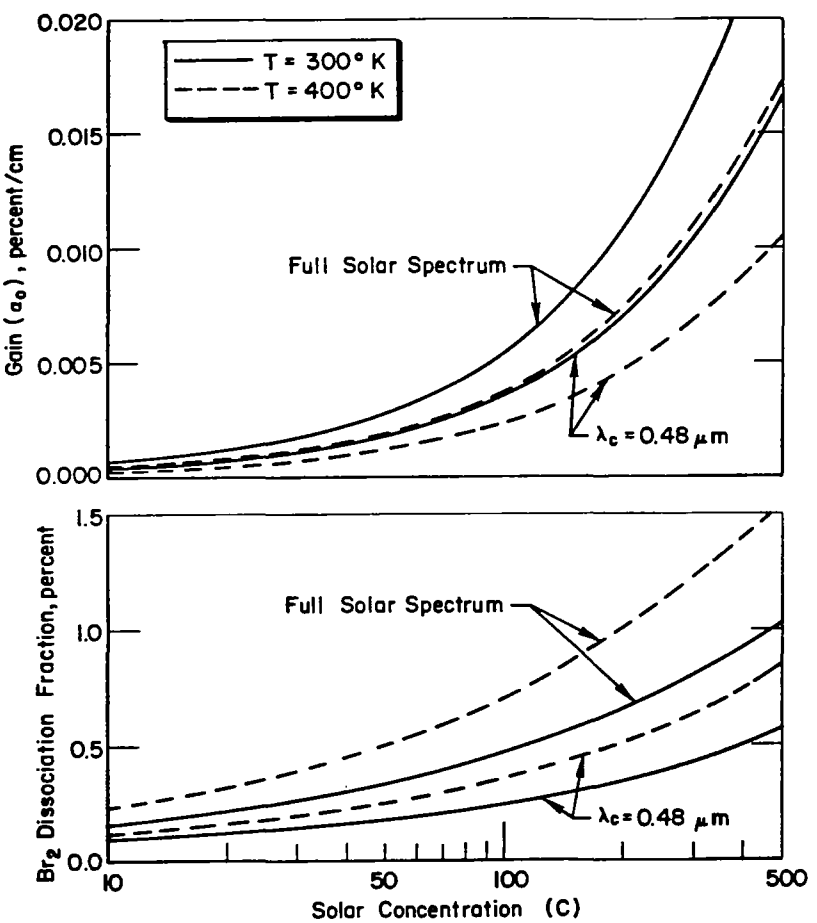

Figure 2.2-5. Small-signal gain coefficient and molecular bromine dissociation fraction as functions of solar concentration ratio.

For a 100-MW laser based on this concept, we estimate that the necessary solar collection area will exceed that required by the 5-GW baseline photoelectric/microwave concept. The shortcomings of this lasing scheme are easily isolated by examination of photon economics and energetics. Under best conditions, only 34% of the absorbed solar photons produce excitation of the upper laser level. One absorbed solar photon of average energy 2.6 eV produces one 0.457-eV Br* atom which liberates "1/2" (f=0.50) laser photon having an energy of only 0.112 eV, representing a loss of almost all of the original photon's energy to heat. To improve this situation, the upper-level energy of the lasing molecule should be in close proximity to the Br* energy (3685 cm^{-1}), the Br*-deactivation rate coefficient (k_1) should be large accompanied by efficient branching to the E-V transfer reaction ($f \simeq 1$), and the lower-level lasing energy should be as close to the ground state as possible. In this connection, the 001→010 transition in HCN may be a better choice than $^{13}C^{16}O_2$. As shown in Figure 2.2-6, the porbability of Br* quenching per collision with a HCN molecule is better than with many other hydrides and the branching fraction is larger ($F \simeq 0.9$). The HCN laser, like the $^{13}C^{16}O_2$ laser, cannot operate at high temperatures so waste heat disposal is still a major problem.

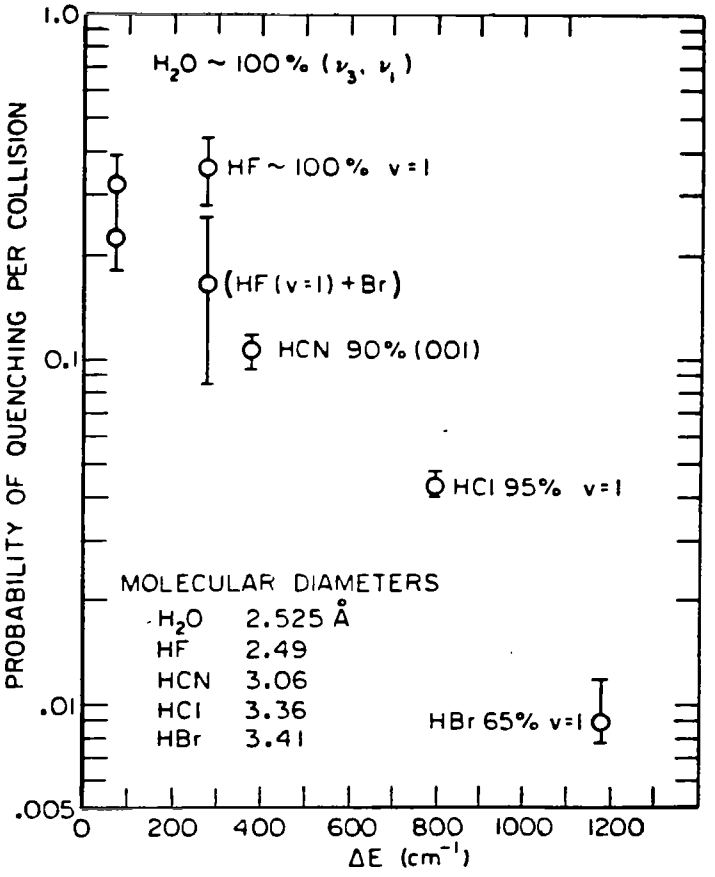

Figure 2.2-6. Probability of quenching per collision vs. energy defect for all hydrides known to quench Br* via E-V transfer.[17] The percentages listed beside each data point correspond to the branching fraction f.

2.3 OPTICALLY PUMPED ALKALI-METAL ATOMIC-TRANSITION LASERS

Golger et al.[26] recently proposed a scheme for direct solar pumping of an atomic-transition alkali-metal laser. Their calculations estimate that an extractable laser power of $\simeq$ 7 kW is obtainable from a 0.4×0.1×25 m^3 volume using a solar concentration ratio of 20 and a gas mixture consisting of cesium vapor and xenon gas. Operation at a temperature of 650°K gives a cesium dimer (Cs_2) concentration ~ 10^{15} cm^3. Absorption of part of the incident solar flux produces excited cesium molecules (Cs_2^*) in the $A^1\Sigma_u^+$ state:

$$Cs_2(X^1\Sigma_g^+) + h\nu_{pump}(445\text{-}523\ nm) \rightarrow Cs_2^*(A^1\Sigma_u^+)$$

Collision induced dissociation then produces one Cs atom in the upper laser level ($7^2S_{\frac{1}{2}}$) and one Cs atom in the ground state ($6^2S_{\frac{1}{2}}$):

$$Cs_2^* + Xe \rightarrow Cs(7^2S_{1/2}) + Cs(6^2S_{1/2}) + Xe$$

Stimulated emission is then possible between the 7S and 6P states:

$$Cs(7^2S_{1/2}) \rightarrow Cs(6^2P_{1/2}) + h\nu_{laser}(1358.9\ nm)$$
$$\rightarrow Cs(6^2P_{3/2}) + h\nu_{laser}(1469.5\ nm)$$

The lower lasing level [$Cs(6^2P_{1/2,3/2})$] cannot be depopulated radiatively because these are the resonant states and optical emission will not escape the medium efficiently. Instead, operation at high buffer gas pressure promotes formation of the rare-gas excimer CsRg:

$$Cs(6^2P_{1/2,3/2}) + Xe \rightarrow CsXe^{*(1,2)}$$

[τ ~ 1 μsec removal rate at P_{Xe} = 30 atm]

Radiative de-excitation is followed immediately by dissociation of the repulsive ground state; this optical emission is not absorbed by the medium:

$$CsXe^{*(1,2)} \rightarrow CsXe + h\nu_{1,2} \rightarrow Cs + Xe$$

The atmospheric transmission efficiencies of both wavelengths emitted by this laser, however, are very poor. Analogous kinetic schemes for the other alkali-metal atoms were examined to determine if more favorable transitions exist, as listed in Table 2.3-1. Operation with Li, Na, or K will be difficult because of the temperatures required to maintain the necessary vapor pressures and because excitation of the X→A transition requires ultraviolet light. The Rb line at 1.3237 μm may yield a viable alternative. Detailed kinetic modeling will be necessary to establish the operating parameters of this system, and

Table 2.3-1. Alkali-metal atomic transitions pumped by photodissociation of alkali dimer states.

Atom	Transition	ν, cm^{-1}	λ, μm	Transmission Efficiency*
Li	$3^2S_{1/2} \rightarrow 2^2P_{1/2}$	12302.5	0.8128	excellent
	$\rightarrow 2^2P_{3/2}$	12302.1	0.8129	excellent
Na	$4^2S_{1/2} \rightarrow 3^2P_{1/2}$	8783.7	1.1385	very poor
	$\rightarrow 3^2P_{3/2}$	8766.5	1.1407	poor
K	$5^2S_{1/2} \rightarrow 4^2P_{1/2}$	8041.6	1.2435	excellent
	$\rightarrow 4^2P_{3/2}$	7983.9	1.2525	fair
Rb	$6^2S_{1/2} \rightarrow 5^2P_{1/2}$	7554.6	1.3237	fair
	$\rightarrow 5^2P_{3/2}$	7317.0	1.3667	very poor
Cs	$7^2S_{1/2} \rightarrow 6^2P_{1/2}$	7358.9	1.3589	very poor
	$\rightarrow 6^2P_{3/2}$	6805.0	1.4695	very poor

*Estimated based on the HITRAN spectral curves given in R. A. McClatchey and J. E. A. Selby, "Atmospheric attenuation of laser radiation from 0.76 to 31.25 μm," AFCRL-TR-74-0003 (1974); excellent -- >95%, fair -- 50-90%, poor -- <10%, very poor -- ≈0% (attenuation due to molecular absorption only).

atmospheric propagation calculations are needed to quantitize the transmission efficiency.

2.4 RARE-EARTH VAPOR-COMPLEX LASERS

Lasing on various electronic states in rare-earth, actinide, and transition metal ions held in an insulating crystal host is well known and highly documented. More recently, the trivalent rare-earth lanthanides have been investigated[27-31] in an effort to develop flowing gas lasers having superior performance compared with their solid-state counterparts. In particular, high average-power operation is possible if waste heat can be removed in a flow cycle, and the stringent system constraints dictated by nonlinear optical properties of the solid-state host can be relaxed.

Gaseous trivalent rare earths (RE^{3+}) which have been investigated include two component transition metal-trihalide molecular complexes [e.g., $RECl_3 \cdot (AlCl_3)_x$] that are generated thermochemically[27-30] and $RE(thd)_3$ chelates.[31] The former complexes require an operating temperature of 800°K to achieve a RE^{3+} concentration of about 5×10^{17} ions/cm^3; by contrast, the $RE(thd)_3$ chelates (2,2,6,6-tetramethyl-3,5-heptanedione) have a significantly higher vapor pressure and permit a low operating temperature, i.e., 10 Torr at about

230°C. Furthermore, the $RE(thd)_3$ chelates are thermally stable and optically resilient so that prolonged operation appears feasible.[31] To date, only neodymium (Nd^{3+}) and terbium (Tb^{3+}) complexes lasing at 1.06 μm and 0.545 μm, respectively, have been studied. Collisional deactivation rates and radiative lifetimes are suitable for pulsed operation with possible laser-fusion applications.

Cw operation of other rare-earth vapor complexes may be possible using other lasing ions having transition wavelengths more suited to efficient atmospheric propagation. Numerous possibilities exist, as illustrated by the transitions shown in Figures 2.4-1 and 2.4-2. In particular, the $Dy^{2+}(^5I_7 \rightarrow {}^5I_8)$ transition at 2.36 μm, the $Ho^{3+}(^5I_7 \rightarrow {}^5I_8)$ transition at 2.06 μm, and the $Er^{3+}(^4I_{13/2} \rightarrow {}^4I_{15/2})$ transition at 1.62 μm are interesting possibilities. It remains to be determined if their radiative lifetimes are sufficiently long and their collisional deactivation rates are sufficiently small to permit cw operation. All of these ions have strong absorption structure in the visible and near infrared so that pumping via concentrated solar radiation may be possible. The kinetics of each lasing compound must be examined in detail to determine if direct solar pumped laser operation is feasible.

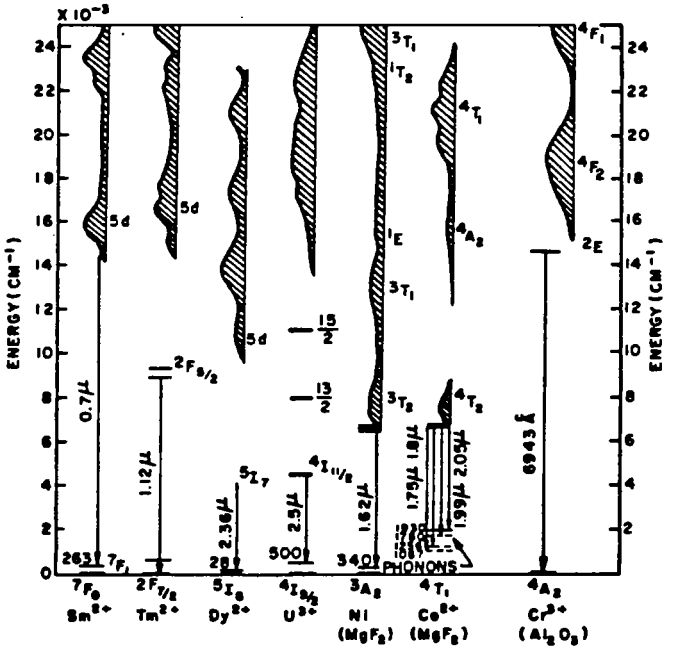

Figure 2.4-1. Energy levels and laser transitions of divalent rare-earth, actinide, and transition metal ions.

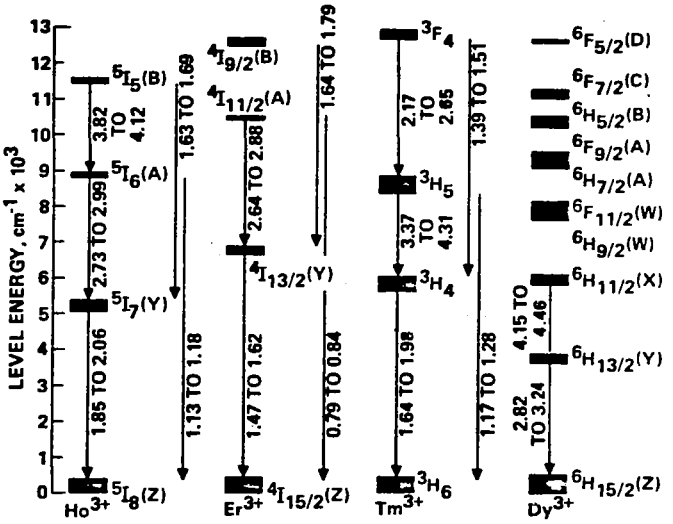

Figure 2.4-2. Energy levels and laser transitions of trivalent rare-earth ions.

2.5 CONCLUSIONS AND RECOMMENDATIONS

Photoexcited E-V transfer lasers, optically pumped alkali-metal atomic-transition lasers, and rare-earth vapor-complex lasers have been discussed as potential candidates for direct solar excitation and application to the SPS concept. The Br*-$^{13}C^{16}O_2$ E-V transfer laser, which was kinetically modeled in some detail, is not a viable concept because of its small lasing-mode power density and large thermal-energy generation rate. The Br*-HCN laser is a better candidate, although the problems associated with waste-heat management may be insurmountable. In particular, E-V lasers using molecules such as CO_2 and HCN must operate at low temperature (<400°K), requiring waste-heat radiators with large areas. The optically pumped atomic-transition Rb laser and various (Dy^{3+}, Ho^{3+}, Er^{3+}) rare-earth vapor-complex lasers were also identified as potential SPS candidates, although detailed modeling was not performed. Kinetic data for various radiative and collisional processes are unknown for many of the excited states of interest and further experimental research is warranted. Sufficient information exists, however, to determine if direct solar pumping is feasible and if the laser operating parameters are appropriate for the SPS.

A number of additional laser candidates exist which were not considered in this study. Because the viability of the overall laser-SPS concept hinges on finding a suitable advanced laser system capable of achieving a satellite specific mass $\lesssim$ 5 kg/kW,[1] further research is needed to adequately model both the Rb atomic-transition laser and the rare-earth vapor-complex lasers as well as all other potentially viable laser schemes involving direct pumping.

2.6 REFERENCES

[1] R. E. Beverly III, "SPS-laser environmental impact study," Final Technical Report to Rockwell International Corporation, Space Operations and Satellite Systems Division on Contract No. M9M 8BNB-896662D (1979); submitted to Space Solar Power Review.

[2] R. E. Beverly III, "Meteorological effects on laser beam propagation," Final Technical Report to Rockwell International Corporation, Space Operations and Satellite Systems Division on Contract No. MOL 8GNS-897409D (1980).

[3] R. Taussig et al., "Design investigation of solar powered lasers for space applications," Mathematical Sciences Northwest Final Technical Report to NASA Lewis Research Center on Contract No. NAS3-21134 (1979).

[4] A. B. Petersen, C. Wittig, and S. R. Leone, "Infrared molecular lasers pumped by electronic-vibrational energy transfer from Br ($4^2P_{1/2}$): CO_2, N_2O, HCN, and C_2H_2," Appl. Phys. Lett. 27, 305 (1975).

[5] A. J. Grimley and P. L. Houston, "Electronic to vibrational energy transfer from $I(5^2P_{1/2})$. I. HCl, HBr, and NO; II. H_2O, HDO, and D_2O; III. H_2, HD, and D_2," J. Chem. Phys. 68, 3366 (1978); 69, 2339 (1978); 70, 4724 (1979).

[6] R. E. Beverly III, "Pressure-broadened iodine-laser-amplifier kinetics and a comparison of diluent effectiveness," Opt. Commun. 15, 204 (1975).

[7] G. A. Fisk, "The effects of chemical kinetics and starting material regeneration on the efficiency of the iodine laser amplifier," Sandia Laboratories Report No. SAND77-0880 (1977).

[8] A. B. Petersen, C. Wittig, and S. R. Leone, "Electronic-to-vibrational pumped CO_2 laser operating at 4.3, 10.6, and 14.1 μm," J. Appl. Phys. 47, 1051 (1976).

[9] A. B. Petersen and C. Wittig, "Line-tunable CO_2 laser operating in the region 2280-2360 cm^{-1} pumped by energy transfer from Br($4^2P_{1/2}$)," J. Appl. Phys. 48, 3665 (1977).

[10] A. Hariri and C. Wittig, "Electronic to vibrational energy transfer from Br($4^2P_{1/2}$) to CO_2, COS, and CS_2," J. Chem. Phys. 67, 4454 (1977).

[11]H. Reisler and C. Wittig, "Temperature dependence of electronic to vibrational energy transfer from $Br(4^2P_{1/2})$ to $^{12}CO_2$ and $^{13}CO_2$," J. Chem. Phys. 69, 3729 (1978).

[12]S. R. Leone and F. J. Wodarczyk, "Laser-excited electronic-to vibrational energy transfer from $Br(4^2P_{1/2})$ to HCl and HBr," J. Chem. Phys. 60, 314 (1974).

[13]H. Reisler and C. Wittig, "Temperature dependence of the quenching of $Br(4^2P_{1/2})$ by CO_2 and HCl with accompanying vibrational excitation," J. Chem. Phys. 68, 3308 (1978).

[14]A. B. Petersen, L. W. Braverman, and C. Wittig, "H_2O, NO, and N_2O infrared lasers pumped directly and indirectly by electronic-vibrational energy transfer," J. Appl. Phys. 48, 230 (1977).

[15]F. J. Wodarczyk and P. B. Sackett, "Electronic-to-vibrational energy transfer from $Br(4^2P_{1/2})$ to HF," Chem. Phys. 12, 65 (1976).

[16]A. Hariri, A. B. Petersen, and C. Wittig, "Electronic-vibrational energy transfer from $Br(4^2P_{1/2})$ to HCN, and deactivation of HCN(001)," J. Chem. Phys. 65, 1872 (1976).

[17]A. Hariri and C. Wittig, "Electronic to vibrational energy transfer from $Br(4^2P_{1/2})$ to H_2O," J. Chem. Phys. 68, 2109 (1978).

[18]J. K. K. Ip and G. Burns, "Recombination of Br atoms by flash photolysis over a wide temperature range. II. Br_2 in He, Ne, Ar, Kr, N_2, and O_2," J. Chem. Phys. 51, 3414 (1969).

[19]R. L. Taylor and S. Bitterman, "Survey of vibrational relaxation data for processes important in the CO_2-N_2 laser system," Rev. Mod. Phys. 41, 26 (1969); S. A. Wutzke et al., "CW pin discharge laser," Westinghouse Research Laboratories Final Technical Report on Contract No. N00014-73-C-0318 (1974).

[20]G. H. Suits, "Natural sources," in The Infrared Handbook, W. L. Wolfe and G. J. Zissis, eds. (Office of Naval Research, Arlington, VA, 1978), Ch. 3, pp. 3-35 to 3-36.

[21]T. G. Lindeman and J. R. Wiesenfeld, "Photodissociation of Br_2 in the visible continuum," J. Chem. Phys. 70, 2882 (1979).

[22]C. P. Hemenway, T. G. Lindeman, and J. R. Wiesenfeld, "Measurement of the $A^3\Pi_{1u} \leftarrow X^1\Sigma_g^+$ continuum absorptivity in Br_2," J. Chem. Phys. 70, 3560 (1979).

[23]T. W. Meyer, C. K. Rhodes, and H. A. Haus, "High-resolution line broadening and collisional studies in CO_2 using nonlinear spectroscopic techniques," Phys. Rev. A 12, 1993 (1975).

[24]R. T. Pack, "Pressure broadening of the dipole and Raman lines of CO_2 by He and Ar. Temperature dependence," J. Chem. Phys. 70, 3424 (1979).

[25]Estimate based on the known mass-dependence of the pressure broadening coefficient on reduced mass.

[26]A. L. Golger, L. I. Gudzenko, and S. I. Yakovlenko, "Direct conversion of solar energy into laser radiation," Sov. J. Quant. Electron. 8, 1118 (1978).

[27]R. R. Jacobs, W. F. Krupke, J. P. Hessler, and W. T. Carnall, "Deactivation on the $Nd^{3+}(4F_{3/2})$ level in neodymium chloride-aluminum chloride vapor complexes," Opt. Commun. 21, 395 (1977).

[28]R. R. Jacobs and W. F. Krupke, "Trivalent rare earth molecular vapor laser systems," in Electronic Transition Lasers II, L. E. Wilson, S. N. Suchard, and J. I. Steinfeld, eds. (MIT Press, Cambridge, MA, 1977), pp. 246.

[29]R. R. Jacobs and W. F. Krupke, "Optical gain at 1.06 μm in the neodymium chloride-aluminum chloride vapor complex," Appl. Phys. Lett. 32, 31 (1978).

[30]R. R. Jacobs and W. F. Krupke, "Kinetics and fusion laser potential for the terbium chloride-aluminum chloride vapor complex," Appl. Phys. Lett. 35, 126 (1979).

[31]R. R. Jacobs and W. F. Krupke, "Excited-state kinetics for $Nd(thd)_3$ and $Tb(thd)_3$ chelate vapor and prospects for fusion laser media," Appl. Phys. Lett. 34, 497 (1979).

APPENDIX

POWER AVAILABILITY, TRANSMISSION FREQUENCY, AND PERSISTENCE FREQUENCY DATA

Statistical calculations of the seasonal and annual power availabilities, transmission frequencies, and persistence frequencies were performed for each of the proposed receptor sites. Computer generated tabular data are presented here with the results grouped by region. Average power availability data for all sites within each region are then presented. The sites are identified by the weather stations providing observational sky-cover data. The tabular data are organized as follows:

Because transmission frequencies and persistence frequencies predicted at a low transmission efficiency oftentimes required an extrapolation of the actual T-K curve, these results are subject to greater possible error. Hence, predicted frequencies of 1.00, for instance, should be construed to read $\geq$ 0.95.

FREQUENCY THAT TRANSMISSION EFFICIENCY EXCEEDS SPECIFIED VALUE--

AT-1: GRIFFISS AFB (ROME), NY N 43 14 W 075 24 ELEV 504 FT

	WINTER			SPRING			SUMMER			FALL		
TRANS.	1	2	3	1	2	3	1	2	3	1	2	3
.1	.91	1.00	1.00	.93	.99	.99	.96	.99	.99	.94	.99	.99
.2	.61	.96	1.00	.69	.97	.99	.81	.98	.99	.73	.97	.99
.3	.39	.55	1.00	.52	.65	.99	.70	.78	.99	.57	.68	.99
.4	.37	.39	1.00	.49	.51	.99	.66	.68	.99	.53	.56	.99
.5	.33	.36	.40	.44	.48	.52	.59	.64	.70	.48	.52	.57
.6	.29	.31	.38	.39	.42	.50	.52	.56	.67	.43	.46	.55
.7	.25	.26	.36	.34	.36	.48	.45	.48	.65	.38	.40	.52
.8	.21	.22	.26	.29	.30	.35	.37	.39	.47	.33	.34	.39
.9	.16	.18	.21	.23	.25	.29	.27	.30	.36	.26	.29	.32

	ANNUAL		
TRANS.	1	2	3
.1	.93	.99	.99
.2	.71	.97	.99
.3	.55	.67	.99
.4	.51	.53	.99
.5	.46	.50	.55
.6	.41	.44	.52
.7	.36	.38	.50
.8	.30	.31	.37
.9	.23	.26	.29

AVERAGE POWER AVAIABILITY--

AT-1: GRIFFISS AFB (ROME), NY N 43 14 W 075 24 ELEV 504 FT

	MODEL		
SEASON	1	2	3
WINTER	.33	.42	.60
SPRING	.43	.50	.66
SUMMER	.54	.60	.72
FALL	.46	.53	.68
ANNUAL	.44	.51	.66

FREQUENCY THAT TRANSMISSION EFFICIENCY EXCEEDS SPECIFIED VALUE
FOR A PERSISTENCE TIME OF 480.0 MINUTES--

AT-1: GRIFFISS AFB (ROME), NY N 43 14 W 075 24 ELEV 504 FT

	WINTER			SPRING			SUMMER			FALL		
TRANS.	1	2	3	1	2	3	1	2	3	1	2	3
.1	.16	.17	1.00	.22	.24	1.00	.25	.28	1.00	.25	.27	1.00
.2	.14	.15	.15	.20	.21	.21	.22	.23	.24	.23	.24	.24
.3	.13	.13	.14	.18	.19	.20	.20	.20	.22	.21	.22	.23
.4	.12	.12	.12	.17	.17	.18	.18	.19	.19	.20	.20	.21
.5	.11	.12	.12	.16	.17	.17	.17	.18	.18	.19	.20	.20
.6	.11	.11	.11	.16	.16	.16	.16	.17	.17	.19	.19	.19
.7	.10	.11	.11	.15	.15	.16	.15	.16	.16	.18	.18	.19
.8	.09	.10	.11	.13	.14	.15	.13	.15	.15	.15	.17	.18
.9	.05	.06	.10	.06	.09	.14	.06	.09	.14	.08	.11	.17

	ANNUAL		
TRANS.	1	2	3
.1	.22	.24	1.00
.2	.20	.21	.21
.3	.18	.19	.19
.4	.17	.17	.17
.5	.16	.16	.17
.6	.15	.16	.16
.7	.14	.15	.15
.8	.13	.14	.15
.9	.06	.09	.14

FREQUENCY THAT TRANSMISSION EFFICIENCY EXCEEDS SPECIFIED VALUE--

AT-2: QUANTICO, VIRGINIA N 38 30 W 077 18 ELEV 11 FT

	WINTER			SPRING			SUMMER			FALL		
TRANS.	1	2	3	1	2	3	1	2	3	1	2	3
.1	.94	.99	.99	.94	.99	.99	.95	.99	.99	.96	.99	.99
.2	.74	.98	.99	.76	.98	.99	.79	.98	.99	.81	.98	.99
.3	.59	.70	.99	.62	.72	.99	.67	.76	.99	.69	.78	.99
.4	.56	.58	.99	.57	.60	.99	.63	.66	.99	.66	.68	.99
.5	.51	.55	.60	.51	.56	.62	.57	.62	.67	.61	.64	.70
.6	.46	.49	.57	.45	.48	.59	.50	.54	.65	.55	.58	.67
.7	.41	.43	.55	.39	.41	.56	.43	.46	.62	.50	.52	.65
.8	.35	.37	.42	.33	.34	.40	.33	.35	.45	.42	.44	.51
.9	.27	.30	.34	.24	.28	.32	.22	.27	.32	.33	.36	.41

	ANNUAL		
TRANS.	1	2	3
.1	.95	.99	.99
.2	.78	.98	.99
.3	.64	.74	.99
.4	.61	.63	.99
.5	.55	.59	.65
.6	.49	.52	.62
.7	.43	.45	.60
.8	.36	.37	.44
.9	.27	.30	.35

AVERAGE POWER AVAIABILITY--

AT-2: QUANTICO, VIRGINIA N 38 30 W 077 18 ELEV 11 FT

	MODEL		
SEASON	1	2	3
WINTER	.49	.55	.69
SPRING	.48	.55	.69
SUMMER	.51	.57	.71
FALL	.56	.62	.74
ANNUAL	.51	.57	.71

FREQUENCY THAT TRANSMISSION EFFICIENCY EXCEEDS SPECIFIED VALUE
FOR A PERSISTENCE TIME OF 480.0 MINUTES--

AT-2: QUANTICO, VIRGINIA N 38 30 W 077 18 ELEV 11 FT

	WINTER			SPRING			SUMMER			FALL		
TRANS.	1	2	3	1	2	3	1	2	3	1	2	3
.1	.26	.29	1.00	.23	.26	1.00	.21	.24	1.00	.31	.34	1.00
.2	.24	.25	.26	.21	.22	.22	.19	.20	.20	.29	.30	.30
.3	.22	.23	.24	.19	.20	.20	.17	.18	.18	.26	.27	.28
.4	.22	.22	.22	.18	.18	.19	.16	.16	.16	.25	.25	.26
.5	.21	.21	.21	.18	.18	.18	.15	.15	.16	.24	.25	.25
.6	.20	.21	.21	.17	.17	.18	.14	.15	.15	.23	.24	.24
.7	.20	.20	.20	.16	.17	.17	.14	.14	.15	.22	.23	.23
.8	.17	.19	.20	.14	.16	.17	.12	.13	.14	.20	.22	.23
.9	.09	.12	.19	.07	.10	.16	.06	.09	.13	.10	.14	.22

	ANNUAL		
TRANS.	1	2	3
.1	.25	.28	1.00
.2	.23	.24	.25
.3	.21	.22	.23
.4	.20	.20	.21
.5	.19	.20	.20
.6	.19	.19	.19
.7	.18	.18	.19
.8	.16	.18	.18
.9	.08	.11	.18

FREQUENCY THAT TRANSMISSION EFFICIENCY EXCEEDS SPECIFIED VALUE--

CN-1: WHITEMAN AFB, MISSOURI N 38 43 W 093 33 ELEV 869 FT

	WINTER			SPRING			SUMMER			FALL		
TRANS.	1	2	3	1	2	3	1	2	3	1	2	3
.1	.94	.99	.99	.94	.99	.99	.97	.99	.99	.95	.99	.99
.2	.73	.98	.99	.74	.97	.99	.88	.99	.99	.80	.98	.99
.3	.57	.68	.99	.59	.69	.99	.80	.86	.99	.69	.77	.99
.4	.55	.57	.99	.57	.58	.99	.78	.80	.99	.67	.68	.99
.5	.54	.55	.57	.55	.56	.59	.75	.77	.80	.65	.66	.69
.6	.52	.53	.56	.52	.54	.58	.72	.74	.79	.62	.64	.68
.7	.49	.50	.55	.49	.50	.56	.68	.70	.77	.59	.61	.67
.8	.45	.46	.50	.44	.45	.50	.62	.63	.69	.55	.56	.60
.9	.38	.42	.45	.36	.40	.44	.49	.56	.61	.45	.50	.54

	ANNUAL		
TRANS.	1	2	3
.1	.95	.99	.99
.2	.79	.98	.99
.3	.66	.75	.99
.4	.64	.66	.99
.5	.62	.64	.66
.6	.60	.61	.65
.7	.56	.58	.64
.8	.52	.53	.57
.9	.42	.47	.51

AVERAGE POWER AVAIABILITY--

CN-1: WHITEMAN AFB, MISSOURI N 38 43 W 093 33 ELEV 869 FT

	MODEL		
SEASON	1	2	3
WINTER	.53	.59	.72
SPRING	.53	.59	.72
SUMMER	.70	.74	.82
FALL	.62	.67	.77
ANNUAL	.59	.65	.76

FREQUENCY THAT TRANSMISSION EFFICIENCY EXCEEDS SPECIFIED VALUE
FOR A PERSISTENCE TIME OF 480.0 MINUTES--

CN-1: WHITEMAN AFB, MISSOURI N 38 43 W 093 33 ELEV 869 FT

	WINTER			SPRING			SUMMER			FALL		
TRANS.	1	2	3	1	2	3	1	2	3	1	2	3
.1	.36	.39	1.00	.34	.38	1.00	.47	.52	1.00	.44	.48	1.00
.2	.33	.34	.35	.31	.32	.33	.41	.43	.45	.40	.41	.42
.3	.30	.31	.32	.28	.29	.30	.36	.38	.40	.36	.37	.39
.4	.28	.29	.29	.26	.27	.27	.33	.34	.35	.34	.35	.36
.5	.27	.28	.28	.24	.25	.26	.30	.32	.33	.32	.33	.34
.6	.25	.26	.27	.23	.24	.24	.28	.29	.30	.31	.31	.32
.7	.24	.25	.26	.21	.22	.23	.25	.27	.28	.29	.30	.31
.8	.21	.23	.24	.18	.21	.22	.21	.24	.26	.25	.28	.29
.9	.10	.15	.23	.09	.13	.20	.11	.15	.24	.12	.18	.28

	ANNUAL		
TRANS.	1	2	3
.1	.40	.44	1.00
.2	.36	.37	.39
.3	.33	.34	.35
.4	.30	.31	.32
.5	.29	.29	.30
.6	.27	.28	.29
.7	.25	.26	.27
.8	.21	.24	.25
.9	.11	.15	.24

FREQUENCY THAT TRANSMISSION EFFICIENCY EXCEEDS SPECIFIED VALUE--

MW-1: CHANUTE AFB (RANTOUL), IL N 40 18 W 088 09 ELEV 747 FT

	WINTER			SPRING			SUMMER			FALL		
TRANS.	1	2	3	1	2	3	1	2	3	1	2	3
.1	.93	.99	.99	.94	.99	.99	.96	.99	.99	.95	1.00	1.00
.2	.68	.97	.99	.72	.97	.99	.84	.98	.99	.80	.98	1.00
.3	.50	.63	.99	.56	.67	.99	.75	.82	.99	.68	.77	1.00
.4	.48	.49	.99	.53	.55	.99	.71	.73	.99	.65	.67	1.00
.5	.44	.47	.50	.48	.52	.56	.65	.70	.75	.62	.64	.68
.6	.41	.43	.48	.44	.47	.54	.60	.63	.72	.58	.60	.67
.7	.38	.39	.47	.40	.41	.52	.54	.56	.70	.54	.55	.65
.8	.34	.35	.39	.34	.36	.41	.46	.48	.55	.49	.50	.55
.9	.29	.31	.34	.28	.30	.34	.36	.40	.45	.42	.45	.48

	ANNUAL		
TRANS.	1	2	3
.1	.94	.99	.99
.2	.76	.98	.99
.3	.62	.72	.99
.4	.59	.61	.99
.5	.55	.58	.62
.6	.51	.53	.60
.7	.46	.48	.58
.8	.41	.42	.47
.9	.34	.36	.40

AVERAGE POWER AVAIABILITY--

MW-1: CHANUTE AFB (RANTOUL), IL N 40 18 W 088 09 ELEV 747 FT

	MODEL		
SEASON	1	2	3
WINTER	.44	.52	.67
SPRING	.47	.54	.68
SUMMER	.60	.65	.76
FALL	.59	.64	.76
ANNUAL	.53	.59	.72

FREQUENCY THAT TRANSMISSION EFFICIENCY EXCEEDS SPECIFIED VALUE
FOR A PERSISTENCE TIME OF 480.0 MINUTES--

MW-1: CHANUTE AFB (RANTOUL), IL N 40 18 W 088 09 ELEV 747 FT

	WINTER			SPRING			SUMMER			FALL		
TRANS.	1	2	3	1	2	3	1	2	3	1	2	3
.1	.29	.30	1.00	.27	.29	1.00	.35	.38	1.00	.41	.43	1.00
.2	.27	.28	.28	.25	.26	.27	.32	.33	.34	.39	.40	.40
.3	.25	.26	.27	.24	.24	.25	.29	.30	.31	.37	.37	.38
.4	.25	.25	.25	.23	.23	.23	.27	.28	.28	.36	.36	.36
.5	.24	.24	.24	.22	.22	.22	.26	.27	.27	.34	.35	.35
.6	.23	.23	.24	.21	.21	.22	.25	.25	.26	.33	.34	.34
.7	.22	.23	.23	.20	.21	.21	.23	.24	.25	.32	.33	.34
.8	.20	.22	.22	.18	.20	.20	.20	.23	.24	.28	.32	.33
.9	.10	.14	.22	.09	.13	.20	.10	.15	.23	.14	.20	.32

	ANNUAL		
TRANS.	1	2	3
.1	.33	.35	1.00
.2	.31	.31	.32
.3	.29	.29	.30
.4	.27	.28	.28
.5	.26	.27	.27
.6	.26	.26	.26
.7	.25	.25	.26
.8	.21	.24	.25
.9	.11	.15	.24

FREQUENCY THAT TRANSMISSION EFFICIENCY EXCEEDS SPECIFIED VALUE--

MW-2: WRIGHT-PATTERSON AFB (DAYTON), OH N 39 50 W 084 03 ELEV 827

	WINTER			SPRING			SUMMER			FALL		
TRANS.	1	2	3	1	2	3	1	2	3	1	2	3
.1	.92	.99	.99	.93	.99	.99	.95	.99	.99	.94	1.00	1.00
.2	.63	.97	.99	.70	.97	.99	.80	.98	.99	.72	.97	1.00
.3	.42	.57	.99	.53	.65	.99	.68	.76	.99	.57	.68	1.00
.4	.41	.42	.99	.51	.52	.99	.65	.67	.99	.55	.56	1.00
.5	.39	.40	.42	.49	.50	.53	.62	.64	.68	.53	.54	.57
.6	.37	.38	.41	.46	.48	.52	.59	.61	.66	.51	.52	.56
.7	.35	.36	.40	.43	.45	.51	.55	.57	.65	.48	.49	.55
.8	.31	.32	.35	.39	.40	.44	.49	.50	.56	.43	.44	.48
.9	.25	.28	.31	.31	.35	.38	.37	.43	.48	.35	.39	.42

	ANNUAL		
TRANS.	1	2	3
.1	.93	.99	.99
.2	.71	.97	.99
.3	.55	.67	.99
.4	.53	.54	.99
.5	.51	.52	.55
.6	.48	.50	.54
.7	.45	.47	.53
.8	.40	.41	.46
.9	.32	.36	.40

AVERAGE POWER AVAIABILITY--

MW-2: WRIGHT-PATTERSON AFB (DAYTON), OH N 39 50 W 084 03 ELEV 827

	MODEL		
SEASON	1	2	3
WINTER	.39	.47	.64
SPRING	.48	.54	.69
SUMMER	.58	.64	.75
FALL	.51	.58	.71
ANNUAL	.49	.56	.70

FREQUENCY THAT TRANSMISSION EFFICIENCY EXCEEDS SPECIFIED VALUE
FOR A PERSISTENCE TIME OF 480.0 MINUTES--

MW-2: WRIGHT-PATTERSON AFB (DAYTON), OH N 39 50 W 084 03 ELEV 827

	WINTER			SPRING			SUMMER			FALL		
TRANS.	1	2	3	1	2	3	1	2	3	1	2	3
.1	.24	.26	1.00	.30	.33	1.00	.35	.40	1.00	.34	.37	1.00
.2	.22	.22	.23	.27	.28	.29	.31	.32	.33	.31	.31	.32
.3	.20	.20	.21	.24	.25	.26	.26	.28	.29	.28	.28	.30
.4	.18	.19	.19	.22	.23	.23	.24	.25	.25	.26	.26	.27
.5	.17	.18	.18	.21	.22	.22	.22	.23	.23	.24	.25	.26
.6	.16	.17	.17	.20	.20	.21	.19	.21	.22	.23	.24	.24
.7	.15	.16	.16	.18	.19	.20	.17	.18	.20	.21	.22	.23
.8	.13	.15	.15	.15	.18	.19	.14	.16	.18	.18	.21	.22
.9	.06	.09	.15	.08	.11	.17	.07	.10	.16	.09	.13	.21

	ANNUAL		
TRANS.	1	2	3
.1	.31	.34	1.00
.2	.27	.28	.29
.3	.24	.25	.26
.4	.23	.23	.24
.5	.21	.22	.22
.6	.20	.20	.21
.7	.18	.19	.20
.8	.15	.17	.18
.9	.08	.11	.17

FREQUENCY THAT TRANSMISSION EFFICIENCY EXCEEDS SPECIFIED VALUE--

NE-1: PEASE AFB (PORTSMOUTH), NH N 43 05 W 070 49 ELEV 101 FT

	WINTER			SPRING			SUMMER			FALL		
TRANS.	1	2	3	1	2	3	1	2	3	1	2	3
.1	.94	1.00	1.00	.94	.99	.99	.94	1.00	1.00	.94	.99	.99
.2	.73	.97	1.00	.72	.97	.99	.75	.98	1.00	.76	.98	.99
.3	.57	.68	1.00	.57	.68	.99	.61	.71	1.00	.62	.72	.99
.4	.56	.57	1.00	.55	.56	.99	.58	.60	1.00	.60	.62	.99
.5	.54	.55	.57	.52	.54	.57	.56	.58	.61	.58	.60	.62
.6	.52	.53	.56	.50	.52	.56	.53	.55	.59	.55	.57	.61
.7	.49	.50	.55	.47	.48	.54	.49	.51	.58	.52	.54	.60
.8	.45	.46	.50	.42	.43	.48	.43	.44	.50	.47	.48	.53
.9	.36	.41	.44	.33	.37	.41	.32	.38	.42	.36	.42	.47

	ANNUAL		
TRANS.	1	2	3
.1	.94	.99	.99
.2	.74	.97	.99
.3	.59	.70	.99
.4	.57	.59	.99
.5	.55	.57	.59
.6	.52	.54	.58
.7	.49	.51	.57
.8	.44	.45	.50
.9	.34	.39	.44

AVERAGE POWER AVAIABILITY--

NE-1: PEASE AFB (PORTSMOUTH), NH N 43 05 W 070 49 ELEV 101 FT

	MODEL		
SEASON	1	2	3
WINTER	.52	.58	.71
SPRING	.50	.57	.70
SUMMER	.52	.59	.72
FALL	.55	.61	.73
ANNUAL	.52	.59	.72

FREQUENCY THAT TRANSMISSION EFFICIENCY EXCEEDS SPECIFIED VALUE
FOR A PERSISTENCE TIME OF 480.0 MINUTES--

NE-1: PEASE AFB (PORTSMOUTH), NH N 43 05 W 070 49 ELEV 101 FT

	WINTER			SPRING			SUMMER			FALL		
TRANS.	1	2	3	1	2	3	1	2	3	1	2	3
.1	.34	.38	1.00	.31	.35	1.00	.30	.34	1.00	.35	.39	1.00
.2	.30	.31	.33	.27	.28	.30	.25	.26	.28	.30	.31	.33
.3	.27	.28	.29	.24	.25	.26	.21	.22	.24	.26	.27	.29
.4	.25	.25	.26	.22	.22	.23	.18	.19	.20	.24	.24	.25
.5	.23	.24	.24	.20	.21	.22	.16	.17	.18	.22	.22	.23
.6	.21	.22	.23	.18	.19	.20	.14	.15	.16	.19	.20	.22
.7	.19	.20	.21	.16	.18	.19	.12	.13	.14	.17	.19	.20
.8	.16	.18	.20	.14	.16	.17	.09	.11	.12	.14	.17	.18
.9	.08	.12	.18	.07	.10	.15	.05	.07	.11	.07	.10	.16

	ANNUAL		
TRANS.	1	2	3
.1	.32	.37	1.00
.2	.28	.29	.31
.3	.24	.26	.27
.4	.22	.23	.23
.5	.20	.21	.22
.6	.18	.19	.20
.7	.16	.17	.18
.8	.13	.15	.17
.9	.07	.10	.15

FREQUENCY THAT TRANSMISSION EFFICIENCY EXCEEDS SPECIFIED VALUE--

NC-1: ELLSWORTH AFB (RAPID CITY), SD N 44 09 W 103 06 ELEV 3276 FT

	WINTER			SPRING			SUMMER			FALL		
TRANS.	1	2	3	1	2	3	1	2	3	1	2	3
.1	.93	.99	.99	.93	.99	.99	.97	.99	.99	.95	.99	.99
.2	.71	.97	.99	.69	.97	.99	.86	.99	.99	.79	.98	.99
.3	.55	.66	.99	.52	.64	.99	.77	.83	.99	.67	.75	.99
.4	.54	.54	.99	.52	.52	.99	.77	.77	.99	.66	.66	.99
.5	.50	.53	.55	.47	.51	.52	.72	.76	.78	.63	.65	.67
.6	.47	.48	.54	.44	.45	.52	.69	.70	.77	.61	.62	.66
.7	.45	.46	.53	.42	.43	.51	.67	.68	.76	.59	.59	.66
.8	.43	.44	.45	.40	.41	.43	.63	.65	.67	.56	.57	.59
.9	.23	.33	.41	.19	.30	.38	.31	.49	.61	.31	.46	.55

	ANNUAL		
TRANS.	1	2	3
.1	.95	.99	.99
.2	.76	.98	.99
.3	.63	.72	.99
.4	.62	.63	.99
.5	.58	.61	.63
.6	.55	.56	.62
.7	.53	.54	.62
.8	.50	.52	.54
.9	.26	.39	.49

AVERAGE POWER AVAIABILITY--

NC-1: ELLSWORTH AFB (RAPID CITY), SD N 44 09 W 103 06 ELEV 3276 FT

	MODEL		
SEASON	1	2	3
WINTER	.48	.55	.69
SPRING	.46	.53	.68
SUMMER	.66	.71	.80
FALL	.60	.65	.76
ANNUAL	.55	.61	.73

FREQUENCY THAT TRANSMISSION EFFICIENCY EXCEEDS SPECIFIED VALUE
FOR A PERSISTENCE TIME OF 480.0 MINUTES--

NC-1: ELLSWORTH AFB (RAPID CITY), SD N 44 09 W 103 06 ELEV 3276 FT

	WINTER			SPRING			SUMMER			FALL		
TRANS.	1	2	3	1	2	3	1	2	3	1	2	3
.1	.20	.28	1.00	.16	.24	1.00	.26	.39	1.00	.28	.38	1.00
.2	.20	.20	.20	.15	.16	.16	.25	.26	.26	.27	.27	.28
.3	.19	.19	.19	.14	.15	.15	.24	.24	.25	.26	.26	.27
.4	.18	.18	.18	.14	.14	.14	.23	.23	.24	.26	.26	.26
.5	.18	.18	.18	.14	.14	.14	.23	.23	.23	.25	.25	.25
.6	.18	.18	.18	.14	.14	.14	.22	.22	.23	.25	.25	.25
.7	.17	.17	.18	.13	.13	.14	.22	.22	.22	.24	.25	.25
.8	.15	.17	.17	.12	.13	.13	.19	.21	.22	.22	.24	.25
.9	.08	.11	.17	.06	.09	.13	.10	.14	.21	.11	.16	.24

	ANNUAL		
TRANS.	1	2	3
.1	.23	.32	1.00
.2	.22	.22	.22
.3	.21	.21	.21
.4	.20	.20	.21
.5	.20	.20	.20
.6	.20	.20	.20
.7	.19	.19	.20
.8	.17	.19	.19
.9	.09	.12	.19

FREQUENCY THAT TRANSMISSION EFFICIENCY EXCEEDS SPECIFIED VALUE--

NC-2: HILL AFB (OGDEN), UTAH N 41 07 W 111 58 ELEV 4787 FT

	WINTER			SPRING			SUMMER			FALL		
TRANS.	1	2	3	1	2	3	1	2	3	1	2	3
.1	.94	.99	.99	.94	.99	.99	.98	.99	.99	.97	.99	.99
.2	.72	.97	.99	.75	.98	.99	.93	.99	.99	.85	.99	.99
.3	.57	.68	.99	.61	.71	.99	.89	.92	.99	.77	.83	.99
.4	.54	.56	.99	.58	.60	.99	.86	.88	.99	.75	.76	.99
.5	.51	.54	.57	.55	.57	.61	.84	.86	.89	.73	.74	.77
.6	.48	.50	.55	.52	.54	.59	.81	.83	.87	.70	.72	.76
.7	.44	.46	.54	.48	.50	.58	.77	.79	.86	.67	.68	.74
.8	.38	.39	.45	.43	.44	.49	.72	.73	.78	.62	.63	.67
.9	.30	.34	.37	.33	.38	.42	.58	.66	.71	.52	.57	.61

	ANNUAL		
TRANS.	1	2	3
.1	.96	.99	.99
.2	.81	.98	.99
.3	.71	.78	.99
.4	.68	.70	.99
.5	.66	.68	.71
.6	.63	.65	.69
.7	.59	.61	.68
.8	.54	.55	.60
.9	.43	.48	.53

AVERAGE POWER AVAIABILITY--

NC-2: HILL AFB (OGDEN), UTAH N 41 07 W 111 58 ELEV 4787 FT

	MODEL		
SEASON	1	2	3
WINTER	.49	.56	.70
SPRING	.52	.59	.72
SUMMER	.78	.81	.87
FALL	.69	.73	.81
ANNUAL	.62	.67	.77

FREQUENCY THAT TRANSMISSION EFFICIENCY EXCEEDS SPECIFIED VALUE
FOR A PERSISTENCE TIME OF 480.0 MINUTES--

NC-2: HILL AFB (OGDEN), UTAH N 41 07 W 111 58 ELEV 4787 FT

	WINTER			SPRING			SUMMER			FALL		
TRANS.	1	2	3	1	2	3	1	2	3	1	2	3
.1	.29	.32	1.00	.31	.35	1.00	.56	.62	1.00	.50	.54	1.00
.2	.26	.27	.28	.28	.29	.30	.50	.52	.54	.46	.47	.49
.3	.23	.24	.25	.24	.26	.27	.44	.46	.48	.43	.44	.45
.4	.22	.22	.23	.22	.23	.24	.41	.42	.43	.40	.41	.42
.5	.20	.21	.22	.21	.21	.22	.38	.40	.41	.39	.39	.40
.6	.19	.20	.20	.19	.20	.21	.36	.37	.38	.37	.38	.39
.7	.18	.18	.19	.17	.18	.19	.33	.35	.36	.35	.36	.37
.8	.15	.17	.18	.14	.17	.18	.28	.32	.34	.30	.34	.35
.9	.07	.11	.17	.07	.10	.16	.14	.20	.31	.15	.22	.34

	ANNUAL		
TRANS.	1	2	3
.1	.41	.46	1.00
.2	.38	.39	.40
.3	.34	.35	.36
.4	.31	.32	.33
.5	.30	.30	.31
.6	.28	.29	.30
.7	.26	.27	.28
.8	.22	.25	.26
.9	.11	.16	.25

FREQUENCY THAT TRANSMISSION EFFICIENCY EXCEEDS SPECIFIED VALUE--

NW-1: FORT LEWIS (GRAY), WASHINGTON N 47 05 W 122 35 ELEV 311 FT

	WINTER			SPRING			SUMMER			FALL		
TRANS.	1	2	3	1	2	3	1	2	3	1	2	3
.1	.90	.99	.99	.93	.99	.99	.95	.99	.99	.93	1.00	1.00
.2	.58	.96	.99	.69	.97	.99	.79	.98	.99	.68	.97	1.00
.3	.34	.51	.99	.51	.64	.99	.67	.76	.99	.50	.63	1.00
.4	.31	.33	.99	.47	.49	.99	.63	.66	.99	.47	.49	1.00
.5	.27	.30	.34	.41	.45	.51	.59	.62	.67	.42	.45	.50
.6	.24	.26	.32	.35	.38	.48	.54	.57	.65	.38	.40	.48
.7	.20	.21	.30	.30	.32	.45	.49	.51	.62	.33	.35	.46
.8	.17	.18	.21	.25	.26	.31	.44	.45	.50	.29	.30	.34
.9	.13	.14	.16	.19	.22	.25	.38	.40	.43	.23	.25	.28

	ANNUAL		
TRANS.	1	2	3
.1	.93	.99	.99
.2	.68	.97	.99
.3	.50	.63	.99
.4	.47	.49	.99
.5	.42	.45	.50
.6	.38	.40	.48
.7	.33	.35	.46
.8	.29	.30	.34
.9	.23	.25	.28

AVERAGE POWER AVAIABILITY--

NW-1: FORT LEWIS (GRAY), WASHINGTON N 47 05 W 122 35 ELEV 311 FT

	MODEL		
SEASON	1	2	3
WINTER	.29	.38	.57
SPRING	.40	.48	.64
SUMMER	.56	.62	.74
FALL	.42	.49	.65
ANNUAL	.42	.49	.65

FREQUENCY THAT TRANSMISSION EFFICIENCY EXCEEDS SPECIFIED VALUE
FOR A PERSISTENCE TIME OF 480.0 MINUTES--

NW-1: FORT LEWIS (GRAY), WASHINGTON N 47 05 W 122 35 ELEV 311 FT

	WINTER			SPRING			SUMMER			FALL		
TRANS.	1	2	3	1	2	3	1	2	3	1	2	3
.1	.12	.13	1.00	.19	.20	1.00	.37	.39	1.00	.22	.24	1.00
.2	.11	.11	.12	.17	.17	.18	.35	.35	.36	.20	.21	.22
.3	.10	.10	.10	.15	.16	.16	.33	.33	.34	.19	.19	.20
.4	.09	.09	.09	.14	.15	.15	.31	.32	.32	.18	.18	.18
.5	.08	.09	.09	.14	.14	.14	.30	.31	.31	.17	.17	.17
.6	.08	.08	.08	.13	.13	.14	.29	.29	.30	.16	.16	.17
.7	.07	.08	.08	.12	.13	.13	.28	.28	.29	.15	.16	.16
.8	.06	.07	.08	.10	.12	.12	.24	.27	.28	.13	.15	.15
.9	.03	.05	.07	.05	.07	.12	.12	.17	.27	.07	.09	.15

	ANNUAL		
TRANS.	1	2	3
.1	.22	.24	1.00
.2	.21	.21	.22
.3	.19	.20	.20
.4	.18	.18	.19
.5	.17	.18	.18
.6	.16	.17	.17
.7	.16	.16	.17
.8	.14	.15	.16
.9	.07	.10	.15

FREQUENCY THAT TRANSMISSION EFFICIENCY EXCEEDS SPECIFIED VALUE--

SC-1: LITTLE ROCK AFB, ARKANSAS N 34 55 W 092 09 ELEV 311 FT

	WINTER			SPRING			SUMMER			FALL		
TRANS.	1	2	3	1	2	3	1	2	3	1	2	3
.1	.93	.99	.99	.94	.99	.99	.97	.99	.99	.95	1.00	1.00
.2	.71	.97	.99	.75	.98	.99	.86	.99	.99	.78	.98	1.00
.3	.56	.67	.99	.61	.71	.99	.78	.84	.99	.66	.75	1.00
.4	.54	.55	.99	.59	.60	.99	.76	.78	.99	.64	.65	1.00
.5	.52	.54	.56	.57	.58	.61	.73	.75	.79	.62	.64	.66
.6	.51	.52	.55	.54	.56	.60	.70	.72	.77	.60	.61	.65
.7	.48	.49	.54	.51	.53	.59	.66	.68	.75	.57	.58	.64
.8	.45	.46	.49	.46	.47	.52	.60	.61	.67	.53	.54	.58
.9	.38	.42	.44	.38	.42	.46	.47	.54	.59	.44	.49	.52

	ANNUAL		
TRANS.	1	2	3
.1	.95	.99	.99
.2	.78	.98	.99
.3	.65	.74	.99
.4	.63	.65	.99
.5	.61	.63	.65
.6	.59	.60	.64
.7	.56	.57	.63
.8	.51	.52	.56
.9	.42	.47	.50

AVERAGE POWER AVAIABILITY--

SC-1: LITTLE ROCK AFB, ARKANSAS N 34 55 W 092 09 ELEV 311 FT

	MODEL		
SEASON	1	2	3
WINTER	.52	.58	.71
SPRING	.55	.61	.73
SUMMER	.68	.72	.81
FALL	.60	.65	.76
ANNUAL	.59	.64	.75

FREQUENCY THAT TRANSMISSION EFFICIENCY EXCEEDS SPECIFIED VALUE
FOR A PERSISTENCE TIME OF 480.0 MINUTES--

SC-1: LITTLE ROCK AFB, ARKANSAS N 34 55 W 092 09 ELEV 311 FT

	WINTER			SPRING			SUMMER			FALL		
TRANS.	1	2	3	1	2	3	1	2	3	1	2	3
.1	.37	.40	1.00	.36	.40	1.00	.45	.50	1.00	.43	.46	1.00
.2	.35	.36	.36	.33	.34	.35	.40	.41	.43	.40	.41	.42
.3	.32	.33	.34	.30	.31	.32	.35	.37	.38	.37	.38	.39
.4	.31	.31	.32	.28	.29	.29	.32	.33	.34	.35	.35	.36
.5	.30	.30	.31	.27	.27	.28	.30	.31	.32	.33	.34	.34
.6	.29	.29	.30	.25	.26	.27	.27	.29	.30	.32	.32	.33
.7	.27	.28	.29	.24	.24	.25	.25	.26	.28	.30	.31	.32
.8	.24	.27	.28	.20	.23	.24	.21	.24	.26	.26	.29	.30
.9	.12	.17	.27	.10	.15	.23	.10	.15	.23	.13	.19	.29

	ANNUAL		
TRANS.	1	2	3
.1	.40	.44	1.00
.2	.37	.38	.39
.3	.34	.35	.36
.4	.32	.32	.33
.5	.30	.31	.31
.6	.28	.29	.30
.7	.26	.27	.28
.8	.23	.26	.27
.9	.11	.16	.25

FREQUENCY THAT TRANSMISSION EFFICIENCY EXCEEDS SPECIFIED VALUE--

SC-2: BARKSDALE AFB (SHREVEPORT), LA N 32 30 W 093 40 ELEV 177 FT

	WINTER			SPRING			SUMMER			FALL		
TRANS.	1	2	3	1	2	3	1	2	3	1	2	3
.1	.93	1.00	1.00	.95	.99	.99	.97	.99	.99	.96	.99	.99
.2	.70	.97	1.00	.76	.98	.99	.89	.99	.99	.84	.98	.99
.3	.54	.66	1.00	.62	.72	.99	.82	.87	.99	.75	.82	.99
.4	.51	.53	1.00	.59	.61	.99	.78	.80	.99	.72	.74	.99
.5	.47	.50	.54	.54	.57	.62	.73	.77	.82	.68	.71	.75
.6	.44	.46	.52	.49	.52	.60	.67	.70	.79	.64	.66	.73
.7	.41	.42	.50	.45	.46	.58	.60	.63	.77	.60	.62	.71
.8	.37	.38	.42	.39	.40	.46	.51	.53	.62	.55	.56	.61
.9	.33	.35	.37	.33	.35	.38	.38	.43	.49	.48	.51	.54

	ANNUAL		
TRANS.	1	2	3
.1	.95	.99	.99
.2	.80	.98	.99
.3	.68	.77	.99
.4	.65	.67	.99
.5	.60	.64	.68
.6	.56	.59	.66
.7	.51	.53	.64
.8	.46	.47	.53
.9	.38	.41	.45

AVERAGE POWER AVAIABILITY--

SC-2: BARKSDALE AFB (SHREVEPORT), LA N 32 30 W 093 40 ELEV 177 FT

	MODEL		
SEASON	1	2	3
WINTER	.47	.54	.68
SPRING	.52	.58	.71
SUMMER	.66	.70	.80
FALL	.65	.69	.79
ANNUAL	.57	.63	.75

FREQUENCY THAT TRANSMISSION EFFICIENCY EXCEEDS SPECIFIED VALUE
FOR A PERSISTENCE TIME OF 480.0 MINUTES--

SC-2: BARKSDALE AFB (SHREVEPORT), LA N 32 30 W 093 40 ELEV 177 FT

	WINTER			SPRING			SUMMER			FALL		
TRANS.	1	2	3	1	2	3	1	2	3	1	2	3
.1	.32	.34	1.00	.32	.34	1.00	.37	.40	1.00	.47	.49	1.00
.2	.31	.31	.32	.30	.30	.31	.33	.34	.36	.44	.45	.46
.3	.29	.30	.30	.28	.29	.29	.30	.31	.32	.42	.43	.44
.4	.28	.28	.29	.27	.27	.28	.28	.29	.29	.41	.41	.41
.5	.27	.28	.28	.26	.27	.27	.27	.28	.28	.39	.40	.40
.6	.27	.27	.27	.25	.26	.26	.26	.26	.27	.38	.39	.39
.7	.26	.26	.27	.24	.25	.25	.24	.25	.26	.37	.38	.38
.8	.23	.26	.26	.22	.24	.25	.21	.24	.25	.33	.37	.37
.9	.12	.17	.26	.11	.16	.24	.11	.15	.24	.16	.24	.36

	ANNUAL		
TRANS.	1	2	3
.1	.37	.39	1.00
.2	.35	.35	.36
.3	.32	.33	.34
.4	.31	.31	.32
.5	.30	.30	.31
.6	.29	.30	.30
.7	.28	.29	.29
.8	.25	.28	.28
.9	.12	.18	.27

FREQUENCY THAT TRANSMISSION EFFICIENCY EXCEEDS SPECIFIED VALUE--

SC-3: KIRTLAND AFB (ALBUQUERQUE), NM N 35 03 W 106 37 ELEV 5352 F

	WINTER			SPRING			SUMMER			FALL		
TRANS.	1	2	3	1	2	3	1	2	3	1	2	3
.1	.96	.99	.99	.97	.99	.99	.98	.99	.99	.98	.99	.99
.2	.83	.98	.99	.87	.99	.99	.91	.99	.99	.90	.99	.99
.3	.74	.81	.99	.80	.85	.99	.85	.89	.99	.84	.89	.99
.4	.72	.73	.99	.78	.79	.99	.82	.84	.99	.83	.84	.99
.5	.69	.71	.74	.75	.77	.80	.79	.81	.85	.80	.82	.84
.6	.67	.68	.72	.72	.73	.79	.75	.77	.83	.78	.79	.83
.7	.63	.65	.71	.68	.69	.77	.70	.72	.82	.75	.76	.82
.8	.59	.60	.64	.62	.63	.69	.63	.65	.72	.70	.71	.76
.9	.51	.55	.58	.53	.57	.61	.52	.57	.62	.62	.66	.70

	ANNUAL		
TRANS.	1	2	3
.1	.97	.99	.99
.2	.88	.99	.99
.3	.81	.86	.99
.4	.79	.80	.99
.5	.76	.78	.81
.6	.73	.74	.79
.7	.69	.71	.78
.8	.64	.65	.70
.9	.55	.59	.63

AVERAGE POWER AVAIABILITY--

SC-3: KIRTLAND AFB (ALBUQUERQUE), NM N 35 03 W 106 37 ELEV 5352 F

	MODEL		
SEASON	1	2	3
WINTER	.66	.71	.80
SPRING	.71	.74	.82
SUMMER	.73	.76	.84
FALL	.77	.80	.86
ANNUAL	.72	.75	.83

FREQUENCY THAT TRANSMISSION EFFICIENCY EXCEEDS SPECIFIED VALUE
FOR A PERSISTENCE TIME OF 480.0 MINUTES--

SC-3: KIRTLAND AFB (ALBUQUERQUE), NM N 35 03 W 106 37 ELEV 5352 F

	WINTER			SPRING			SUMMER			FALL		
TRANS.	1	2	3	1	2	3	1	2	3	1	2	3
.1	.50	.53	1.00	.52	.55	1.00	.50	.54	1.00	.61	.64	1.00
.2	.47	.48	.49	.49	.50	.51	.46	.47	.49	.58	.59	.60
.3	.45	.46	.47	.46	.47	.48	.42	.43	.45	.56	.57	.58
.4	.43	.44	.44	.44	.44	.45	.40	.40	.41	.54	.55	.55
.5	.42	.43	.43	.42	.43	.44	.37	.38	.39	.53	.53	.54
.6	.41	.41	.42	.41	.41	.42	.35	.36	.37	.51	.52	.53
.7	.39	.40	.41	.39	.40	.41	.33	.34	.36	.50	.50	.51
.8	.35	.39	.40	.34	.39	.40	.28	.32	.34	.44	.49	.50
.9	.17	.25	.39	.17	.25	.38	.14	.20	.32	.22	.32	.49

	ANNUAL		
TRANS.	1	2	3
.1	.53	.57	1.00
.2	.50	.51	.52
.3	.47	.48	.49
.4	.45	.46	.46
.5	.44	.44	.45
.6	.42	.43	.44
.7	.40	.41	.42
.8	.35	.40	.41
.9	.18	.25	.39

FREQUENCY THAT TRANSMISSION EFFICIENCY EXCEEDS SPECIFIED VALUE--

SC-4: SHEPPARD AFB (WICHITA FALLS), TX N 33 58 W 098 29 ELEV 1015

	WINTER			SPRING			SUMMER			FALL		
TRANS.	1	2	3	1	2	3	1	2	3	1	2	3
.1	.95	.99	.99	.95	.99	.99	.98	.99	.99	.97	.99	.99
.2	.78	.98	.99	.80	.98	.99	.91	.99	.99	.87	.99	.99
.3	.66	.75	.99	.68	.77	.99	.85	.89	.99	.79	.84	.99
.4	.64	.65	.99	.66	.68	.99	.82	.84	.99	.77	.78	.99
.5	.61	.63	.66	.62	.65	.69	.78	.81	.85	.74	.76	.79
.6	.58	.60	.65	.58	.61	.67	.74	.76	.83	.71	.73	.78
.7	.55	.56	.63	.54	.56	.65	.68	.71	.81	.67	.69	.76
.8	.51	.52	.56	.50	.51	.55	.62	.63	.70	.63	.64	.68
.9	.47	.49	.51	.44	.46	.49	.53	.57	.61	.58	.60	.63

	ANNUAL		
TRANS.	1	2	3
.1	.96	.99	.99
.2	.84	.99	.99
.3	.75	.81	.99
.4	.72	.74	.99
.5	.69	.71	.75
.6	.65	.67	.73
.7	.61	.63	.71
.8	.57	.57	.62
.9	.50	.53	.56

AVERAGE POWER AVAIABILITY--

SC-4: SHEPPARD AFB (WICHITA FALLS), TX N 33 58 W 098 29 ELEV 1015

	MODEL		
SEASON	1	2	3
WINTER	.60	.65	.76
SPRING	.60	.65	.76
SUMMER	.73	.76	.84
FALL	.71	.75	.83
ANNUAL	.66	.70	.80

FREQUENCY THAT TRANSMISSION EFFICIENCY EXCEEDS SPECIFIED VALUE
FOR A PERSISTENCE TIME OF 480.0 MINUTES--

SC-4: SHEPPARD AFB (WICHITA FALLS), TX N 33 58 W 098 29 ELEV 1015

	WINTER			SPRING			SUMMER			FALL		
TRANS.	1	2	3	1	2	3	1	2	3	1	2	3
.1	.46	.48	1.00	.43	.45	1.00	.52	.55	1.00	.57	.59	1.00
.2	.45	.45	.46	.41	.42	.42	.49	.50	.51	.55	.56	.56
.3	.43	.44	.44	.40	.40	.41	.46	.47	.48	.53	.54	.55
.4	.42	.43	.43	.38	.39	.39	.44	.45	.46	.52	.53	.53
.5	.42	.42	.42	.37	.38	.38	.43	.43	.44	.51	.52	.52
.6	.41	.41	.42	.36	.37	.37	.41	.42	.43	.50	.51	.51
.7	.40	.40	.41	.35	.36	.37	.39	.40	.41	.49	.50	.50
.8	.36	.40	.40	.31	.35	.36	.35	.39	.40	.44	.49	.50
.9	.18	.26	.40	.16	.23	.35	.17	.25	.38	.22	.32	.49

	ANNUAL		
TRANS.	1	2	3
.1	.49	.51	1.00
.2	.48	.48	.49
.3	.46	.46	.47
.4	.44	.45	.45
.5	.43	.44	.44
.6	.42	.43	.43
.7	.41	.42	.42
.8	.36	.41	.41
.9	.18	.26	.40

FREQUENCY THAT TRANSMISSION EFFICIENCY EXCEEDS SPECIFIED VALUE--

SC-5: CONNALLY AFB (WACO), TEXAS N 38 38 W 097 04 ELEV 475 FT

	WINTER			SPRING			SUMMER			FALL		
TRANS.	1	2	3	1	2	3	1	2	3	1	2	3
.1	.94	.99	.99	.95	.99	.99	.98	.99	.99	.97	.99	.99
.2	.74	.97	.99	.77	.98	.99	.92	.99	.99	.86	.99	.99
.3	.59	.70	.99	.64	.73	.99	.87	.91	.99	.77	.83	.99
.4	.56	.58	.99	.60	.63	.99	.84	.86	.99	.74	.76	.99
.5	.53	.55	.59	.55	.59	.64	.79	.83	.87	.70	.73	.77
.6	.49	.51	.57	.50	.53	.62	.73	.76	.85	.67	.69	.75
.7	.46	.47	.56	.45	.47	.60	.67	.69	.83	.63	.64	.74
.8	.42	.42	.46	.39	.41	.46	.57	.59	.68	.58	.59	.64
.9	.37	.39	.41	.33	.35	.39	.44	.49	.56	.51	.54	.57

	ANNUAL		
TRANS.	1	2	3
.1	.96	.99	.99
.2	.82	.98	.99
.3	.72	.79	.99
.4	.69	.71	.99
.5	.64	.68	.72
.6	.60	.62	.70
.7	.55	.57	.68
.8	.49	.50	.56
.9	.41	.44	.48

AVERAGE POWER AVAIABILITY--

SC-5: CONNALLY AFB (WACO), TEXAS N 38 38 W 097 04 ELEV 475 FT

	MODEL		
SEASON	1	2	3
WINTER	.52	.58	.71
SPRING	.53	.59	.72
SUMMER	.71	.75	.83
FALL	.67	.71	.80
ANNUAL	.61	.66	.77

FREQUENCY THAT TRANSMISSION EFFICIENCY EXCEEDS SPECIFIED VALUE
FOR A PERSISTENCE TIME OF 480.0 MINUTES--

SC-5: CONNALLY AFB (WACO), TEXAS N 38 38 W 097 04 ELEV 475 FT

	WINTER			SPRING			SUMMER			FALL		
TRANS.	1	2	3	1	2	3	1	2	3	1	2	3
.1	.36	.38	1.00	.32	.34	1.00	.43	.47	1.00	.50	.52	1.00
.2	.35	.35	.35	.30	.30	.31	.39	.40	.42	.48	.48	.49
.3	.33	.33	.34	.28	.28	.29	.36	.37	.38	.46	.46	.47
.4	.32	.32	.33	.27	.27	.27	.34	.35	.35	.44	.45	.45
.5	.31	.32	.32	.26	.26	.27	.32	.33	.34	.43	.43	.44
.6	.30	.31	.31	.25	.25	.26	.31	.31	.32	.42	.42	.43
.7	.30	.30	.30	.24	.24	.25	.29	.30	.31	.40	.41	.42
.8	.26	.29	.30	.21	.24	.24	.25	.28	.29	.36	.40	.41
.9	.13	.19	.29	.10	.15	.23	.12	.18	.28	.18	.26	.40

	ANNUAL		
TRANS.	1	2	3
.1	.40	.43	1.00
.2	.38	.39	.39
.3	.36	.36	.37
.4	.34	.35	.35
.5	.33	.34	.34
.6	.32	.32	.33
.7	.31	.31	.32
.8	.27	.30	.31
.9	.13	.19	.30

FREQUENCY THAT TRANSMISSION EFFICIENCY EXCEEDS SPECIFIED VALUE--

SE-1: HUNTSVILLE, ALABAMA N 34 42 W 86 35 ELEV 644 FT

	WINTER			SPRING			SUMMER			FALL		
TRANS.	1	2	3	1	2	3	1	2	3	1	2	3
.1	.92	1.00	1.00	.95	.99	.99	.97	.99	.99	.96	1.00	1.00
.2	.68	.97	1.00	.77	.98	.99	.86	.99	.99	.81	.98	1.00
.3	.50	.63	1.00	.64	.74	.99	.76	.83	.99	.70	.78	1.00
.4	.48	.49	1.00	.61	.63	.99	.72	.75	.99	.67	.69	1.00
.5	.45	.47	.50	.57	.60	.64	.65	.70	.77	.63	.66	.70
.6	.42	.43	.48	.53	.55	.63	.59	.63	.74	.60	.62	.68
.7	.39	.40	.47	.48	.50	.60	.52	.55	.70	.56	.57	.66
.8	.36	.37	.40	.44	.45	.50	.44	.45	.54	.52	.53	.57
.9	.31	.33	.35	.35	.39	.43	.31	.36	.42	.44	.47	.51

	ANNUAL		
TRANS.	1	2	3
.1	.95	1.00	1.00
.2	.78	.98	1.00
.3	.65	.74	1.00
.4	.62	.64	1.00
.5	.58	.61	.65
.6	.53	.56	.63
.7	.49	.51	.61
.8	.44	.45	.50
.9	.35	.39	.43

AVERAGE POWER AVAIABILITY--

SE-1: HUNTSVILLE, ALABAMA N 34 42 W 86 35 ELEV 644 FT

	MODEL		
SEASON	1	2	3
WINTER	.45	.52	.67
SPRING	.55	.60	.73
SUMMER	.60	.65	.76
FALL	.61	.66	.77
ANNUAL	.55	.61	.73

FREQUENCY THAT TRANSMISSION EFFICIENCY EXCEEDS SPECIFIED VALUE
FOR A PERSISTENCE TIME OF 480.0 MINUTES--

SE-1: HUNTSVILLE, ALABAMA N 34 42 W 86 35 ELEV 644 FT

	WINTER			SPRING			SUMMER			FALL		
TRANS.	1	2	3	1	2	3	1	2	3	1	2	3
.1	.30	.32	1.00	.35	.37	1.00	.30	.34	1.00	.43	.45	1.00
.2	.29	.29	.30	.33	.33	.34	.28	.28	.29	.41	.42	.42
.3	.28	.28	.29	.31	.31	.32	.25	.26	.27	.40	.40	.41
.4	.27	.27	.27	.30	.30	.30	.24	.24	.25	.39	.39	.39
.5	.27	.27	.27	.29	.29	.30	.23	.24	.24	.38	.38	.39
.6	.26	.27	.27	.28	.29	.29	.22	.23	.23	.37	.38	.38
.7	.26	.26	.26	.28	.28	.28	.21	.22	.22	.36	.37	.37
.8	.23	.26	.26	.24	.27	.28	.19	.21	.22	.32	.36	.37
.9	.12	.17	.26	.12	.18	.27	.09	.13	.21	.16	.23	.36

	ANNUAL		
TRANS.	1	2	3
.1	.34	.37	1.00
.2	.33	.33	.34
.3	.31	.31	.32
.4	.30	.30	.30
.5	.29	.30	.30
.6	.29	.29	.29
.7	.28	.28	.29
.8	.25	.28	.28
.9	.12	.18	.27

FREQUENCY THAT TRANSMISSION EFFICIENCY EXCEEDS SPECIFIED VALUE--

SE-2: MACDILL AFB (TAMPA), FLORIDA N 27 51 W 082 30 ELEV 13 FT

	WINTER			SPRING			SUMMER			FALL		
TRANS.	1	2	3	1	2	3	1	2	3	1	2	3
.1	.96	.99	.99	.97	.99	.99	.97	.99	.99	.97	.99	.99
.2	.82	.98	.99	.86	.99	.99	.86	.99	.99	.87	.99	.99
.3	.72	.79	.99	.78	.84	.99	.77	.83	.99	.79	.85	.99
.4	.69	.71	.99	.76	.77	.99	.73	.76	.99	.76	.78	.99
.5	.67	.69	.72	.73	.75	.78	.69	.72	.77	.73	.75	.79
.6	.64	.66	.70	.70	.72	.77	.65	.68	.75	.70	.72	.77
.7	.60	.62	.69	.67	.68	.75	.59	.62	.73	.66	.67	.76
.8	.55	.56	.61	.61	.62	.67	.51	.52	.61	.59	.60	.67
.9	.44	.50	.54	.48	.55	.60	.36	.43	.49	.46	.53	.58

	ANNUAL		
TRANS.	1	2	3
.1	.97	.99	.99
.2	.85	.99	.99
.3	.76	.83	.99
.4	.74	.76	.99
.5	.71	.73	.77
.6	.67	.69	.75
.7	.63	.65	.73
.8	.56	.58	.64
.9	.44	.50	.55

AVERAGE POWER AVAIABILITY--

SE-2: MACDILL AFB (TAMPA), FLORIDA N 27 51 W 082 30 ELEV 13 FT

	MODEL		
SEASON	1	2	3
WINTER	.63	.68	.78
SPRING	.68	.72	.81
SUMMER	.63	.67	.78
FALL	.68	.72	.81
ANNUAL	.65	.70	.79

FREQUENCY THAT TRANSMISSION EFFICIENCY EXCEEDS SPECIFIED VALUE
FOR A PERSISTENCE TIME OF 480.0 MINUTES--

SE-2: MACDILL AFB (TAMPA), FLORIDA N 27 51 W 082 30 ELEV 13 FT

	WINTER			SPRING			SUMMER			FALL		
TRANS.	1	2	3	1	2	3	1	2	3	1	2	3
.1	.43	.47	1.00	.46	.51	1.00	.33	.39	1.00	.44	.50	1.00
.2	.39	.40	.41	.41	.42	.44	.28	.29	.31	.40	.41	.43
.3	.35	.36	.38	.36	.37	.39	.22	.24	.26	.35	.36	.38
.4	.33	.33	.34	.33	.34	.35	.19	.20	.21	.32	.33	.34
.5	.31	.32	.32	.30	.31	.32	.17	.18	.19	.30	.31	.32
.6	.29	.30	.31	.28	.29	.30	.14	.15	.17	.27	.28	.30
.7	.27	.28	.29	.25	.27	.28	.11	.13	.14	.25	.26	.28
.8	.23	.26	.27	.21	.24	.26	.08	.10	.12	.21	.24	.26
.9	.11	.16	.26	.10	.15	.24	.04	.06	.10	.10	.15	.24

	ANNUAL		
TRANS.	1	2	3
.1	.42	.47	1.00
.2	.37	.38	.40
.3	.32	.33	.35
.4	.29	.30	.31
.5	.27	.28	.29
.6	.24	.26	.27
.7	.22	.23	.25
.8	.18	.21	.23
.9	.09	.13	.21

FREQUENCY THAT TRANSMISSION EFFICIENCY EXCEEDS SPECIFIED VALUE--

SE-3: DOBBINS AFB (MARIETTA), GA N 33 55 W 084 32 ELEV 1068 FT

	WINTER			SPRING			SUMMER			FALL		
TRANS.	1	2	3	1	2	3	1	2	3	1	2	3
.1	.93	.99	.99	.95	.99	.99	.97	.99	.99	.96	.99	.99
.2	.71	.97	.99	.78	.98	.99	.85	.99	.99	.82	.98	.99
.3	.55	.67	.99	.66	.75	.99	.75	.83	.99	.72	.79	.99
.4	.53	.54	.99	.62	.65	.99	.71	.74	.99	.69	.71	.99
.5	.49	.52	.55	.58	.61	.66	.65	.70	.76	.65	.68	.72
.6	.45	.47	.54	.53	.56	.64	.58	.62	.73	.61	.63	.70
.7	.42	.43	.52	.49	.50	.62	.51	.53	.70	.57	.59	.68
.8	.38	.39	.43	.43	.44	.50	.42	.44	.52	.52	.53	.58
.9	.33	.35	.38	.36	.38	.42	.30	.35	.40	.45	.48	.51

	ANNUAL		
TRANS.	1	2	3
.1	.95	.99	.99
.2	.79	.98	.99
.3	.67	.76	.99
.4	.64	.66	.99
.5	.59	.63	.67
.6	.54	.57	.65
.7	.50	.51	.63
.8	.44	.45	.51
.9	.36	.39	.43

AVERAGE POWER AVAIABILITY--

SE-3: DOBBINS AFB (MARIETTA), GA N 33 55 W 084 32 ELEV 1068 FT

	MODEL		
SEASON	1	2	3
WINTER	.49	.55	.69
SPRING	.55	.61	.73
SUMMER	.59	.64	.75
FALL	.62	.67	.77
ANNUAL	.56	.62	.74

FREQUENCY THAT TRANSMISSION EFFICIENCY EXCEEDS SPECIFIED VALUE
FOR A PERSISTENCE TIME OF 480.0 MINUTES--

SE-3: DOBBINS AFB (MARIETTA), GA N 33 55 W 084 32 ELEV 1068 FT

	WINTER			SPRING			SUMMER			FALL		
TRANS.	1	2	3	1	2	3	1	2	3	1	2	3
.1	.32	.34	1.00	.35	.37	1.00	.29	.32	1.00	.45	.47	1.00
.2	.31	.31	.32	.33	.33	.34	.26	.27	.28	.42	.43	.44
.3	.29	.30	.30	.31	.31	.32	.24	.24	.25	.40	.41	.42
.4	.28	.29	.29	.30	.30	.30	.22	.23	.23	.39	.39	.40
.5	.28	.28	.28	.29	.29	.29	.21	.22	.22	.38	.38	.39
.6	.27	.27	.28	.28	.28	.29	.20	.21	.21	.37	.37	.38
.7	.26	.27	.27	.27	.27	.28	.19	.20	.20	.36	.36	.37
.8	.23	.26	.26	.24	.26	.27	.16	.19	.19	.32	.35	.36
.9	.12	.17	.26	.12	.17	.26	.08	.12	.18	.16	.23	.35

	ANNUAL		
TRANS.	1	2	3
.1	.35	.37	1.00
.2	.33	.34	.34
.3	.31	.32	.32
.4	.30	.30	.30
.5	.29	.29	.30
.6	.28	.28	.29
.7	.27	.27	.28
.8	.24	.27	.27
.9	.12	.17	.26

FREQUENCY THAT TRANSMISSION EFFICIENCY EXCEEDS SPECIFIED VALUE--

SE-4: COLUMBUS AFB, MISSISSIPPI N 33 39 W 088 27 ELEV 219 FT

	WINTER			SPRING			SUMMER			FALL		
TRANS.	1	2	3	1	2	3	1	2	3	1	2	3
.1	.93	.99	.99	.95	.99	.99	.96	.99	.99	.96	.99	.99
.2	.69	.97	.99	.77	.98	.99	.84	.99	.99	.81	.98	.99
.3	.52	.64	.99	.63	.73	.99	.74	.81	.99	.71	.78	.99
.4	.49	.51	.99	.61	.63	.99	.70	.72	.99	.68	.70	.99
.5	.46	.48	.52	.56	.59	.64	.62	.68	.74	.64	.67	.71
.6	.42	.44	.50	.51	.54	.62	.55	.59	.71	.60	.62	.69
.7	.39	.40	.48	.46	.48	.60	.48	.51	.68	.55	.57	.67
.8	.36	.36	.40	.41	.42	.48	.38	.40	.49	.50	.51	.56
.9	.31	.33	.35	.33	.36	.40	.27	.31	.37	.43	.46	.49

	ANNUAL		
TRANS.	1	2	3
.1	.95	.99	.99
.2	.78	.98	.99
.3	.65	.74	.99
.4	.62	.64	.99
.5	.57	.61	.65
.6	.52	.55	.63
.7	.47	.49	.61
.8	.41	.43	.48
.9	.33	.36	.40

AVERAGE POWER AVAIABILITY--

SE-4: COLUMBUS AFB, MISSISSIPPI N 33 39 W 088 27 ELEV 219 FT

	MODEL		
SEASON	1	2	3
WINTER	.46	.53	.67
SPRING	.53	.59	.72
SUMMER	.56	.61	.74
FALL	.61	.66	.77
ANNUAL	.54	.60	.72

FREQUENCY THAT TRANSMISSION EFFICIENCY EXCEEDS SPECIFIED VALUE
FOR A PERSISTENCE TIME OF 480.0 MINUTES--

SE-4: COLUMBUS AFB, MISSISSIPPI N 33 39 W 088 27 ELEV 219 FT

	WINTER			SPRING			SUMMER			FALL		
TRANS.	1	2	3	1	2	3	1	2	3	1	2	3
.1	.31	.32	1.00	.32	.34	1.00	.25	.29	1.00	.42	.44	1.00
.2	.29	.29	.30	.30	.30	.31	.22	.23	.24	.39	.40	.41
.3	.27	.28	.28	.27	.28	.29	.20	.20	.22	.37	.37	.38
.4	.26	.26	.27	.26	.26	.27	.18	.18	.19	.35	.35	.36
.5	.25	.25	.26	.25	.25	.26	.17	.17	.18	.34	.34	.35
.6	.24	.24	.25	.24	.24	.25	.16	.16	.17	.32	.33	.34
.7	.23	.24	.24	.23	.23	.24	.14	.15	.16	.31	.32	.32
.8	.20	.23	.23	.20	.22	.23	.12	.14	.15	.27	.30	.31
.9	.10	.14	.22	.10	.14	.22	.06	.09	.14	.13	.19	.30

	ANNUAL		
TRANS.	1	2	3
.1	.32	.35	1.00
.2	.30	.31	.32
.3	.28	.28	.29
.4	.26	.27	.27
.5	.25	.26	.26
.6	.24	.24	.25
.7	.23	.23	.24
.8	.20	.22	.23
.9	.10	.14	.22

FREQUENCY THAT TRANSMISSION EFFICIENCY EXCEEDS SPECIFIED VALUE--

SE-5: FORT BRAGG (FAYETTEVILLE), N CAROLINA N 35 08 W 078 56 ELEV 244

	WINTER			SPRING			SUMMER			FALL		
TRANS.	1	2	3	1	2	3	1	2	3	1	2	3
.1	.94	.99	.99	.95	.99	.99	.95	.99	.99	.96	.99	.99
.2	.73	.97	.99	.77	.98	.99	.78	.98	.99	.83	.98	.99
.3	.59	.69	.99	.64	.73	.99	.65	.74	.99	.72	.80	.99
.4	.57	.58	.99	.61	.63	.99	.62	.64	.99	.70	.72	.99
.5	.54	.56	.59	.57	.60	.64	.55	.60	.65	.66	.69	.72
.6	.50	.52	.57	.52	.55	.62	.48	.52	.63	.62	.64	.71
.7	.47	.48	.56	.48	.50	.61	.42	.44	.61	.57	.59	.69
.8	.43	.44	.48	.42	.44	.49	.34	.36	.43	.52	.53	.58
.9	.38	.40	.43	.35	.38	.41	.24	.27	.33	.44	.47	.51

	ANNUAL		
TRANS.	1	2	3
.1	.95	.99	.99
.2	.78	.98	.99
.3	.65	.74	.99
.4	.62	.64	.99
.5	.58	.61	.65
.6	.53	.56	.63
.7	.49	.50	.62
.8	.43	.44	.50
.9	.35	.38	.42

AVERAGE POWER AVAIABILITY--

SE-5: FORT BRAGG (FAYETTEVILLE), N CAROLINA N 35 08 W 078 56 ELEV 244

	MODEL		
SEASON	1	2	3
WINTER	.53	.59	.72
SPRING	.54	.60	.73
SUMMER	.50	.57	.70
FALL	.62	.67	.78
ANNUAL	.55	.61	.73

FREQUENCY THAT TRANSMISSION EFFICIENCY EXCEEDS SPECIFIED VALUE
FOR A PERSISTENCE TIME OF 480.0 MINUTES--

SE-5: FORT BRAGG (FAYETTEVILLE), N CAROLINA N 35 08 W 078 56 ELEV 244

	WINTER			SPRING			SUMMER			FALL		
TRANS.	1	2	3	1	2	3	1	2	3	1	2	3
.1	.37	.39	1.00	.34	.36	1.00	.23	.25	1.00	.43	.46	1.00
.2	.35	.35	.36	.32	.32	.33	.20	.21	.22	.41	.41	.42
.3	.33	.34	.34	.29	.30	.31	.18	.18	.19	.38	.39	.40
.4	.32	.32	.32	.28	.29	.29	.17	.17	.17	.37	.37	.38
.5	.31	.31	.32	.27	.28	.28	.16	.16	.17	.36	.36	.37
.6	.30	.31	.31	.27	.27	.27	.15	.15	.16	.35	.35	.36
.7	.29	.30	.30	.26	.26	.27	.14	.15	.15	.34	.34	.35
.8	.26	.29	.29	.23	.25	.26	.12	.14	.14	.30	.33	.34
.9	.13	.19	.29	.11	.16	.25	.06	.09	.14	.15	.21	.33

	ANNUAL		
TRANS.	1	2	3
.1	.34	.36	1.00
.2	.32	.33	.33
.3	.30	.30	.31
.4	.28	.29	.29
.5	.28	.28	.28
.6	.27	.27	.28
.7	.26	.26	.27
.8	.23	.25	.26
.9	.11	.16	.25

FREQUENCY THAT TRANSMISSION EFFICIENCY EXCEEDS SPECIFIED VALUE--

SW-1: LUKE AFB (PHOENIX), ARIZONA N 33 32 W 112 23 ELEV 1121 FT

	WINTER			SPRING			SUMMER			FALL		
TRANS.	1	2	3	1	2	3	1	2	3	1	2	3
.1	.97	1.00	1.00	.98	.99	.99	.98	.99	.99	.99	.99	.99
.2	.87	.99	1.00	.92	.99	.99	.93	.99	.99	.94	1.00	.99
.3	.79	.85	1.00	.87	.90	.99	.89	.92	.99	.90	.93	.99
.4	.76	.78	1.00	.84	.86	.99	.86	.88	.99	.88	.90	.99
.5	.73	.75	.79	.81	.83	.87	.82	.85	.89	.86	.88	.91
.6	.69	.71	.77	.77	.80	.85	.78	.81	.87	.83	.84	.89
.7	.65	.67	.76	.74	.75	.84	.73	.75	.86	.79	.81	.88
.8	.61	.62	.66	.69	.70	.74	.67	.68	.74	.75	.76	.80
.9	.54	.57	.60	.62	.64	.68	.58	.61	.66	.69	.71	.74

	ANNUAL		
TRANS.	1	2	3
.1	.98	.99	.99
.2	.91	.99	.99
.3	.86	.90	.99
.4	.84	.85	.99
.5	.80	.83	.86
.6	.77	.79	.85
.7	.73	.74	.83
.8	.68	.69	.74
.9	.61	.63	.67

AVERAGE POWER AVAIABILITY--

SW-1: LUKE AFB (PHOENIX), ARIZONA N 33 32 W 112 23 ELEV 1121 FT

	MODEL		
SEASON	1	2	3
WINTER	.70	.73	.82
SPRING	.77	.80	.86
SUMMER	.77	.80	.86
FALL	.82	.84	.89
ANNUAL	.76	.79	.86

FREQUENCY THAT TRANSMISSION EFFICIENCY EXCEEDS SPECIFIED VALUE
FOR A PERSISTENCE TIME OF 480.0 MINUTES--

SW-1: LUKE AFB (PHOENIX), ARIZONA N 33 32 W 112 23 ELEV 1121 FT

	WINTER			SPRING			SUMMER			FALL		
TRANS.	1	2	3	1	2	3	1	2	3	1	2	3
.1	.53	.55	1.00	.61	.63	1.00	.56	.59	1.00	.68	.70	1.00
.2	.51	.52	.53	.58	.59	.60	.53	.54	.55	.66	.66	.67
.3	.49	.50	.51	.56	.57	.58	.50	.51	.52	.64	.64	.65
.4	.48	.48	.49	.55	.55	.56	.48	.49	.49	.62	.63	.63
.5	.47	.47	.48	.54	.54	.55	.47	.47	.48	.61	.61	.62
.6	.46	.46	.47	.52	.53	.54	.45	.46	.47	.59	.60	.61
.7	.45	.45	.46	.51	.52	.53	.43	.44	.45	.58	.59	.60
.8	.40	.44	.45	.45	.51	.51	.38	.43	.44	.52	.58	.58
.9	.20	.28	.44	.23	.33	.50	.19	.27	.42	.26	.37	.57

	ANNUAL		
TRANS.	1	2	3
.1	.60	.62	1.00
.2	.57	.58	.59
.3	.55	.55	.56
.4	.53	.54	.54
.5	.52	.52	.53
.6	.51	.51	.52
.7	.49	.50	.51
.8	.44	.49	.50
.9	.22	.31	.48

FREQUENCY THAT TRANSMISSION EFFICIENCY EXCEEDS SPECIFIED VALUE--

SW-2: MCCLELLAN AFB (SACRAMENTO), CA N 38 40 W 121 24 , ELEV 76 FT

	WINTER			SPRING			SUMMER			FALL		
TRANS.	1	2	3	1	2	3	1	2	3	1	2	3
.1	.95	.99	.99	.97	.99	.99	.99	1.00	1.00	.98	.99	.99
.2	.78	.98	.99	.89	.99	.99	.98	1.00	1.00	.92	.99	.99
.3	.65	.74	.99	.82	.87	.99	.96	.97	1.00	.88	.91	.99
.4	.64	.65	.99	.80	.81	.99	.95	.96	1.00	.86	.87	.99
.5	.60	.63	.65	.76	.79	.82	.94	.95	.96	.84	.86	.88
.6	.57	.58	.64	.73	.75	.81	.92	.93	.96	.82	.83	.87
.7	.54	.55	.63	.70	.71	.79	.91	.91	.95	.79	.80	.86
.8	.50	.51	.55	.64	.65	.70	.88	.88	.91	.75	.76	.80
.9	.47	.48	.50	.59	.61	.64	.84	.85	.87	.70	.72	.74

	ANNUAL		
TRANS.	1	2	3
.1	.97	.99	.99
.2	.89	.99	.99
.3	.83	.87	.99
.4	.81	.82	.99
.5	.79	.81	.83
.6	.76	.77	.82
.7	.73	.74	.81
.8	.69	.70	.74
.9	.65	.67	.69

AVERAGE POWER AVAIABILITY--

SW-2: MCCLELLAN AFB (SACRAMENTO), CA N 38 40 W 121 24 ELEV 76 FT

	MODEL		
SEASON	1	2	3
WINTER	.59	.64	.76
SPRING	.73	.76	.84
SUMMER	.91	.92	.95
FALL	.81	.83	.89
ANNUAL	.76	.79	.86

FREQUENCY THAT TRANSMISSION EFFICIENCY EXCEEDS SPECIFIED VALUE
FOR A PERSISTENCE TIME OF 480.0 MINUTES--

SW-2: MCCLELLAN AFB (SACRAMENTO), CA N 38 40 W 121 24 ELEV 76 FT

	WINTER			SPRING			SUMMER			FALL		
TRANS.	1	2	3	1	2	3	1	2	3	1	2	3
.1	.46	.47	1.00	.58	.60	1.00	.83	.85	1.00	.70	.71	1.00
.2	.44	.44	.45	.56	.56	.57	.81	.82	.83	.68	.68	.69
.3	.42	.42	.43	.53	.54	.55	.79	.80	.81	.65	.66	.67
.4	.41	.41	.41	.52	.52	.52	.78	.79	.79	.64	.64	.65
.5	.40	.41	.41	.51	.51	.52	.77	.78	.78	.63	.64	.64
.6	.40	.40	.40	.50	.50	.51	.76	.77	.77	.62	.63	.63
.7	.39	.39	.40	.49	.49	.50	.75	.76	.76	.61	.62	.62
.8	.35	.39	.39	.43	.48	.49	.68	.75	.76	.55	.61	.62
.9	.17	.25	.39	.22	.31	.48	.34	.49	.75	.27	.40	.61

	ANNUAL		
TRANS.	1	2	3
.1	.64	.66	1.00
.2	.62	.63	.63
.3	.60	.61	.61
.4	.59	.59	.59
.5	.58	.58	.59
.6	.57	.57	.58
.7	.56	.57	.57
.8	.50	.56	.56
.9	.25	.36	.56

FREQUENCY THAT TRANSMISSION EFFICIENCY EXCEEDS SPECIFIED VALUE--

SW-3: NELLIS AFB (LAS VEGAS), NEVADA N 36 15 W 115 02 ELEV 1868 F

	WINTER			SPRING			SUMMER			FALL		
TRANS.	1	2	3	1	2	3	1	2	3	1	2	3
.1	.97	.99	.99	.98	.99	.99	.99	.99	.99	.99	.99	.99
.2	.86	.99	.99	.90	.99	.99	.96	1.00	.99	.94	1.00	.99
.3	.77	.84	.99	.84	.88	.99	.93	.95	.99	.90	.93	.99
.4	.75	.77	.99	.81	.83	.99	.91	.92	.99	.88	.89	.99
.5	.71	.74	.78	.77	.80	.84	.88	.90	.93	.85	.87	.90
.6	.67	.69	.76	.73	.76	.82	.84	.86	.92	.82	.84	.88
.7	.62	.64	.74	.69	.70	.81	.80	.82	.90	.79	.80	.87
.8	.57	.58	.63	.63	.64	.70	.75	.76	.81	.74	.75	.79
.9	.50	.53	.56	.55	.58	.62	.67	.70	.74	.68	.71	.74

	ANNUAL		
TRANS.	1	2	3
.1	.98	.99	.99
.2	.91	.99	.99
.3	.86	.90	.99
.4	.84	.85	.99
.5	.80	.83	.86
.6	.77	.79	.85
.7	.72	.74	.83
.8	.67	.69	.73
.9	.60	.63	.67

AVERAGE POWER AVAIABILITY--

SW-3: NELLIS AFB (LAS VEGAS), NEVADA N 36 15 W 115 02 ELEV 1868 F

	MODEL		
SEASON	1	2	3
WINTER	.67	.71	.81
SPRING	.73	.76	.84
SUMMER	.83	.85	.90
FALL	.81	.84	.89
ANNUAL	.76	.79	.86

FREQUENCY THAT TRANSMISSION EFFICIENCY EXCEEDS SPECIFIED VALUE
FOR A PERSISTENCE TIME OF 480.0 MINUTES--

SW-3: NELLIS AFB (LAS VEGAS), NEVADA N 36 15 W 115 02 ELEV 1868 F

	WINTER			SPRING			SUMMER			FALL		
TRANS.	1	2	3	1	2	3	1	2	3	1	2	3
.1	.49	.51	1.00	.54	.56	1.00	.66	.69	1.00	.68	.70	1.00
.2	.46	.47	.48	.51	.52	.53	.63	.64	.65	.65	.66	.67
.3	.44	.45	.46	.48	.49	.50	.61	.61	.62	.63	.64	.65
.4	.43	.43	.44	.46	.47	.47	.59	.59	.60	.62	.62	.63
.5	.41	.42	.43	.45	.46	.46	.57	.58	.58	.60	.61	.61
.6	.40	.41	.41	.43	.44	.45	.55	.56	.57	.59	.60	.60
.7	.39	.40	.40	.42	.43	.44	.54	.55	.56	.58	.58	.59
.8	.34	.39	.39	.37	.41	.42	.48	.53	.54	.51	.57	.58
.9	.17	.25	.38	.18	.27	.41	.24	.34	.53	.26	.37	.57

	ANNUAL		
TRANS.	1	2	3
.1	.59	.61	1.00
.2	.56	.57	.58
.3	.54	.55	.56
.4	.52	.53	.53
.5	.51	.52	.52
.6	.50	.50	.51
.7	.48	.49	.50
.8	.43	.48	.48
.9	.21	.31	.47

AVERAGE POWER AVAILABILITIES FOR MULTIPLE SITES--Atlantic Region

	MODEL		
SEASON	1	2	3
WINTER	.41	.49	.65
SPRING	.45	.52	.67
SUMMER	.53	.58	.72
FALL	.51	.57	.71
ANNUAL	.48	.54	.69

AVERAGE POWER AVAILABILITIES FOR MULTIPLE SITES-- Central Region

	MODEL		
SEASON	1	2	3
WINTER	.53	.59	.72
SPRING	.53	.59	.72
SUMMER	.70	.74	.82
FALL	.62	.67	.77
ANNUAL	.59	.65	.76

AVERAGE POWER AVAILABILITIES FOR MULTIPLE SITES-- Midwest Region

	MODEL		
SEASON	1	2	3
WINTER	.42	.49	.65
SPRING	.47	.54	.68
SUMMER	.59	.64	.76
FALL	.55	.61	.73
ANNUAL	.51	.57	.71

AVERAGE POWER AVAILABILITIES FOR MULTIPLE SITES--New England Region

SEASON	MODEL 1	2	3
WINTER	.52	.58	.71
SPRING	.50	.57	.70
SUMMER	.52	.59	.72
FALL	.55	.61	.73
ANNUAL	.52	.59	.72

AVERAGE POWER AVAILABILITIES FOR MULTIPLE SITES--North Central Region

SEASON	MODEL 1	2	3
WINTER	.49	.55	.69
SPRING	.49	.56	.70
SUMMER	.72	.76	.84
FALL	.64	.69	.79
ANNUAL	.58	.64	.75

AVERAGE POWER AVAILABILITIES FOR MULTIPLE SITES--Northwest Region

SEASON	MODEL 1	2	3
WINTER	.29	.38	.57
SPRING	.40	.48	.64
SUMMER	.56	.62	.74
FALL	.42	.49	.65
ANNUAL	.42	.49	.65

AVERAGE POWER AVAILABILITIES FOR MULTIPLE SITES--South Central Region

SEASON	MODEL 1	2	3
WINTER	.56	.61	.73
SPRING	.58	.63	.75
SUMMER	.70	.74	.82
FALL	.68	.72	.81
ANNUAL	.63	.68	.78

AVERAGE POWER AVAILABILITIES FOR MULTIPLE SITES--Southeast Region

SEASON	MODEL 1	2	3
WINTER	.51	.57	.71
SPRING	.57	.63	.74
SUMMER	.57	.63	.75
FALL	.63	.68	.78
ANNUAL	.57	.63	.74

AVERAGE POWER AVAILABILITIES FOR MULTIPLE SITES--Southwest Region

SEASON	MODEL 1	2	3
WINTER	.65	.70	.79
SPRING	.74	.77	.85
SUMMER	.84	.86	.90
FALL	.81	.84	.89
ANNUAL	.76	.79	.86

1. REPORT NO.	2. GOVERNMENT ACCESSION NO.	3. RECIPIENT'S CATALOG NO.
NASA CR-3347		

4. TITLE AND SUBTITLE	5. REPORT DATE
Satellite Power Systems (SPS) Laser Studies Vol. 2: Meteorological Effects on Laser Beam Propagation and Direct Solar Pumped Lasers for the SPS	November 1980
	6. PERFORMING ORGANIZATION CODE
7. AUTHOR(S) R. E. Beverly III	8. PERFORMING ORGANIZATION REPORT # SSD 80-0119-2
9. PERFORMING ORGANIZATION NAME AND ADDRESS Rockwell International Space Operations and Satellite Systems Division Columbus, Ohio	10. WORK UNIT NO. M-314
	11. CONTRACT OR GRANT NO. NAS8-32475
12. SPONSORING AGENCY NAME AND ADDRESS National Aeronautics and Space Administration Washington, DC 20546	13. TYPE OF REPORT & PERIOD COVERED Contractor Report June 79 - Mar 80
	14. SPONSORING AGENCY CODE

15. SUPPLEMENTARY NOTES

NASA Marshall Technical Monitor: Charles Guttman
Final Report

16. ABSTRACT

The primary emphasis of this research activity is to investigate the effect of the environment on laser power transmission/reception from space to ground. This activity investigates potential mitigation techniques to minimize the environment effect by a judicious choice of laser operating parameters. Using these techniques, the availability of power at selected sites is determined using statistical meteorological data for each site.

17. KEY WORDS	18. DISTRIBUTION STATEMENT
Satellite Power System (SPS) Laser Power transmission/reception Space Environment	Unclassified - Unlimited Subject Category 44

19. SECURITY CLASSIF. (of this report)	20. SECURITY CLASSIF. (of this page)	21. NO. OF PAGES	22. PRICE
Unclassified	Unclassified	141	A07

For sale by National Technical Information Service, Springfield, Virginia 22161

NASA-Langley, 1980